Summer 2000

Phenomenological Description of Double-Pion Photoproduction

Andry M. Rakotovao
Old Dominion University

PHENOMENOLOGICAL DESCRIPTION OF DOUBLE-PION PHOTOPRODUCTION

by

Andry M. Rakotovao
C.A.P.E.N., 1990, University of Antananarivo, Madagascar
M.S., 1994, Old Dominion University, Norfolk

A Dissertation submitted to the Faculty of
Old Dominion University in Partial Fullfillment of the
Requirement for the Degree of

DOCTOR OF PHILOSOPHY

PHYSICS

OLD DOMINION UNIVERSITY
August 2000

Approved by:

Dr. Winston Roberts (Director)

Dr. Jose Goity

Dr. Gilbert Hoy

Dr. Anatoly Radyushkin

Dr. Linda Vahala

Dr. Wallace Van Orden

ABSTRACT

PHENOMENOLOGICAL DESCRIPTION OF DOUBLE-PION PHOTOPRODUCTION

Andry M. Rakotovao
Old Dominion University, 2000
Director: Dr. Winston Roberts

Double pion photoproduction off proton targets is studied, in the framework of an Effective Lagrangian approach at tree level, based on the coupling of photons and pions to nucleons and resonances. We consider N, $\Delta(1232)$, $N(1440)$, $N(1520)$ and $N(1535)$ as intermediate baryonic states and $\rho-$meson as the intermediate 2π resonance. The general form of the amplitude is presented and total cross sections of the $\gamma p \rightarrow \pi^+\pi^- p$, $\gamma p \rightarrow \pi^0\pi^0 p$ and $\gamma p \rightarrow \pi^+\pi^0 n$ processes are evaluated up to $E_\gamma = 800$ MeV. We fit our theoretical calculation to the experimental data and extract some previously unknown parameters. Furthermore, single pion photoproduction is studied and analysis of the axial anomaly using the $\gamma\pi^+ \rightarrow \pi^+\pi^0$ reaction near threshold is presented.

Acknowledgements

I would like to thank Dr. Winston Roberts for the guidance, patience and support that he has given me during this research project. I greatly appreciate his willingness to share his knowledge and carefully reading the manuscript. Without his effort, this work would not have been accomplished.

I am very grateful to Dr. José Goity, Dr. Gilbert Hoy, Dr. Anatoly Radyushkin, Dr. Linda Vahala and Dr. Wallace Van Orden for their time in reading of this text and making valuable comments.

I would like also to thank other members of the Physics Department, in particular, Dr. James Cox and Mr. Walton Hooks for the assistance that they have provided to me during my work at the Department, and finally I would like to thank the graduate student group, especially Tobias Oed for the friendly atmosphere I have enjoyed during my years at the University.

This work is partially sponsored by the Department of Energy, the National Science Foundation and the Jeffress Foundation.

Table of Contents

List of Tables

List of Figures

Chapter 1

INTRODUCTION AND MOTIVATION

1.1 Status of our understanding of Quantum Chromodynamics

Quantum Chromodynamics (QCD), or the theory of strong interaction, describes the interaction that binds quarks into hadrons. In order to understand this interaction, we need to examine the theory of QCD which is similar to the theory of Quantum Electrodynamics (QED).

The Lagrangian for QED is

$$\mathcal{L}_{QED} = -\frac{1}{4}F^{\mu\nu}F_{\mu\nu} + i\bar{\psi}\gamma^{\mu}D_{\mu}\psi - m_e\bar{\psi}\psi, \tag{1}$$

where

$$F^{\mu\nu} = \partial^{\mu}A^{\nu} - \partial^{\nu}A^{\mu}$$

is the QED field strength tensor and

$$D_{\mu} = \partial_{\mu} - ieA_{\mu}$$

The style specifications used in this thesis follow those of *Physical Review* **D**.

is the so-called covariant derivative. A_μ is the photon field, γ_μ is the Dirac matrix, ψ is the electron field, e is the electric charge of the electron and m_e is its mass.

The Lagrangian for QCD is

$$\mathcal{L}_{QCD} = -\frac{1}{4}G^a_{\mu\nu}G^{\mu\nu}_a + i\sum_q \bar{\psi}^i_q \gamma^\mu (D_\mu)_{ij}\psi^j_q - \sum_q m_q \bar{\psi}^i_q \psi_{qi}, \tag{2}$$

where

$$G^a_{\mu\nu} = \partial_\mu A^a_\nu - \partial_\nu A^a_\mu + g_s f_{abc} A^b_\mu A^c_\nu$$

is the QCD field strength tensor, A^a_μ $(a = 1, 2, ...8)$ are the gluon fields and ψ_{qi} are the quark fields with color i and flavor q.

$$(D_\mu)_{ij} = \delta_{ij}\partial_\mu - ig_s \sum_a \frac{\lambda^a_{ij}}{2} A^a_\mu$$

is the covariant derivative, where g_s is a coupling constant and f_{abc} are the structure constants of the SU(3) algebra defined by

$$\left[\frac{\lambda^a}{2}, \frac{\lambda^b}{2}\right] = i f_{abc}\frac{\lambda^c}{2}.$$

The main difference between the QED Lagrangian and that of QCD is the extra term $g_s f_{abc} A^b_\mu A^c_\nu$ which is seen in the QCD Lagrangian. In fact, there is a single gauge boson in QED, namely the photon. In QCD, there are eight gauge bosons, the gluons which carry color charge, and they can interact with each other. In QED, photons do not couple to each other since they are chargeless. Thus, we note that the previous extra term represents the coupling between gluons.

The existence of the gluon-gluon interaction leads to an important property of QCD, the so-called 'asymptotic freedom'. To explain this, let us examine the so called 'running coupling constant', a coupling constant that varies with the energy scale.

In both theories, the running 'fine structure' constants $\alpha(Q^2)$ and $\alpha_s(Q^2)$, where $Q^2 = -q^2$ and q is the four-momentum transferred during the interactions, are used to measure the strength of interactions between two charged particles. These coupling constants are respectively

$$\alpha(Q^2) = \frac{e^2(Q^2)}{4\pi}$$

and

$$\alpha_s(Q^2) = \frac{g_s^2(Q^2)}{4\pi}$$

for QED and QCD, where e is the electron charge and g_s is the QCD coupling constant already defined in the above Lagrangian.

The behavior of the running coupling constants in the two theories are very different. In QED, virtual e^+e^- pairs surround the electron and create the effect of charge screening, similar to a dielectric medium, so that the apparent charge is less than the true charge. Thus, photons must probe through this medium when two electrons interact with each other and the strength of the interaction therefore depends on the energy and momentum of the transmitted photons. As Q^2 increases, the resolution of the photon probe increases and smaller distances are probed. Then, we begin to penetrate the dielectric medium and see the bare charge. Consequently, the running coupling constant increases with Q^2.

In QCD, a quark is not only surrounded by a cloud of quark-antiquark ($q\bar{q}$) pairs but also by gluons, which are also color charged. As it turns out, this additional contribution reverses the effect from ($q\bar{q}$) and leads to an antiscreening effect. When contributions up to one loop level are considered, the running coupling constant of QCD is [1]

$$\alpha_s(Q^2) = \frac{4\pi}{b_0 \ln(\frac{Q^2}{\Lambda^2_{QCD}})},$$

where Λ_{QCD} is the QCD scale parameter, which has a value somewhere between 0.1 GeV and 0.5 GeV, and b_0 is a positive parameter.

We observe that the running coupling constant decreases with increasing Q^2. This means that if the separation between the two quarks is small, the strength of the interaction between them is weak and they behave like almost free particles. This is the property of the 'asymptotic freedom'. On the other hand, if the distance that separates the two quarks increases, the strength of the interaction

increases as well. This is because of the self-coupling of the gluons which implies that the exchanged gluons attract each other.

Isolated quarks have never been observed and this has led to the hypothesis of quark confinement. It is believed that the only particle states that we can observe are colorless states. Since quarks have color, we cannot observe a free quark. As a result, quarks and antiquarks are bound into the so-called 'hadrons'. The hadrons that are fermions are called baryons, and the hadrons that are bosons are called mesons. It is assumed that baryons are bound states of three valence quarks $(q_1q_2q_3)$, while mesons are bound states of one valence quark and one valence antiquark $(q_1\bar{q}_2)$. Not all combinations of quarks and antiquarks are allowed since the outcome must be colorless. Combinations such qqq and $q\bar{q}$ have been observed, while combinations such $qq\bar{q}$ and qq are thought not to exist.

With the development of Quantum Chromodynamics as the theoretical framework of the strong interactions, different techniques have been proposed to describe the structure of hadrons and extract hadron properties. Among these is the 'perturbative' technique which is similar to what is used to solve QED. This technique works well at short distance, or at large Q^2 when QCD is asymptotically free. As the distance between the two quarks increases, or as Q^2 decreases, the running coupling constant $\alpha_s(Q^2)$ becomes large. Perturbation theory breaks down and QCD is said to be confined. Consequently, we need other techniques to solve QCD.

One of the most promising techniques is the so-called 'Lattice QCD' [2] which begins to give some insight into rigorous results, especially for heavy mesons. In this approach, quarks are located at lattice sites and gluons on the links between these sites. Thus, an effective interquark potential is studied and hadron properties are calculated. The Feynman path integral technique is usually used to perform numerical calculation. However, application of lattice QCD to many physical processes is limited to available computer power.

Another approach that has been extensively studied is the QCD sum rules approach [3, 4]. The fundamental idea in this method is a systematic separation of the short distance properties of quarks, which are well known from perturbative

QCD, from long distance properties, which can not be calculated but which may be parametrized using experimental input. The theoretical tool which is almost ideally suited for the purpose of the sum rule method is the Wilson operator product expansion, in which the time ordered product of currents is expressed in terms of the Wilson coefficients and the average vacuum expectation values of quark and gluons condensate operators. The Wilson coefficient functions contain the short distance information and can be calculated by perturbative techniques. The vacuum matrix elements contain the hadron properties at large distance and are determined entirely by non-perturbative techniques. The effect of the short and long distance separation is built into the Wilson product expansion. The essential part for the method to work is that only if the expectation value of the condensate operator is dominated by non-perturbative effects, then the effect of separating the regions of short and long distances becomes unimportant. Then, transition from the perturbative to the non-perturbative regime can be done, and hadron properties can be expressed in terms of a few QCD parameters.

Another example of these techniques is the quark potential model approach [5] which has been quite successful in providing physical insight into hadron physics. In this approach, a model for a quark potential is proposed and the Hamiltonian is established. The wave function is built and is usually expanded in terms of some known wave functions such as the harmonic-oscillator eigenfunctions. Then, the equations of motion for quarks in hadrons are solved, and approximate solutions of these equations are derived. One of the most successful models in this approach is the nonrelativistic constituent quark model (NRQM). This particular model has provided a simple picture for understanding hadron spectroscopy and has been surprisingly successful in explaining large amounts of data.

Despite the success of these models (NRQM), many physical problems, such as the significance and treatment of the relativistic motion of quarks within hadrons, remain unsolved. Attempts have been made to solve some of the problems by including relativistic effects and other refinements [6] into the models. However, these refinements are unlikely to offer a solution to the most important problem of the so-called 'missing' baryon states. These are the states that appear in the

model but which have not been seen experimentally yet.

One approach that has been used in dealing with the missing states is that of diminishing the number of effective degrees of freedom within the baryons. This is done by replacing the three-quark system with a quark-diquark system [7], with the result that the predicted spectrum contains fewer states. This approach raises the question of whether there is any diquark clustering within the baryons. Indeed, potential model [8] studies and lattice simulations [9] show that there is little evidence for such clustering in baryons of light quarks unless they have large orbital angular momentum.

An improved model has been made by S. Capstick and W. Roberts [10] in which a relativized model of baryon resonances is used to calculate the πN amplitudes for resonant states. Comparison between the theoretical πN amplitudes and the extracted experimental amplitudes suggests that, for a group of states which have the same isospin, spin and parity, the missing states have smaller amplitudes than the states (usually lighter) which are seen. We note that this result was first suggested by Koniuk and Isgur [11, 12]. This result may therefore explain the apparent absence of many predicted states from the partial-wave analyses. These missing states are weakly coupled to the πN states, but should be eventually seen. Another finding in this model is that states which are close in mass and which have similar couplings to the πN production channels are likely to mix in the presence of many open decay channels. Such mixing could easily make one state more likely and one state less likely to be produced. What is noticeably absent in this analysis is therefore the treatment of coupled-channel effects in the spectroscopy and the decay-channel couplings of these states. On the other hand, the model can be considered reliable for states which are appreciably separated in mass and coupling strength from other states with similar isospin, spin and parity.

We summarize this section by noting that many QCD techniques and QCD inspired quark models have had great success in predicting new hadronic states and progress has been made in extracting hadron properties. However, many physical problems remain unsolved at the present time, in particular, the problem

of the missing states. If these missing states couple weakly with the πN channel, then they have to be sought elsewhere. Thus, new approaches need to be found in explaining the source of these states.

In this quest for better approach to extracting hadron properties, electromagnetic transition amplitudes are beginning to provide powerful tests of the quality of emerging models. Thus, for excited-baryon spectroscopy, there is a continuing need to determine accurately the photocouplings of baryon resonances, from the high quality experimental data, and to contrast them with their best theoretical estimates. At the Thomas Jefferson National Accelerator Facility (TJNAF), a continuous electron beam is produced and study of photocouplings of baryons with polarized or non-polarized targets and electron or photon beams with high precision is possible. Various experimental results need a careful theoretical analysis and this work is part of that effort.

1.2 The $N^\star$ program at TJNAF and double pion photoproduction

The $N^\star$ program at TJNAF is aimed at studying many properties of baryon states. Included in these studies are the search for the missing baryon resonances and 'exotic states' such as 'hybrids'. Hybrids are states which have constituent quarks and one or more excited gluons. Other $N^\star$ studies at TJNAF include that of the structure of the Roper resonance [$N^\star(1440)$] [13], the $\Lambda(1405)$ and other low-lying resonances such as the $\Lambda(1520)$ and $\Sigma(1385)$, and that of the couplings of nucleons to strange matter [14, 15].

πN scattering experiments have been extensively performed in the past to probe the πN couplings of ground states and excited baryons [16, 17, 18, 10]. However, one of the best prospects [19] for discovery of new baryon states, such as those missing from the analyses of pion elastic scattering, is the electromagnetic production of multiple pions. If we believe that these states are missing because of a weak coupling to the πN channel, then processes which form these excited

baryon states electromagnetically are favorable, and some means of decay other than πN are also favorable. Therefore, one possibility for producing the missing states is to use a photon or electron beam to probe the nucleon targets. Meson and baryon resonance channels such as ρN and $\Delta\pi$ are produced in the photo- and electroexcitation of a nucleon [20]. These intermediate states in turn will decay and produce the channel $\pi\pi N$. The process $\gamma N \rightarrow X \rightarrow \pi N$ where X represents a missing baryon may also occur but its cross section is expected to be relatively small compared to that from the known baryons. Therefore, one way to look for the missing states is the use of the double pion photoproduction.

Double pion photoproduction experiments have been studied in the past [21, 22, 23, 24, 25] and two experiments on the proton [26, 27] have been done recently at Mainz and Bonn. In addition, several experiments related to the double pion photo- and electroproduction have been already approved at Jefferson Laboratory's Hall B, where the CEBAF Large Acceptance Spectrometer (CLAS) is located. This detector allows good particle identification so that electrons, pions, kaons, protons, and deuterons can be separated, as well as neutrals such as photons and neutrons.

As an example of these experiments is the study of the $\gamma p \rightarrow p\pi^+\pi^-$ process [28]. All of the final state particles are charged and so will be easily detected. The invariant mass of the two pions will be examined to look for intermediate states in the $\gamma p \rightarrow p\rho$, and similarly the invariant mass of one pion and the proton can be reconstructed to look for missing baryons, for example, in the $\Delta\pi$ channel. Models of the strong decays of these missing states predict sizeable decay widths [11, 20] into these channels.

A few experiments using an unpolarized photon beam and an unpolarized target have been partially completed at TJNAF, and the analyses are still underway. In the near future, one expects to have both polarized beam and target. Many high-precision data such as total cross sections will be extracted from these experiments, and a systematic, comprehensive calculation for this process must be undertaken. By comprehensive, it is meant that all possible effects must be

included, even small ones, as these 'small' effects may provide very valuable information.

A theoretical calculation of double pion photoproduction was first done by L. Lüke and P. Söding in 1970, by including a few Feynman diagrams [29]. Calculations with more diagrams have been carried out recently by Oset *et al.* using a different approach [30, 31]. This approach reproduces fairly well the experimental cross sections of some isospin channels below $E_\gamma = 800$ MeV. They attempt to fit the recent Mainz data [26] by including a number of resonant and non-resonant terms in their model, and they find that the dominant feature of their cross section results come from neither $\gamma N \to \rho N \to \pi\pi N$ nor $\gamma N \to \Delta\pi \to \pi\pi N$, but from the interference of one $\Delta\pi$ resonant contribution with one of their non-resonant terms. It is not at all intuitive that such an interference term should dominate the cross section, in any energy range. On the other hand, a systematic analysis of two-pion photoproduction processes that is similar to those which exist for single pion photoproduction [32, 33] has not, as far as we know, yet been attempted. Our model is based on the couplings of photons and pions to nucleons and resonances using effective Lagrangians. We set up a general model independent amplitude which is gauge invariant and Lorentz covariant to ensure the independence of the amplitude on the choice of the frame. The model leads to a set of Feynman diagrams at tree level where two- and three- point nucleon Born terms, including the seagull terms, are taken into account. These terms are believed to provide a large contribution to the cross section at low energy. Vector meson exchanges and nucleon resonance excitations are also discussed. In this way, we include the ρ-meson as an intermediate 2π resonance as well as the baryonic states such as $\Delta(1232)$, $N(1440)$, $N(1520)$ and $N(1535)$. We do not include resonances such as $\Delta(1600)$ and $N(1620)$ and higher since our calculation goes up to Lab. energy $E_\gamma = 800$ MeV or total energy $W = 1540$ MeV.

Another issue that we can discuss from this calculation is the study of the chiral anomaly using the $\gamma p \to \pi^+\pi^0 n$ reaction at low t where t is the square of the momentum transfert between the two nucleons. From the measurement of the cross section, the $\gamma \to 3\pi$ structure function ($F^{3\pi}$) can be extracted at low

t, and its momentum dependence can be evaluated. In the chiral limit, ($F^{3\pi}$) is related to the $\pi^0 \rightarrow 2\gamma$ amplitude. Within the context of the chiral anomaly, which successfully predicts the decay of the π^0, the $\gamma \rightarrow 3\pi$ vertex can be used to evaluate the validity of chiral symmetry in QCD.

The main objective of this work is to reproduce the cross sections of the three different processes related to double pion-photoproduction with proton target from threshold to $E_\gamma = 800$ MeV, by fitting our theoretical calculation to the experimental data. These three processes are $\gamma p \rightarrow \pi^+\pi^- p$, $\gamma p \rightarrow \pi^+\pi^0 n$ and $\gamma p \rightarrow \pi^0\pi^0 p$. One outcome of the fit is that we may determine some previously unknown parameters required to describe the model. This means that double pion photoproduction can provide new ways of testing our understanding of hadron structure, by way of the couplings of new vertices such as $N_1^* N_2^* \pi$, $N_1^* N_2^* \gamma$ and $N_1^* N_2^* \rho$ where the N_i^* are baryon resonances. We note that this is essentially what is done in analysis of pion-nucleon elastic scattering data, from which we have essentially all of the information on the baryon spectrum that is presented in the Particle Data listing [34]. Clearly, cross section data alone will not be enough to delimit the possible choices of parameters that can provide good fits to the available and expected data. There is an essential need for high quality polarization data. This will be crucial if we are to exploit the many opportunities lurking in the shadows of this process. However, our results should provide an idea of the structures of these fitted vertices as well as the magnitudes of the theoretical values (including the range of uncertainty) of the corresponding parameters in treating other or related nuclear processes.

This thesis is organized as follows. In chapter 2, a description of single pion photoproduction is introduced as a test for our model. In chapter 3, we present the formalism of the effective Lagrangian and results for the single pion photoproduction calculation. In chapter 4, we describe the generalized invariant amplitude, the kinematics and the cross section of the double pion photoproduction process, and all the possible different Feynman diagrams involved at tree level. Chapter 5 is devoted to discussing the results that we obtain from the fits, and in chapter 6 the study of the axial anomaly using the $\gamma\pi^+ \rightarrow \pi^+\pi^0$ reaction near threshold

is presented. A summary and our conclusions are given in chapter 7. Appendices detail kinematic analyses of the process as well as different Lagrangians, coupling constants, isospin operators and isospin coefficients that would be helpful for further understanding of the analysis.

Chapter 2

SINGLE PION PHOTOPRODUCTION

2.1 Kinematics

In this chapter, we examine the process

$$\gamma(k) + N(p_1) \rightarrow \pi(Q) + N(p_2)$$

where k, p_1, Q, p_2 are, respectively, the momenta of the incident photon, target nucleon, pion and recoil nucleon.

The usual Mandelstam variables are

$$\begin{aligned} s &= (k+p_1)^2 = (Q+p_2)^2, \\ u &= (k-p_2)^2 = (Q-p_1)^2, \\ t &= (Q-k)^2 = (p_1-p_2)^2, \end{aligned} \tag{3}$$

where $s+t+u = 2M^2 + m_\pi^2 + k^2$. M and m_π denote the masses of the nucleon and the pion. It is easier to work in the center of mass of the final nucleon and the π where the experimental observables are calculated. The relations (3), in the center of mass system become

$$\begin{aligned} s &= W^2 = (E_1 + k_0)^2, \\ u &= M^2 + k^2 - 2k_0E_2 - 2|\vec{Q}||\vec{k}|\cos\theta, \\ t &= m_\pi^2 + k^2 - 2k_0w + 2|\vec{Q}||\vec{k}|\cos\theta, \end{aligned}$$

where $\cos(\theta) = \frac{\vec{Q}\cdot\vec{k}}{|\vec{Q}||\vec{k}|}$, with θ being the c.o.m. scattering angle of the pion and W is the total c.o.m energy. The energies and momenta are

$$\begin{aligned} k_0 &= \frac{W^2 + k^2 - M^2}{2W}, \quad E_1 = \frac{W^2 - k^2 + M^2}{2W}, \\ w &= \frac{W^2 + m_\pi^2 - M^2}{2W}, \quad E_2 = \frac{W^2 - m_\pi^2 + M^2}{2W}, \\ |\vec{p_1}| &= |\vec{k}| = \sqrt{k_0^2 - k_2}, \\ |\vec{p_2}| &= |\vec{Q}| = \sqrt{w^2 - m_\pi^2}, \end{aligned}$$

where $k = (k_0, \vec{k})$, $p_1 = (E_1, -\vec{k})$, $Q = (w, \vec{Q})$ and $p_2 = (E_2, -\vec{Q})$.

For photoproduction, $k^2 = 0$ and the relation between the energy E_γ of the photon in the lab. frame and the c.o.m. energy is

$$E_\gamma = \frac{W^2 - M^2}{2M}.$$

2.2 Invariant amplitude

The invariant matrix element $i\mathcal{M}_{fi}$ can be written as

$$i\mathcal{M}_{fi} = \bar{u}(p_2)O^\mu\epsilon_\mu u(p_1), \tag{4}$$

where $u(p_1)$ and $u(p_2)$ are the Dirac spinors for the initial and final nucleons, respectively. O^μ describes the current operator produced by the strongly interacting hadrons, and ϵ^μ the photon polarization vector.

The hadronic current can be expressed as

$$O^\mu = \sum_j B_j \mathcal{N}_j^\mu, \tag{5}$$

where the B_j are Lorentz invariant scalars that we call 'amplitude coefficients'. Because of the pseudoscalar nature of the π meson, the only Dirac matrices that enter in equation (5) are γ_5, $\gamma_5\gamma_\mu$, and $\gamma_5\gamma_\mu\gamma_\nu$. Taking into account the Dirac equations for the initial and final nucleons, both on shell,

$$\not{p}_1 u_1 = M u_1, \quad \not{p}_2 u_2 = M u_2,$$

and conservation of the four-momentum ($p_1 + k = p_2 + Q$), we can form eight covariant matrices. They are

$$\begin{aligned}
\mathcal{N}_1^\mu &= \gamma_5\gamma.k\gamma^\mu, & \mathcal{N}_5^\mu &= \gamma_5\gamma^\mu, \\
\mathcal{N}_2^\mu &= \gamma_5 p_1^\mu, & \mathcal{N}_6^\mu &= \gamma_5\gamma.k p_1^\mu, \\
\mathcal{N}_3^\mu &= \gamma_5 p_2^\mu, & \mathcal{N}_7^\mu &= \gamma_5\gamma.k p_2^\mu, \\
\mathcal{N}_4^\mu &= \gamma_5 k^\mu, & \mathcal{N}_8^\mu &= \gamma_5\gamma.k k^\mu.
\end{aligned} \tag{6}$$

Any other pseudoscalar can be reduced to a linear combination of the $\mathcal{N}_j^\mu$. Current conservation (gauge invariance) $k_\mu O^\mu = 0$, yields two conditions on the B_j. They are

$$\begin{aligned}
B_1 k^2 + p_1.k B_2 + p_2.k B_3 + k^2 B_4 &= 0, \\
B_5 + p_1.k B_6 + p_2.k B_7 + k^2 B_8 &= 0.
\end{aligned} \tag{7}$$

Solving for B_2 and B_5 and using the condition $\epsilon.k = 0$, the number of amplitude coefficients is reduced to four for the photoproduction, and the general amplitude becomes

$$i\mathcal{M}_{fi} = \bar{u}(p_2)\left\{ B_1\left(-\frac{1}{2}\gamma_\mu\gamma_\nu\right) + B_3\left(-\frac{p_{1\mu}p_{2\nu}}{p_1.k}\right) + B_6\gamma_\nu p_{1\mu} + B_7\gamma_\nu p_{2\mu} \right\} F^{\mu\nu} u(p_1), \tag{8}$$

where $F^{\mu\nu} = \epsilon^\mu k^\nu - \epsilon^\nu k^\mu$ is the electromagnetic field tensor. It is obvious that other forms of $i\mathcal{M}_{fi}$ can be obtained by eliminating a different set of the B_j.

2.3 C.G.L.N. and helicity amplitudes

The invariant amplitude $i\mathcal{M}_{fi}$ can be rewritten in terms of amplitudes corresponding to a definite parity and angular momentum state. The matrix elements appearing in equation (8) are first written in two-component form

$$i\mathcal{M}_{fi} = \frac{4\pi W}{M}\chi_f^\dagger F \chi_i, \tag{9}$$

where χ_i and χ_f are, respectively, the initial and final nucleon Pauli spinors. The amplitude F can be written in the familiar form [35]

$$F = i\vec{\sigma}.\vec{\epsilon}F_1 + \vec{\sigma}.\hat{p}_2\vec{\sigma}.(\hat{k}\times\vec{\epsilon})F_2 + i\vec{\sigma}.\hat{k}\hat{p}_2.\vec{\epsilon}F_3 + i\vec{\sigma}.\hat{p}_2\hat{p}_2.\vec{\epsilon}F_4. \tag{10}$$

The relations among the amplitudes F_j and B_j are derived by reducing equation (8) into two component spinors. In this way, we obtain

$$\begin{aligned}
F_1 &= \sqrt{E_2+M}\left\{ -B_1 k_0 \frac{W+M}{\sqrt{E_1+M}} - (B_6 p_1.k + B_7 p_2.k)\sqrt{E_1+M}\right\},\\
F_2 &= \frac{k_0\sqrt{E_2-M}}{\sqrt{E_1+M}}\left\{ (B_6 p_1.k + B_7 p_2.k) - B_1(W+M)\right\},\\
F_3 &= (B_3 - B_7(W+M))k_0\sqrt{E_2^2-M^2}\frac{\sqrt{E_2+M}}{\sqrt{E_1+M}},\\
F_4 &= (-B_3\sqrt{E_1+M} - B_7 k_0\frac{W+M}{\sqrt{E_1+M}})(M-E_2)\sqrt{E_2+M},
\end{aligned} \tag{11}$$

where F_1, F_2, F_3, F_4 are the well-known Chew-Goldberger-Low-Nambu (CGLN) amplitudes [36].

We complete this section by discussing the relation among the CGLN amplitudes and the helicity amplitudes. In the c.o.m. system, we quantize the initial and final spins along the directions of $\hat{k}$ and $\hat{Q}$. We choose the $z-$axis along the photon momentum, namely

$$\hat{k} = \frac{\vec{k}}{|\vec{k}|} = (0,0,1), \qquad \hat{Q} = \frac{\vec{Q}}{|\vec{Q}|} = (\sin\theta, 0, \cos\theta).$$

The spinors of the initial and final nucleons are respectively

$$\chi^i_{+\frac{1}{2}} = \begin{pmatrix} 1 \\ 0 \end{pmatrix}, \quad \chi^i_{-\frac{1}{2}} = \begin{pmatrix} 0 \\ 1 \end{pmatrix},$$

and

$$\chi^f_{+\frac{1}{2}} = \begin{pmatrix} \cos(\frac{\theta}{2}) \\ \sin(\frac{\theta}{2}) \end{pmatrix}, \quad \chi^f_{-\frac{1}{2}} = \begin{pmatrix} -\sin(\frac{\theta}{2}) \\ \cos(\frac{\theta}{2}) \end{pmatrix},$$

with

$$\vec{\sigma}.\hat{k}\chi^i_{\pm\frac{1}{2}} = \pm\chi^i_{\pm\frac{1}{2}},$$

and

$$\vec{\sigma}.\hat{Q}\chi^f_{\pm\frac{1}{2}} = \pm\chi^f_{\pm\frac{1}{2}}.$$

For the initial and final nucleons, spins up (respectively along $\hat{k}$ and $\hat{Q}$) correspond, in the c.o.m. frames, to negative helicities.

The photon polarization has two independent components. They are $\epsilon_\gamma(+1) = -\frac{1}{\sqrt{2}}(0, 1, i, 0)$ for positive helicity, and $\epsilon_\gamma(-1) = \frac{1}{\sqrt{2}}(0, 1, -i, 0)$ for negative helicity.

Using the relations above, equation (9) can be rewritten [37]

$$\begin{aligned} H_{\lambda_\gamma,\lambda_1,\lambda_2} = & - \frac{1}{\sqrt{2}}(\lambda_\gamma + 2\lambda_1)\left[\cos(\frac{\theta}{2})\delta_{\lambda_2,-\lambda_1} - 2\lambda_2\sin(\frac{\theta}{2})\delta_{-\lambda_2,-\lambda_1}\right](F_1 + 4\lambda_1\lambda_2 F_2) \\ & + \frac{1}{\sqrt{2}}\sin(\theta)\left[\cos(\frac{\theta}{2})\delta_{\lambda_2,\lambda_1} - 2\lambda_2\sin(\frac{\theta}{2})\delta_{-\lambda_2,\lambda_1}\right](2\lambda_1 F_3 + 2\lambda_2 F_4), \end{aligned}$$

where λ_γ, λ_1, λ_2 are, respectively, the helicities of the photon, target nucleon and recoil nucleon. The above amplitude represents $2 \times 2 \times 2 = 8$ complex numbers. However, by the virtue of parity invariance, there are four relations between these amplitudes and consequently, we have 4 independent amplitudes. They are [38]

$$\begin{aligned} H_{+1,-\frac{1}{2},-\frac{1}{2}} = H_1 = & - \frac{1}{\sqrt{2}}\sin(\theta)\cos(\frac{\theta}{2})(F_3 + F_4), \\ H_{+1,+\frac{1}{2},-\frac{1}{2}} = H_2 = & \sqrt{2}\cos(\frac{\theta}{2})[(F_2 - F_1) + \sin^2(\frac{\theta}{2})(F_3 - F_4)], \\ H_{+1,-\frac{1}{2},+\frac{1}{2}} = H_3 = & \frac{1}{\sqrt{2}}\sin(\theta)\sin(\frac{\theta}{2})(F_3 - F_4), \\ H_{+1,+\frac{1}{2},+\frac{1}{2}} = H_4 = & \sqrt{2}\sin(\frac{\theta}{2})[(F_1 + F_2) + \cos^2(\frac{\theta}{2})(F_3 + F_4)]. \end{aligned}$$

The other four are obtained through the relation

$$H_{\lambda_\gamma,\lambda_1,\lambda_2} = (-1)^{\lambda_\gamma+\lambda_1+\lambda_2} H_{-\lambda_\gamma,-\lambda_1,-\lambda_2}.$$

2.4 Cross section

The cross section of the process is

$$d\sigma = \frac{|\mathcal{M}_{fi}|^2}{4\sqrt{(p_1.k)^2 - M^2k^2}} d\phi_2(p_1+k, p_2+Q), \tag{12}$$

where the phase space $d\phi_2$ is given by

$$d\phi_2(p_1+k, p_2+Q) = (2\pi)^4\delta^4(p_1+k-p_2-Q)\frac{d^3p_2}{(2\pi)^3 2E_2}\frac{d^3Q}{(2\pi)^3 2w}.$$

Integrating over d^3Q, we find

$$d\phi_2 = \frac{d^3p_2}{(2\pi)^2 4E_2 w}\delta(W - E_2 - w),$$

or

$$d\phi_2 = \frac{|\vec{p_2}|^2 d\Omega_2 d|\vec{p_2}|}{(2\pi)^2 4E_2 w}\delta(W - \sqrt{M^2+|\vec{p_2}|^2} - \sqrt{m_\pi^2+|\vec{p_2}|^2}).$$

Now, we use the $\delta-$function property

$$\delta(f(x)) = \sum_i \frac{\delta(x-x_i)}{|f'(x_i)|},$$

where x_i are the zeroes of $f(x)$. In our case, $f(x) = W - \sqrt{M^2+|\vec{p_2}|^2} - \sqrt{m_\pi^2+|\vec{p_2}|^2}$ with the variable $x = |\vec{p_2}|$, the derivative of $f(x)$ is $f'(x) = -\frac{|\vec{p_2}|}{\sqrt{M^2+|\vec{p_2}|^2}} - \frac{|\vec{p_2}|}{\sqrt{m_\pi^2+|\vec{p_2}|^2}} = -\frac{|\vec{p_2}|}{E_2} - \frac{|\vec{p_2}|}{w} = -\frac{|\vec{p_2}|W}{E_2 w}$. Thus, the phase space becomes

$$d\phi_2 = \frac{|\vec{p_2}| d\Omega_2}{4(2\pi)^2 W},$$

and the cross section is

$$d\sigma = \frac{|\vec{p_2}||\mathcal{M}_{fi}|^2 d\Omega_2}{16(2\pi)^2 W(p_1.k)}.$$

Hence, integrating over the azimutal angle ϕ_2 of the recoil nucleon, averaging over the initial spin of the nucleon and initial photon polarization, and summing over the spin of the recoil nucleon, we obtain the expression

$$d\sigma = \frac{1}{2(2j+1)} \frac{|\vec{p_2}||\mathcal{M}_{fi}|^2 d\cos(\theta)}{32\pi W(p_1.k)}, \tag{13}$$

where j is the spin of the nucleon, and $|\vec{p_2}| = |\vec{Q}| = \frac{\sqrt{[W^2-(M+m_\pi)^2][W^2-(M-m_\pi)^2]}}{2W}$ is the magnitude of one of the outgoing 3-momenta written in the center of mass system.

Finally, the square of the amplitude $|\mathcal{M}_{fi}|^2$ in the cross section has the form

$$|\mathcal{M}_{fi}|^2 = \sum_{i,j=1,3,6,7} B_i B_j^* F_{ij},$$

where the sixteen quantities F_{ij} depend on scalar products and masses only. The F_{ij} are symmetric in i and j and the non-trivial ones are

$$\begin{aligned}
F_{11} = \quad & 16\left(\frac{s-M^2}{2}\right)\left(\frac{M^2-u}{2}\right), \\
F_{13} = \quad & 4\left[M^2\left(\frac{s-M^2}{2}\right) - 2\left(M^2-\frac{t}{2}\right)\left(\frac{M^2-u}{2}\right)\right. \\
& + \left. M^2\left(\frac{M^2-u}{2}\right)^2 / \left(\frac{s-M^2}{2}\right)\right], \\
F_{16} = \quad & 8M\left(\frac{s-M^2}{2}\right)\left[\left(\frac{s-M^2}{2}\right) + \left(\frac{M^2-u}{2}\right)\right], \\
F_{17} = \quad & 8M\left(\frac{M^2-u}{2}\right)\left[\left(\frac{s-M^2}{2}\right) + \left(\frac{M^2-u}{2}\right)\right], \\
F_{33} = \quad & 4M^4\left\{\left[\left(\frac{s-M^2}{2}\right)^2 + \left(\frac{M^2-u}{2}\right)^2\right] / \left(\frac{s-M^2}{2}\right)^2\right\} \\
& - 4\left(M^2-\frac{t}{2}\right)\left[M^2 - 2M^2\left(\frac{M^2-u}{2}\right) / \left(\frac{s-M^2}{2}\right)\right. \\
& + \left. 2\left(M^2-\frac{t}{2}\right)\left(\frac{M^2-u}{2}\right) / \left(\frac{s-M^2}{2}\right) - M^2\left(\frac{M^2-u}{2}\right)^2 / \left(\frac{s-M^2}{2}\right)^2\right], \\
F_{36} = \quad & 4M\left\{M^2\left(\frac{s-M^2}{2}\right) - 2\left(\frac{M^2-u}{2}\right)\left[\left(M^2-\frac{t}{2}\right)\right.\right. \\
& + \left.\left. M^2\left(\frac{M^2-u}{2}\right) / \left(\frac{s-M^2}{2}\right)\right]\right\},
\end{aligned}$$

$$
\begin{aligned}
F_{37} = \quad & 4M\left\{ M^2\left(\frac{s-M^2}{2}\right) - 2\left(\frac{M^2-u}{2}\right)\left[\left(M^2-\frac{t}{2}\right)\right.\right. \\
+ \quad & \left.\left. M^2\left(\frac{M^2-u}{2}\right)/\left(\frac{s-M^2}{2}\right)\right]\right\}, \\
F_{66} = \quad & 8\left(\frac{s-M^2}{2}\right)^2\left[M^2+\left(M^2-\frac{t}{2}\right)\right], \\
F_{67} = \quad & 4M^2\left[\left(\frac{s-M^2}{2}\right)+\left(\frac{M^2-u}{2}\right)\right]^2, \\
F_{77} = \quad & 8\left(\frac{M^2-u}{2}\right)^2\left[M^2+\left(M^2-\frac{t}{2}\right)\right],
\end{aligned}
$$

and the rest of the terms are obtained through the relation $F_{ij} = F^{\dagger}_{ji}$.

2.5 Polarization observables

When a polarization measurement is made, we obtain a number, or an observable, which is a sum or difference of bilinear products of helicity amplitudes, for instance. We can define sixteen polarization observables. However, since there are only four independent helicity amplitudes, these sixteen observables are not independent. Here, we use the usual Basel convention with the $z-$axis being the beam direction and the $y-$axis the normal to the $(x,z)-$reaction plane (this is the convention that we already chose at the beginning of this chapter, so previous results can be used in the following calculation). The $z'-$axis is in the direction of the scattered meson. $y' = y$ and $x' = y \times z'$.

To carry out the calculation of these observables, it is easier to rewrite equation (10) as

$$F = A + \vec{\sigma}.\vec{B}, \tag{14}$$

where $A = F_2(\hat{p}_2 \times \hat{k}).\vec{\epsilon}$ and $\vec{B} = i[F_1 - F_2(\hat{p}_2.\hat{k})]\vec{\epsilon} + i(F_3+F_4)(\hat{p}_2.\vec{\epsilon})\hat{k} + iF_4(\hat{p}_2.\vec{\epsilon})$. The square of the modulus of $\mathcal{M}$ is

$$|\mathcal{M}|^2 = (\frac{4\pi W}{M})^2 \chi_i^{\dagger} F^{\dagger} \chi_f \chi_f^{\dagger} F \chi_i, \tag{15}$$

with

$$\chi^{\dagger}_{i,f}\chi_{i,f} = \frac{1}{2}(1 + \vec{\sigma}.\vec{\lambda}_{i,f}), \tag{16}$$

and $\vec{\lambda_i} = \lambda_{ix}\vec{x} + \lambda_{iy}\vec{y} + \lambda_{iz}\vec{z}$ and $\vec{\lambda_f} = \lambda_{fx}\vec{x} + \lambda_{fy}\vec{y} + \lambda_{fz}\vec{z}$ are the polarization vectors of the initial and final nucleons, both expressed in the $(x, y, z)-$frame. Written in the $(x', y', z')-$frame, $\vec{\lambda_f}$ becomes $\vec{\lambda_f} = \lambda'_{fx}\vec{x'} + \lambda'_{fy}\vec{y'} + \lambda'_{fz}\vec{z'}$, where $\vec{x'} = \cos(\theta)\vec{x} - \sin(\theta)\vec{z}$, $\vec{y'} = \vec{y}$, and $\vec{z'} = \sin(\theta)\vec{x} + \cos(\theta)\vec{z}$.

As a result, $|\mathcal{M}|^2$ can be rewritten as the trace of the products of $\sigma-$matrices,

$$|\mathcal{M}|^2 = (\frac{4\pi W}{M})^2\frac{1}{4}Tr[(1 + \vec{\sigma}.\vec{\lambda_f})(A + \vec{\sigma}.\vec{B})(1 + \vec{\sigma}.\vec{\lambda_i})(A^{\dagger} + \vec{\sigma}.\vec{B}^{\dagger})]. \tag{17}$$

In expanding the equation (17), we use the relations,

$$\begin{aligned}
&Tr[\sigma_i] = 0,\\
&Tr[\sigma_i\sigma_j] = 2\delta_{ij},\\
&Tr[\sigma_i\sigma_j\sigma_k] = 2i\epsilon_{ijk},\\
&Tr[\sigma_i\sigma_j\sigma_k\sigma_l] = 2(\delta_{ij}\delta_{kl} + \delta_{il}\delta_{jk} - \delta_{ik}\delta_{jl}),
\end{aligned}$$

and

$$\begin{aligned}
(\vec{\epsilon}.\vec{X}_1)(\vec{\epsilon}^{*}.\vec{X}_2) = \quad & \frac{1}{2}\{\vec{X}_1.\vec{X}_2 - \frac{\vec{k}.\vec{X}_1\vec{k}.\vec{X}_2}{|\vec{k}|^2} - i\Lambda_c\frac{\vec{k}.(\vec{X}_1 \times \vec{X}_2)}{|\vec{k}|}\\
+ \quad & \Lambda_l(2\vec{u}.\vec{X}_1\vec{v}.\vec{X}_2 + \frac{\vec{k}.\vec{X}_1\vec{k}.\vec{X}_2}{|\vec{k}|^2} - \vec{X}_1.\vec{X}_2)\},
\end{aligned} \tag{18}$$

where Λ_c is the degree of circular polarization and Λ_l the degree of linear polarization. $\vec{u} = (\cos(\phi), \sin(\phi), 0)$, $\vec{v} = (-\sin(\phi), \cos(\phi), 0)$, where $\phi = (\vec{x}, \vec{u})$ is the linear polarization angle. Therefore, $|\mathcal{M}|^2$ can be rewritten in terms of the nucleon polarization vector coordinates λ_{ix},λ_{iy}, λ_{iz}, λ'_{fx}, λ'_{fy}, λ'_{fz}, and the beam polarization angle ϕ. Polarization observables are extracted from $|\mathcal{M}|^2$ as the coefficients of these coordinates or their products. These observables are given in table I. We note that observables from triple polarization [39] can also be defined and expressed in terms of the linear combination of the bilinear products $H_iH_j^{*}$.

However, since there are only sixteen bilinear products, we can obtain all of them from the sixteen observables already defined from single and double polarizations. Therefore, complete information can be obtained without measuring or defining a triple polarization.

The precise relation between observables and the experiments considered in table I is as follows. For polarized beam and polarized target, the differential cross section is

$$\begin{aligned}\frac{d\sigma}{dt} = & \left.\frac{d\sigma}{dt}\right|_{unpolarized} \Big\{ 1 - P_T\Sigma\cos(2\phi) + P_x\left[-P_T H\sin(2\phi) + P_o F\right] \\ & - P_y\left[-T + P_T P\cos(2\phi)\right] - P_z\left[-P_T G\sin(2\phi) + P_o E\right] \Big\}, \end{aligned} \tag{19}$$

where (P_x, P_y, P_z) is the polarization of the target, P_T is the transverse polarization of the beam at angle ϕ to the reaction plane, and P_O is the degree of right circular polarization of the beam.

For polarized beam and polarized recoil, the differential cross section is

$$\begin{aligned}\rho_f\frac{d\sigma}{dt} = & \left.\frac{d\sigma}{dt}\right|_{unpolarized} \Big\{ 1 + \sigma_y P - P_T\cos(2\phi)(\Sigma + \sigma_y T) \\ & - P_T\sin(2\phi)(O_x\sigma_x + O_z\sigma_z) - (P_o(C_x\sigma_x + C_z\sigma_z) \Big\} \end{aligned} \tag{20}$$

and for both polarized target and recoil, it is given by

$$\begin{aligned}\rho_f\frac{d\sigma}{dt} = & \left.\frac{d\sigma}{dt}\right|_{unpolarized} \Big\{ 1 + \sigma_y P + P_x(T_x\sigma_x + T_z\sigma_z) \\ & + P_y(T + \Sigma\sigma_y) - P_z(L_x\sigma - L_z\sigma_z) \Big\}, \end{aligned} \tag{21}$$

where $\rho_f = \frac{1}{2}(1 + \vec{\sigma}.\vec{P}_f)$ is the density matrix of the recoil nucleon, and P_f is its polarization.

TABLE I: Table of polarization observables for the single pion photoproduction process [38]; we show in the third column the experiments required to extract the physical observables given in the first column. In the $\{P_\gamma, P_T, P_R\}$ notation, $P_\gamma \equiv (L(\phi), c)$ is the polarization of the beam where $L(\phi)$ represents the beam linearly polarized at angle ϕ to the scattering plane, and c represents the circularly polarized beam. $P_T \equiv$ (x,y,z) gives the direction of the target polarization and $P_R \equiv$ (x',y',z') is that of the recoil nucleon polarization.

Symbol	Helicity representation	Experiment required
$d\sigma/dt$	$\|H_1\|^2 + \|H_2\|^2 + \|H_3\|^2 + \|H_4\|^2$	{-;-;-}
$\Sigma d\sigma/dt$	$2\mathrm{Re}(H_3 H_2^* - H_4 H_1^*)$	$\{L(\frac{\pi}{2}, 0)$;-;-}, {-;y;y}
$T d\sigma/dt$	$2\mathrm{Im}(H_3 H_4^* - H_2 H_1^*)$	$\{L(\frac{\pi}{2}, 0)$;-;y}, {-;y;-}
$P d\sigma/dt$	$2\mathrm{Im}(H_2 H_4^* - H_3 H_1^*)$	$\{L(\frac{\pi}{2}, 0)$;y;-}, {-;-;y}
$T_x d\sigma/dt$	$2\mathrm{Re}(H_3 H_2^* + H_4 H_1^*)$	{-;x;x'}
$T_z d\sigma/dt$	$2\mathrm{Re}(H_3 H_4^* - H_2 H_1^*)$	{-;x;z'}
$L_x d\sigma/dt$	$2\mathrm{Re}(H_2 H_4^* - H_3 H_1^*)$	{-;z;x'}
$L_z d\sigma/dt$	$\|H_2\|^2 + \|H_3\|^2 - \|H_1\|^2 - \|H_4\|^2$	{-;z;z'}
$G d\sigma/dt$	$-2\mathrm{Im}(H_3 H_2^* + H_4 H_1^*)$	$\{L(\pm\frac{\pi}{4}, 0)$;z;-}
$H d\sigma/dt$	$-2\mathrm{Im}(H_3 H_1^* + H_2 H_4^*)$	$\{L(\pm\frac{\pi}{4}, 0)$;x;-}
$F d\sigma/dt$	$2\mathrm{Re}(H_2 H_1^* + H_3 H_4^*)$	{c;x;-}
$E d\sigma/dt$	$\|H_2\|^2 - \|H_3\|^2 - \|H_1\|^2 + \|H_4\|^2$	{c;z;-}
$O_x d\sigma/dt$	$-2\mathrm{Im}(H_2 H_1^* + H_3 H_4^*)$	$\{L(\pm\frac{\pi}{4}, 0)$;-;x'}
$O_z d\sigma/dt$	$-2\mathrm{Im}(H_2 H_3^* + H_4 H_1^*)$	$\{L(\pm\frac{\pi}{4}, 0)$;-;z'}
$C_x d\sigma/dt$	$-2\mathrm{Re}(H_2 H_4^* + H_3 H_1^*)$	{c;-;x'}
$C_z d\sigma/dt$	$\|H_2\|^2 - \|H_3\|^2 + \|H_1\|^2 - \|H_4\|^2$	{c;-;z'}

Chapter 3

FORMALISM OF THE EFFECTIVE LAGRANGIAN

We use an effective Lagrangian approach [40, 41] at tree level to calculate the amplitude coefficients B_j defined in the previous chapter. In this approach, we treat all particles as essentially point-like; any structure in these particles will be accounted for by the introduction of appropriate form factors. Vertices corresponding to individual couplings of photons and pions to nucleons and resonances are established and 'Feynman' diagrams describing the given processes are drawn. For each of these diagrams, the contribution to each of the B_j is extracted, and the B_j are thus built from a number of such diagrams. We note that this calculation has been done previously with success around the Δ-energy region [40, 32, 33] and up to $E_\gamma = 1.0$ GeV [42].

Feynman diagrams for single pion photoproduction are shown in figure 1. Solid lines represent the ground state nucleons, thick solid lines are baryon resonances, wavy lines are photons, dashed lines are pions, and curly lines are vector mesons. Diagrams (a), (b), (c) and (d) are the Born terms. This means that the intermediate particles are ground state nucleons. Diagram (e) is the t-channel ρ or ω vector meson exchange term and diagrams (f) and (g) are the s- and u-channel nucleon resonance terms. In this work, $\Delta(1232)$, $N(1440)$, $N(1520)$ and the $N(1535)$ are included as resonant states.

Expressions for all Lagrangians are given below and the corresponding vertices along with the propagators are shown in a later section.

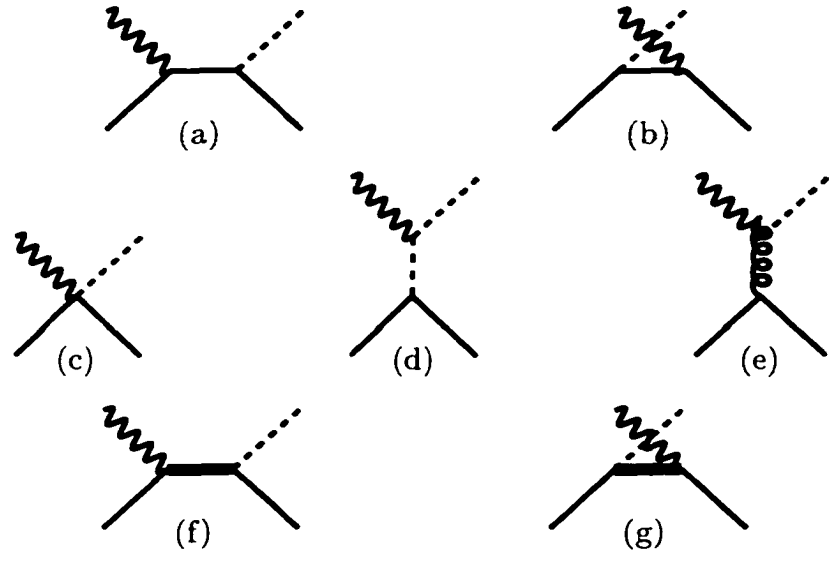

FIG. 1: Feynman diagrams for single pion photoproduction. Diagrams (a) and (b) are the direct s-channel and the crossed u-channel nucleon Born terms. Diagram (c) represents the equivalence breaking term and diagram (d) corresponds to the pion exchange term. Solid lines represent nucleons, dashed lines are pions and wavy lines are photons. Diagram (e) is the t-channel ρ or ω vector meson exchange term (curly lines). Diagrams (f) and (g) are the s- and u-channel nucleon resonance terms. Thick solid lines are nucleon resonances. In this work, the nucleon resonances are the $\Delta(1232)$, $N(1440)$, $N(1520)$ and $N(1535)$.

3.1 Born terms

The Lagrangians for the vertex interactions for the Born terms shown in figure 1 are

$$\begin{aligned}
\mathcal{L}_{NN\gamma} &= \bar{N}\left(-\frac{e}{2}(1+\tau_3)\gamma_\mu A^\mu + \frac{e}{4M}(k_s+\tau_3 k_v)\gamma_\mu\gamma_\nu F^{\mu\nu}\right)N + H.c.,\\
\mathcal{L}_{NN\pi} &= \bar{N}\frac{f_{\pi NN}}{m_\pi}\gamma_5\gamma_\mu\tau_j(\partial^\mu\phi_j)N + H.c.,\\
\mathcal{L}_{NN\gamma\pi} &= \bar{N}\gamma_5\frac{f_{\pi NN}}{m_\pi}\tau_i\epsilon_{ij3}\gamma_\mu A^\mu\phi_j N + H.c.,\\
\mathcal{L}_{\gamma\pi\pi} &= e\epsilon_{i3j}\phi_i\partial_\mu\phi_j A^\mu + H.c., \qquad (22)
\end{aligned}$$

where $F^{\nu\lambda} = \partial^\nu A^\lambda - \partial^\lambda A^\nu$ is the electromagnetic field strength tensor. N is a generic notation for the nucleon and ϕ for the pion. k_s and k_v are the isoscalar and isovector anomalous magnetic moments for the nucleons. They are respectively $k_s = \frac{1}{2}(k_p + k_n)$ and $k_v = \frac{1}{2}(k_p - k_n)$, where $k_p = 1.79$ nuclear magnetons (nm) and $k_n = -1.91$ nm. $f_{\pi NN}$ is the coupling constant for the πNN coupling and τ_i the isospin operator for $I = \frac{1}{2}$.

We note that the Lagrangian $\mathcal{L}_{NN\gamma\pi}$ exists only if a charged pion (π^+, π^-) is present. This term arises from minimal substitution in the $NN\pi$ vertex. However, it may also come from chiral transformation in the $NN\gamma$ vertex.

3.2 Vector meson couplings

The vertices involving the ρ or the ω-meson are described by the Lagrangians

$$\begin{aligned}
\mathcal{L}_{V\pi\gamma} &= \frac{g_{V\pi\gamma}}{m_\pi}\epsilon^{\alpha\beta\mu\nu}(A_\gamma)_\beta(\partial_\mu(A_V)_\alpha)(\partial_\nu\phi_\pi) + H.c.,\\
\mathcal{L}_{VNN} &= \bar{N}I_{j1}\left\{-G_v^{(V)}\gamma^\mu(A^*{}_{Vj1})_\mu + \frac{G_t^{(V)}}{2M}\gamma^\mu\gamma^\nu\partial_\mu(A^*{}_{Vj1})_\nu\right\}N + H.c., \qquad (23)
\end{aligned}$$

where ϕ presents a pion field, N is the nucleon field and V is a generic notation for the vector meson. I_{j1} is τ_j for the ρ-meson and 1 for the ω-meson and A_{Vj1}

is A_{V3} for ρ-meson and A_{V1} for the ω-meson. $g_{V\pi\gamma}$, $G_v^{(V)}$ and $G_t^{(V)}$ are coupling constants and $\epsilon^{\mu\nu\alpha\beta}$ is the fourth rank pseudo-tensor defined by

$$\begin{cases} \pm 1 & \text{for } \mu = 0, \nu = 1, \alpha = 2, \beta = 3 \text{ and any even/odd permutation} \\ 0 & \text{if any two indices are equal.} \end{cases}$$

In this calculation, we use the standard values [43, 44] of $G_v^{(\rho)}$ and $G_t^{(\rho)}$ such that $G_v^{(\rho)} = 2.66$ and $G_t^{(\rho)} = G_v^{(\rho)} K_\rho$, where $K_\rho = 3.71$. For the ω meson, the standard values are given by $G_v^{(\omega)} = 3G_v^{(\rho)}$ and $G_t^{(\omega)} = G_v^{(\omega)} K_\omega$, where $K_\omega = -0.12$. However, we note that the coupling constant $G_v^{(\omega)}$ is not precisely determined in magnitude. Most authors [45] agree on a value around 8, while others [46] take a value twice as large. For this reason, we fit the values of $G_v^{(\omega)}$ and $G_t^{(\omega)}$ in this calculation.

3.3 Spin-$\frac{1}{2}$ resonance couplings

The Lagrangians for the $N^*N\gamma$ and $N^*N\pi$ couplings are similar to those of the $NN\gamma$ and $NN\pi$ couplings found in the Born terms except that for the $N^*N\gamma$, the first term (with $\gamma_\mu A^\mu$) is absent because its presence violates gauge invariance. However, it would be present for virtual photons. These Lagrangians are

$$\begin{aligned} \mathcal{L}_{N^*N\gamma} &= \bar{N}^* \frac{e}{2(M_{N^*} + M)} I_5 (k_s^R + \tau_3 k_v^R) \gamma_\mu \gamma_\nu F^{\mu\nu} N + H.c., \\ \mathcal{L}_{N^*N\pi} &= \bar{N}^* \frac{f_{N^*N\pi}}{m_\pi} I_5 \tau_j \gamma_\mu N (\partial^\mu \phi_j) + H.c., \end{aligned} \tag{24}$$

where N^* represents the spinor of the spin-$\frac{1}{2}$ resonance, N the nucleon field and ϕ the pion field. The operator I_5 is either 1 or γ_5 depending on the parity of the resonance. M_{N^*} is the mass of the resonance and M the mass of the nucleon. k_s^R and k_v^R are such that $k_p^R = k_s^R + k_v^R$ and $k_n^R = k_s^R - k_v^R$ where k_p^R and k_n^R are respectively the transition magnetic couplings for proton and neutron targets. We note that these expressions for k_p^R and k_n^R are for the isospin-$\frac{1}{2}$ resonance only. In our calculation, we do not include spin-$\frac{1}{2}$ resonance with isospin $I = \frac{3}{2}$.

3.4 Spin-$\frac{3}{2}$ resonance couplings

The spin-$\frac{3}{2}$ resonant states involved in this energy range ($W = 1.1 - 1.6$ GeV) are the $\Delta(1232)$ and the isospin-$\frac{1}{2}$ $N^*(1520)$ resonances. The effective Lagrangians for the $RN\pi$ and $RN\gamma$ interactions, where R represents the nucleon resonance, are

$$\begin{aligned}
\mathcal{L}_{RN\pi} &= \bar{R}^\mu \frac{f_{RN\pi}}{m_\pi} I_5 I_j \Theta_{\mu\nu}(Z) N(\partial^\nu \phi_j) + H.c., \\
\mathcal{L}^1_{RN\gamma} &= \bar{R}^\mu I_5 T_{1R} \Theta_{\mu\nu}(Y) \gamma_\lambda N F^{\nu\lambda} + H.c., \\
\mathcal{L}^2_{RN\gamma} &= \bar{R}^\mu I_5 T_{2R} \Theta_{\mu\nu}(X) (\partial_\lambda N) F^{\nu\lambda} + H.c.,
\end{aligned} \tag{25}$$

where the operator I_5 is again either 1 or γ_5 and I_j is either τ_j or T_j. R^μ is the vector spinor of the resonance, N the nucleon field and ϕ the pion field.

$\Theta_{\mu\nu}(V)$ is given by $\Theta_{\mu\nu}(V) = g_{\mu\nu} + [\frac{1}{2}(1 + 4V)A_0 + V]\gamma_\mu\gamma_\nu$ where A_0 is an arbitrary parameter defining the so-called 'point transformation' (see appendix D). The interaction Lagrangians given in equation (25) have been constructed in such a way that they are invariant under the same point transformation as the free one. This guarantees that the parameter A_0 that appears in $\Theta_{\mu\nu}(V)$ does not appear in any physical observables. The arbitrary parameters X, Y and Z are called 'off-shell' parameters. Many theoretical attempts have been made to fix these arbitrary parameters but none have been successful [47, 48, 49]. In fact, we choose $A_0 = -1$ and $V = -\frac{1}{2}$ or $A_0 = 0$ and $V = 0$ so that the off-shell terms do not contribute. It has also been proposed that the second coupling in the $\Delta N\gamma$ interaction could be set zero [40, 50] and a particular choice of values of the parameters Z and Y is required. The choice is $Z = \frac{1}{2}$, $Y = 0$ and $T_{2R} = 0$. However, Davidson *et al.* [51] showed that with the constraint $T_{2R} = 0$, the behavior of the electromagnetic amplitudes is not consistent with the experimental data for the transition. We show in appendix G the behavior of the helicity amplitudes of the $\Delta N\gamma$ interaction as $T_{2R} = 0$.

In all these couplings, we have to take into account the isoscalar/isovector nature of the photon ($I = 0$ or $I = 1$). This is done in the case of $I = \frac{1}{2}$

resonances by using $T_{1R} = (k_s^{R(1)} + \tau_3 k_v^{R(1)})$ and $T_{2R} = (k_s^{R(2)} + \tau_3 k_v^{R(2)})$. Note that $I = \frac{3}{2}$ resonances only couple to γN through the isovector component of the photon and therefore have the same coupling constants $T_3 k_v^{R(1)}$ and $T_3 k_v^{R(2)}$ for the γp and γn couplings. Here, τ_3 is the isospin operator for $I = \frac{1}{2}$ and T_3 is the $I = \frac{1}{2}$ to $I = \frac{3}{2}$ operator.

3.5 Vertices and coupling constants

The vertices corresponding to the previous Lagrangians are given below.

$$\mathcal{M}_{\gamma NN} = \bar{u}(p_f)(-e\frac{1+\tau_3}{2} \not{\epsilon} + e\frac{k_s+\tau_3 k_v}{4M}\gamma_\mu\gamma_\nu F^{\mu\nu})u(p_i),$$

$$\mathcal{M}_{\pi NN} = \bar{u}(p_f)\frac{f_{\pi NN}}{m_\pi}\tau_j\gamma_5 \not{Q}_j u(p_i),$$

$$\mathcal{M}_{\gamma\pi\pi} = -2q_\pi\epsilon.Q,$$

$$\mathcal{M}_{\pi\gamma NN} = \bar{u}(p_f)\frac{f_{\pi NN}}{m_\pi}\tau_i\epsilon_{ij3}\gamma_5 \not{\epsilon}_j u(p_i),$$

$$\mathcal{M}_{\gamma N^\star N} = \bar{u}(p_f)T_2^\star I_5\gamma_\mu\gamma_\nu F^{\mu\nu}u(p_i),$$

$$\mathcal{M}_{\pi N^\star N} = \bar{u}(p_f)\frac{f_{\pi N^\star N}}{m_\pi}\tau_j I_5 \not{Q}_j u(p_i),$$

$$\mathcal{M}_{\pi N^o N} = \bar{u}(p_f)I_5\frac{f_{\pi N^o N}}{m_\pi}T_j\Theta_{\mu\nu}(Z)Q_j^\nu u^\mu(p_i),$$

$$\mathcal{M}^1_{\gamma N^o N} = \bar{u}^\mu(p_f)I_5 T_1\Theta_{\mu\nu}(Y)\gamma_\lambda F^{\lambda\nu}u(p_i),$$

$$\mathcal{M}^2_{\gamma N^o N} = \bar{u}^\mu(p_f)I_5 T_2\Theta_{\mu\nu}(X)p_{N\lambda}F^{\nu\lambda}u(p_i),$$

$$\mathcal{M}_{V\pi\gamma} = \frac{g_{V\pi\gamma}}{m_\pi}\epsilon^{\alpha\beta\mu\nu}(\epsilon_V)_\alpha\epsilon_\beta(Q_V)_\mu(Q_\pi)_\nu,$$

$$\mathcal{M}_{VNN} = \bar{u}(p_f)I_{j1}(-G_v^{(V)}\gamma^\mu\epsilon^\star_{1\mu} + \frac{G_t^{(V)}}{2M}\gamma^\mu\epsilon^\star_{1\mu} \not{Q}_j)u(p_i).$$

In these expressions, $N^\star$ denotes either the $N(1440)\frac{1}{2}^+$ or the $N(1535)\frac{1}{2}^-$, N^o the $\Delta(1232)\frac{3}{2}^+$ or the $N(1520)\frac{3}{2}^-$, V denotes a vector meson ρ or ω and Q_v represents

its momentum. ϵ_j^μ is the photon polarization where the isospin index 'j' arises from the index 'j' in the term $A^\mu\phi_j$. τ_j is the isospin operator for $I = \frac{1}{2}$ and T_j are the $I = \frac{1}{2}$ to $I = \frac{3}{2}$ operators.

In reproducing the cross sections and other observables, we fit our theoretical calculation to the experimental data and extract some parameters. We employ a CERN fitting routine, MINUIT, to minimize the weighted least-square function χ^2

$$\chi^2 = \sum_{i=1}^{N} \frac{[x_i - f_i(a_1, a_2, ..., a_n)]^2}{\sigma_{x_i}^2}, \tag{26}$$

where N is the number of experimental data points, x_i represent the experimental observables which are the total cross sections, the differential cross sections, and the polarizations in our case, $f_i(a_1, a_2, ..., a_n)$ are the theoretical predictions with a_i being the parameters of the theory, and the σ_{x_i} the standard deviations of the observables. These parameters are the πN and photo-coupling constants of the resonances as well as the two ωNN coupling constants. In this work, there are sixteen such coupling constants. They are $f_{\pi\Delta N}$, $f_{\pi N_{1440}N}$, $f_{\pi N_{1520}N}$, $f_{\pi N_{1535}N}$, $T_1(\Delta \to \gamma N)$, $T_2(\Delta \to \gamma N)$, $T_2^*(N(1440) \to \gamma p)$, $T_2^*(N(1440) \to \gamma n)$, $T_1(N(1520) \to \gamma p)$, $T_2(N(1520) \to \gamma p)$, $T_1(N(1520) \to \gamma n)$, $T_2(N(1520) \to \gamma n)$, $T_2^*(N(1535) \to \gamma p)$, $T_2^*(N(1535) \to \gamma n)$, $G_v^{(\omega)}$ and $G_t^{(\omega)}$.

3.6 Results and discussion

We remark the particular behavior of the Born terms in the $\gamma p \to \pi^+ n$ process which quickly increase at threshold and remain almost constant at higher energies. This is mainly due to the contribution of the s-channel in the Born term and the absence of the γnn charge coupling in the u-channel. We also note the peak at about $W = 1.230$ GeV which is dominated by the s-channel excitation of the Δ particle. In addition, the $N^*(1520)$ and $N^*(1535)$ resonances are found to be important. On the other hand, the $N^*(1440)$ contribution is relatively small for both channels and may not have a significant effect on the observables.

This is somewhat suspicious as its photocouplings and couplings to πN are both reported to be large. Recently, there have been some speculation [52] that the $N^*(1440)$ might be a candidate for the lightest hybrid state, consisting of three valence quarks and one valence gluon. A precise determination of the $N^*(1440)$ photocoupling can provide a powerful tool to distinguish between different internal structures for this hadron.

In figure 2, we show the total cross sections of the $\gamma p \to n\pi^+$ and $\gamma p \to p\pi^0$ processes *vs.* total energy. The fits are obtained by simultaneously fitting the experimental data sets with our theoretical calculation. Parameters extracted from the fit are given in the tables II and III. The value of χ^2 per degree of freedom in this fit is $\chi^2_{DOF} = 2.35$. χ^2_{DOF} is expected to rise as we put more data sets, especially if they come from different sources.

In figures 3-10, we compare our theoretical calculation with measured values of the total cross sections σ, differential cross sections $d\sigma/d\Omega$, photon asymmetry (Σ) and target asymmetry (T) at various angles and for total energies from threshold to 1.6 GeV, for the reactions $\gamma p \to n\pi^+$ and $\gamma p \to p\pi^0$. Note that these fits are obtained by simultaneouly fitting our theoretical calculation to all the data sets. The extracted parameters, total decay widths and helicity amplitudes are shown respectively in tables IV, V, VI and VII. We remark that there is a good agreement between the P.D.G. values and our fit values for the πN couplings to the resonances. However, discrepancies are observed between the P.D.G. values and the fit values for the photocoupling constants to the resonances. We assume that more experimental data sets should be included in the fit to place more constraints on these parameters. However, we recall that the goal of this calculation is to test the model of the 'Effective Lagragian', not to extract parameters. We, therefore limit our number of data sets to a few. The experimental data sets are taken from various sources. However, some data sets may be inconsistent with each other. An inclusion of inconsistent data sets may increase the χ^2 dramatically. Since we do not know and we do not assume which data sets are inconsistent, then we treat all sets on equal footing and give equal weight to all χ^2_i's. We hope the discrepancies amongst the data sets can be resolved by future experimental

research at emerging facilities such as TJNAF.

Contributions from individual resonances are also shown in the figures. For π^+ production, the agreement with the data is generally good for the total cross sections and differential cross sections in the entire energy region under consideration. For the production of neutral pions, our results are also in good agreement with the data through the first resonance region (the Δ-region), but start to deviate from the data at higher energies. We particularly note the discrepancy observed at higher energy for the total cross section (figure 4) of the $\gamma p \rightarrow p\pi^0$ process. This problem may be the result of the truncated set of resonances used in this calculation and a better fit may be obtained by including more resonances such as the $\Delta(1600)$, $N(1620)$ and $N(1650)$. We also remark the strange behavior of the differential cross sections corresponding to $\theta = 120^o$ and $\theta = 130^o$(figure 6) at higher energy for the same process. This may be improved by fitting more data points or including more resonances as we previously stated.

For the polarization observables in both processes, they are reasonably well behaved through the Δ-region, but discrepancies are observed as the energy increases. Again, inclusion of higher resonances may improve our results.

TABLE II: Table of parameters for the single pion photoproduction process. The second column shows parameters that are derived from PDG. The parameters in the third column are obtained by fitting both total cross sections of the $\gamma p \to \pi^+ n$ and $\gamma p \to \pi^0 p$ processes. $\chi^2 = 141$ and the number of points is N=76. These correspond to $\chi^2_{DOF} = 2.35$.

Parameters	P.D.G. values	Fit values
$f_{\pi\Delta N}$	2.16 ± 0.06	2.11
$f_{\pi N_{1440} N}$	0.64 ± 0.09	0.69
$f_{\pi N_{1520} N}$	2.73 ± 0.27	2.36
$f_{\pi N_{1535} N}$	0.29 ± 0.09	0.07
T_1 for $\Delta\gamma N$	0.688 ± 0.022	0.656
T_2 for $\Delta\gamma N$	-0.305 ± 0.047	-0.556
$T_2^\star$ for $N(1440)\gamma p$	$\pm 0.0407 \pm 0.0025$	0.0164
$T_2^\star$ for $N(1440)\gamma n$	$\pm 0.0250 \pm 0.0063$	0.0204
T_1 for $N(1520)\gamma p$	0.620 ± 0.062	0.459
T_2 for $N(1520)\gamma p$	0.350 ± 0.045	0.239
T_1 for $N(1520)\gamma n$	-0.110 ± 0.014	0.1473
T_2 for $N(1520)\gamma n$	0.039 ± 0.021	1.5299
$T_2^\star$ for $N(1535)\gamma p$	$\pm 0.0394 \pm 0.0072$	-0.0024
$T_2^\star$ for $N(1535)\gamma n$	$\pm 0.0259 \pm 0.0165$	4.4932

TABLE III: Table of parameters for the single pion photoproduction process. The second column shows the standard values for $G_v^{(\omega)}$ and $G_t^{(\omega)}$ [45]. The parameters in the third column are obtained by fitting both total cross sections of the $\gamma p \to \pi^+ n$ and $\gamma p \to \pi^0 p$ processes. $\chi^2 = 141$ and the number of points is N=76. These correspond to $\chi^2_{DOF} = 2.35$.

Parameters	Standard values	Fit values
$G_v^{(\omega)}$ for $NN\omega$	7.98	0.494
$G_t^{(\omega)}$ for $NN\omega$	-0.95	-0.813

TABLE IV: Table of parameters for the single pion photoproduction process. The second column gives parameters that are derived from PDG. The parameters in the third column are derived by simultaneously fitting the total cross sections of $\gamma p \rightarrow \pi^+ n$ and $\gamma p \rightarrow \pi^0 p$ with their differential cross sections, their polarized photon asymmetries Σ and their polarized target asymmetries T to some experimental data sets. $\chi^2 = 4013$ and the number of points is N=529. These give $\chi^2_{DOF} = 7.82$

.

Parameters	P.D.G. values	Fit values
$f_{\pi\Delta N}$	2.16 ± 0.06	2.17
$f_{\pi N_{1440} N}$	0.64 ± 0.09	0.72
$f_{\pi N_{1520} N}$	2.73 ± 0.27	2.99
$f_{\pi N_{1535} N}$	0.29 ± 0.09	0.27
T_1 for $\Delta\gamma N$	0.668 ± 0.022	0.664
T_2 for $\Delta\gamma N$	-0.305 ± 0.047	-0.499
$T_2^\star$ for $N(1440)\gamma p$	$\pm 0.0407 \pm 0.0025$	-0.0061
$T_2^\star$ for $N(1440)\gamma n$	$\pm 0.0250 \pm 0.0063$	0.0234
T_1 for $N(1520)\gamma p$	0.620 ± 0.062	0.743
T_2 for $N(1520)\gamma p$	0.350 ± 0.045	0.455
T_1 for $N(1520)\gamma n$	-0.110 ± 0.014	1.038
T_2 for $N(1520)\gamma n$	0.039 ± 0.021	1.659
$T_2^\star$ for $N(1535)\gamma p$	$\pm 0.0394 \pm 0.0072$	-0.068
$T_2^\star$ for $N(1535)\gamma n$	$\pm 0.0259 \pm 0.0165$	0.510

TABLE V: Table of parameters for the single pion photoproduction process. The second column are the standard values of $G_v^{(\omega)}$ and $G_t^{(\omega)}$. The parameters in the third column are derived by simultaneously fitting the total cross sections of $\gamma p \rightarrow \pi^+ n$ and $\gamma p \rightarrow \pi^0 p$ with their differential cross sections, their polarized photon asymmetries Σ and their polarized target asymmetries T to some experimental data sets. $\chi^2 = 4013$ and the number of points is N=529. These give $\chi^2_{DOF} = 7.82$

.

Parameters	Standard values	Fit values
$G_v^{(\omega)}$ for $NN\omega$	7.98	0.512
$G_t^{(\omega)}$ for $NN\omega$	-0.95	-0.792

TABLE VI: Table of decay widths; the second column corresponds to the total decay widths listed in P.D.G. The values in the third column are calculated from the fitted parameters in table VI.

widths	P.D.G. values (GeV)	Fit values
Γ_{Δ}	0.120 ± 0.005	0.118
$\Gamma_{N_{1440}}$	0.350 ± 0.100	0.422
$\Gamma_{N_{1520}}$	0.122 ± 0.012	0.128
$\Gamma_{N_{1535}}$	0.175 ± 0.075	0.131

TABLE VII: Table of helicity amplitudes; we show in the second column the helicity amplitudes given in PDG. The third column shows our calculated helicity amplitudes obtained from the fit.

Helicity amplitudes	P.D.G. values ($\text{GeV}^{-\frac{1}{2}}$)	Fit values
$H_{\frac{1}{2}}, \Delta(1232) \rightarrow \gamma N$	-0.140 ± 0.005	-0.139
$H_{\frac{3}{2}}, \Delta(1232) \rightarrow \gamma N$	-0.258 ± 0.006	-0.247
$H_{\frac{1}{2}}, N(1440) \rightarrow \gamma p$	-0.065 ± 0.004	-0.0097
$H_{\frac{1}{2}}, N(1440) \rightarrow \gamma n$	0.040 ± 0.010	0.0373
$H_{\frac{1}{2}}, N(1520) \rightarrow \gamma p$	-0.024 ± 0.009	-0.051
$H_{\frac{3}{2}}, N(1520) \rightarrow \gamma p$	0.166 ± 0.005	0.160
$H_{\frac{1}{2}}, N(1520) \rightarrow \gamma n$	-0.059 ± 0.009	-0.705
$H_{\frac{3}{2}}, N(1520) \rightarrow \gamma n$	-0.139 ± 0.011	-0.874
$H_{\frac{1}{2}}, N(1535) \rightarrow \gamma p$	0.090 ± 0.012	-0.105
$H_{\frac{1}{2}}, N(1535) \rightarrow \gamma n$	-0.046 ± 0.027	0.755

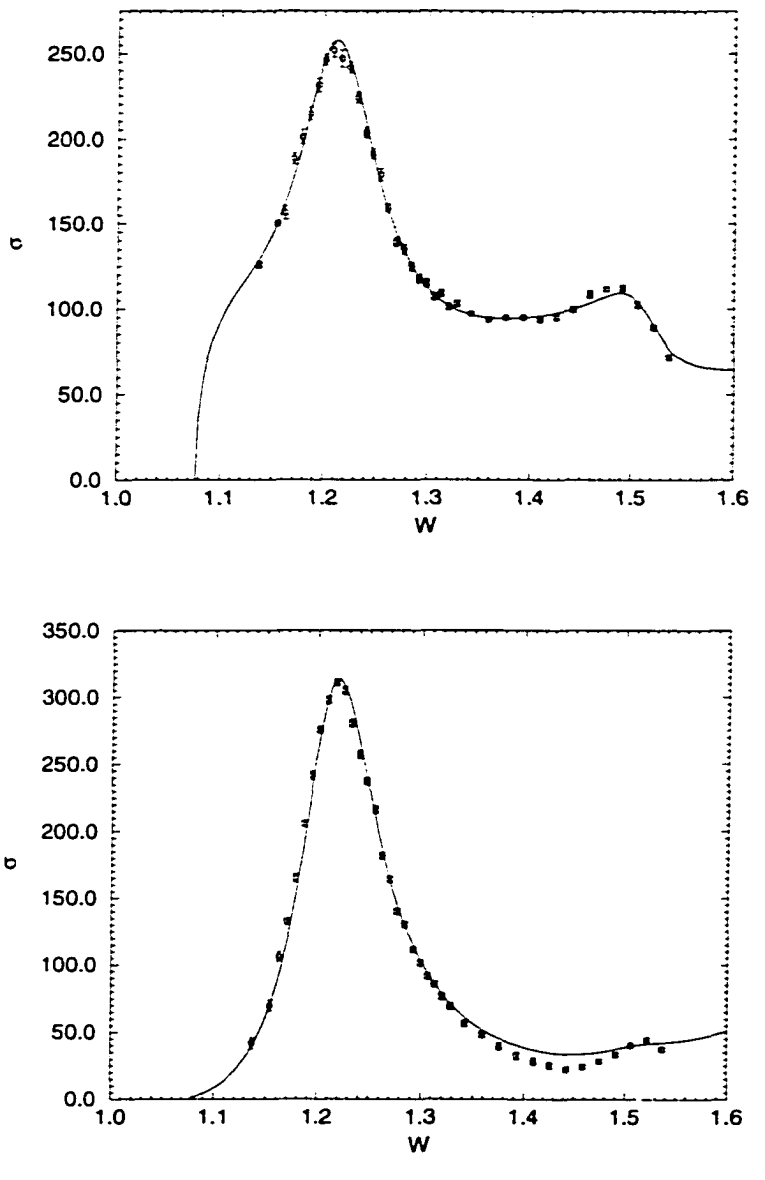

FIG. 2: Total cross sections (μb) of $\gamma p \to \pi^+ n$ and $\gamma p \to \pi^0 p$ *vs.* total energy W(GeV). These plots are obtained by simultaneously fitting both processes. Data points are from FU76TOKY.

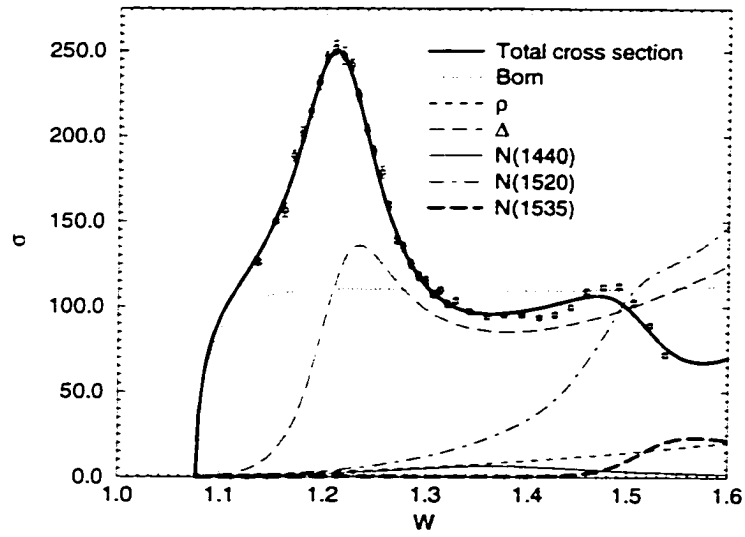

FIG. 3: Total cross section (μb) of $\gamma p \to \pi^+ n$ *vs.* total energy W(GeV). Data points are from FU76TOKY.

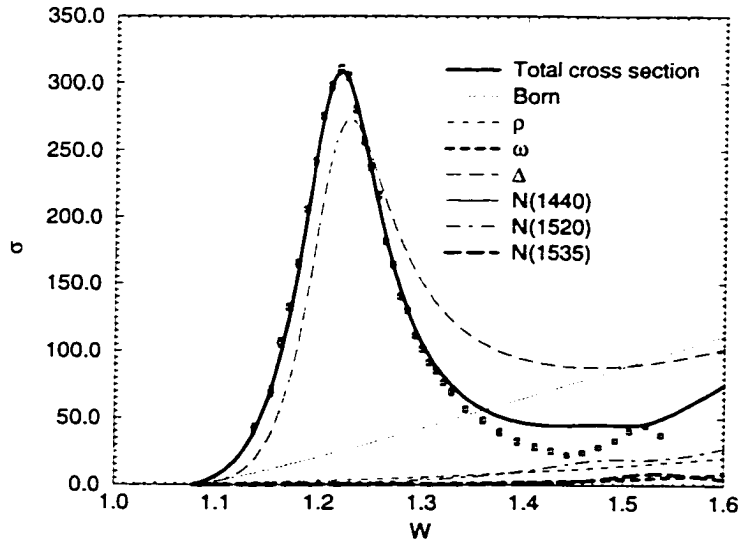

FIG. 4: Total cross section (μb) of $\gamma p \to \pi^0 p$ *vs.* total energy W(GeV). Data points are from FU76TOKY.

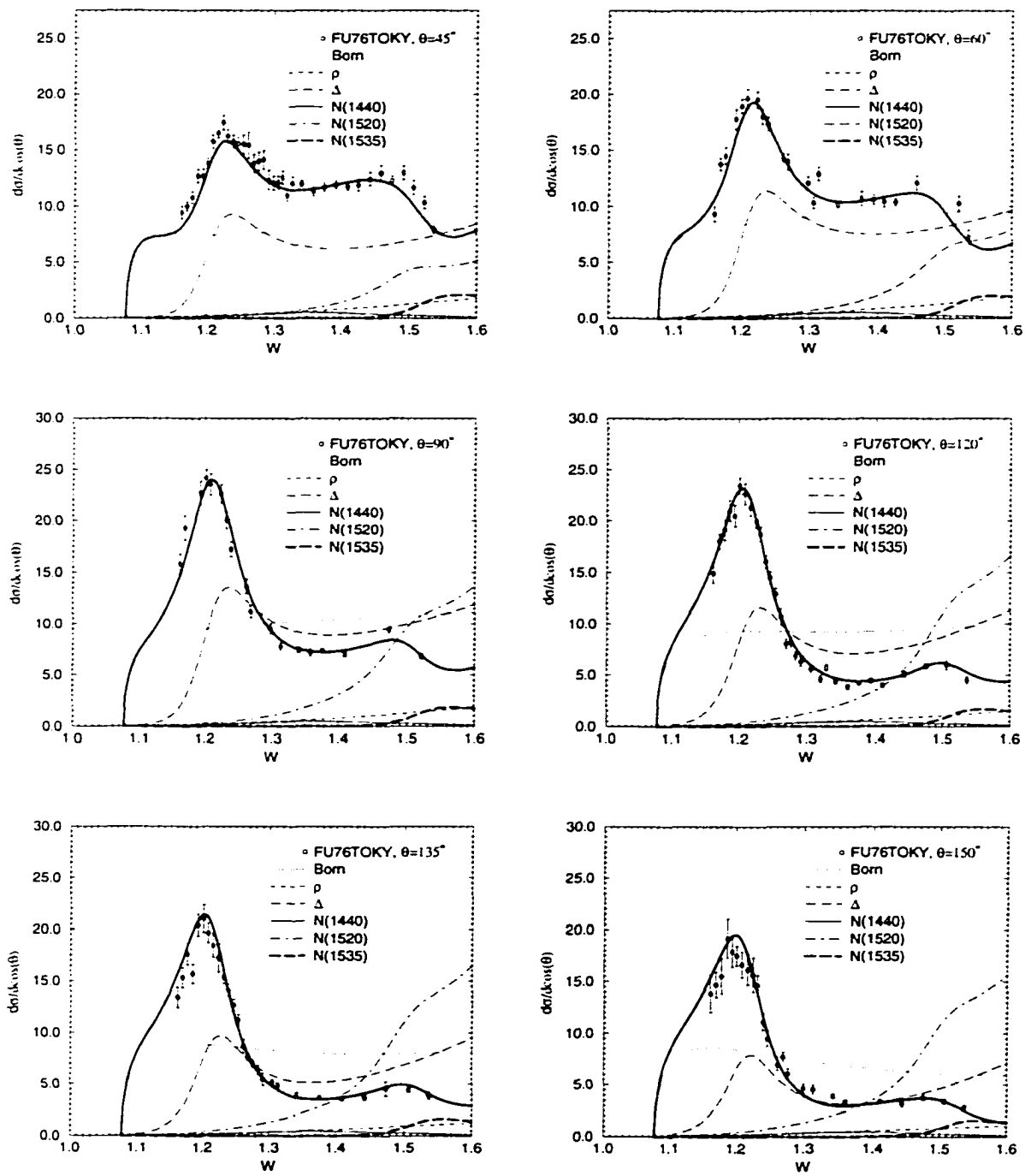

FIG. 5: Differential cross section (μb) of $\gamma p \to \pi^+ n$ *vs.* total energy W(GeV).

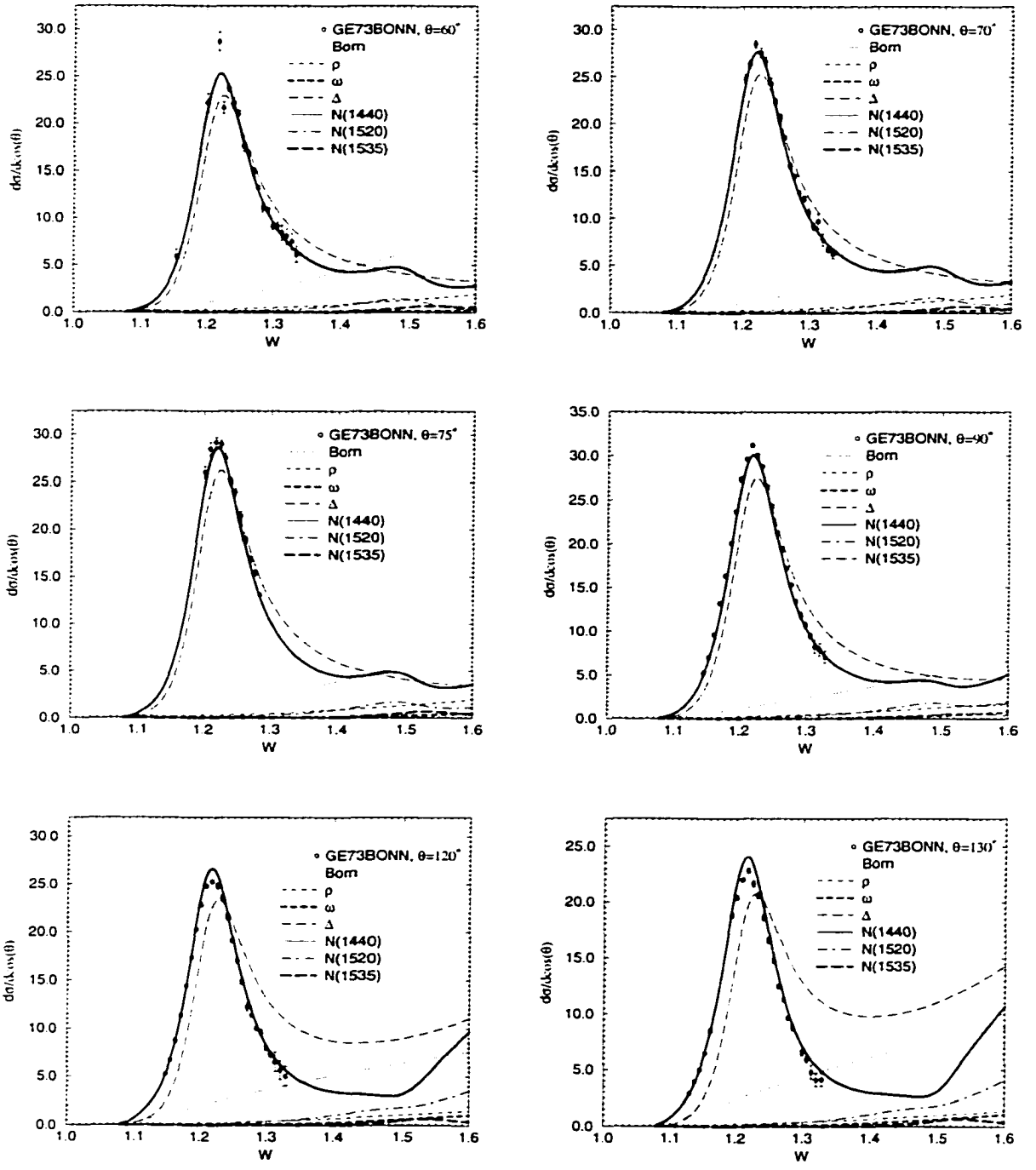

FIG. 6: Differential cross section (μb) of $\gamma p \to \pi^0 p$ *vs.* total energy W(GeV).

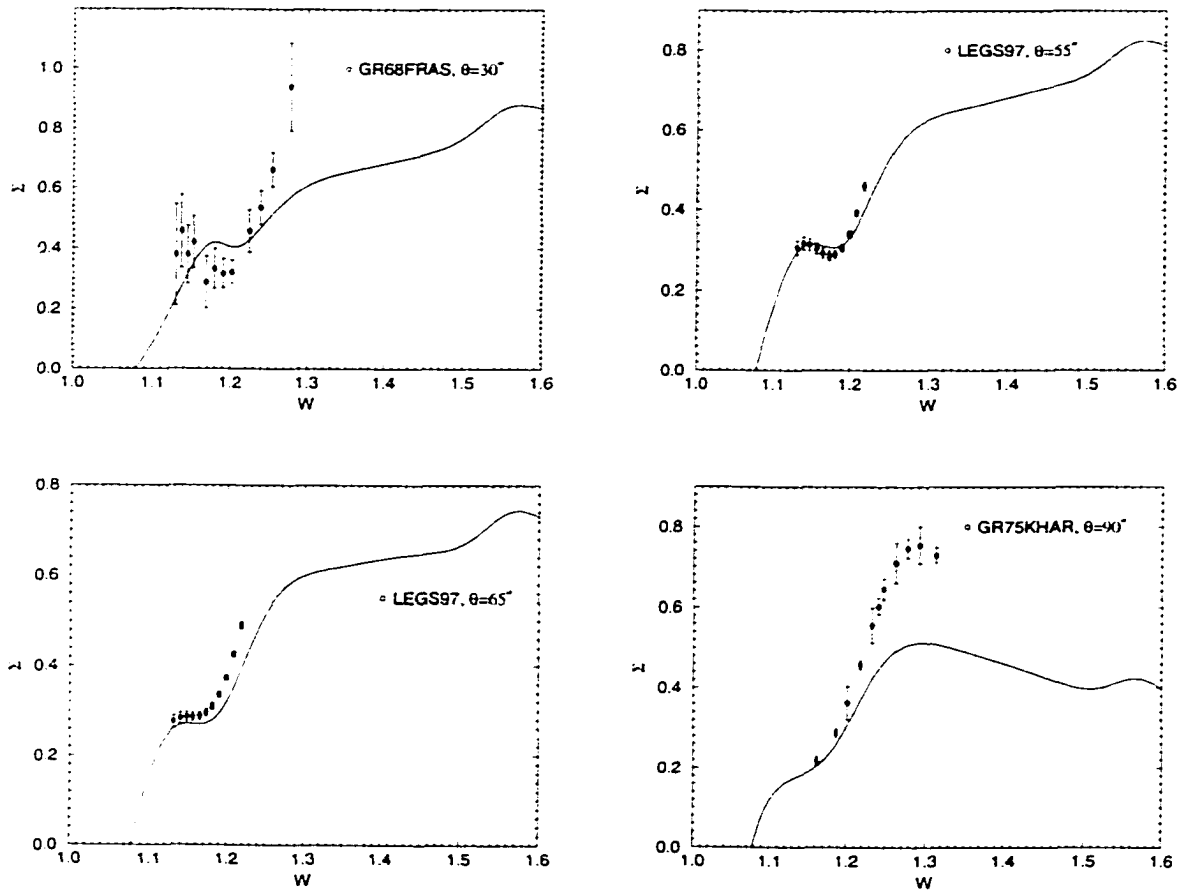

FIG. 7: Σ *vs.* total energy W(GeV) for the $\gamma p \to \pi^+ n$ process.

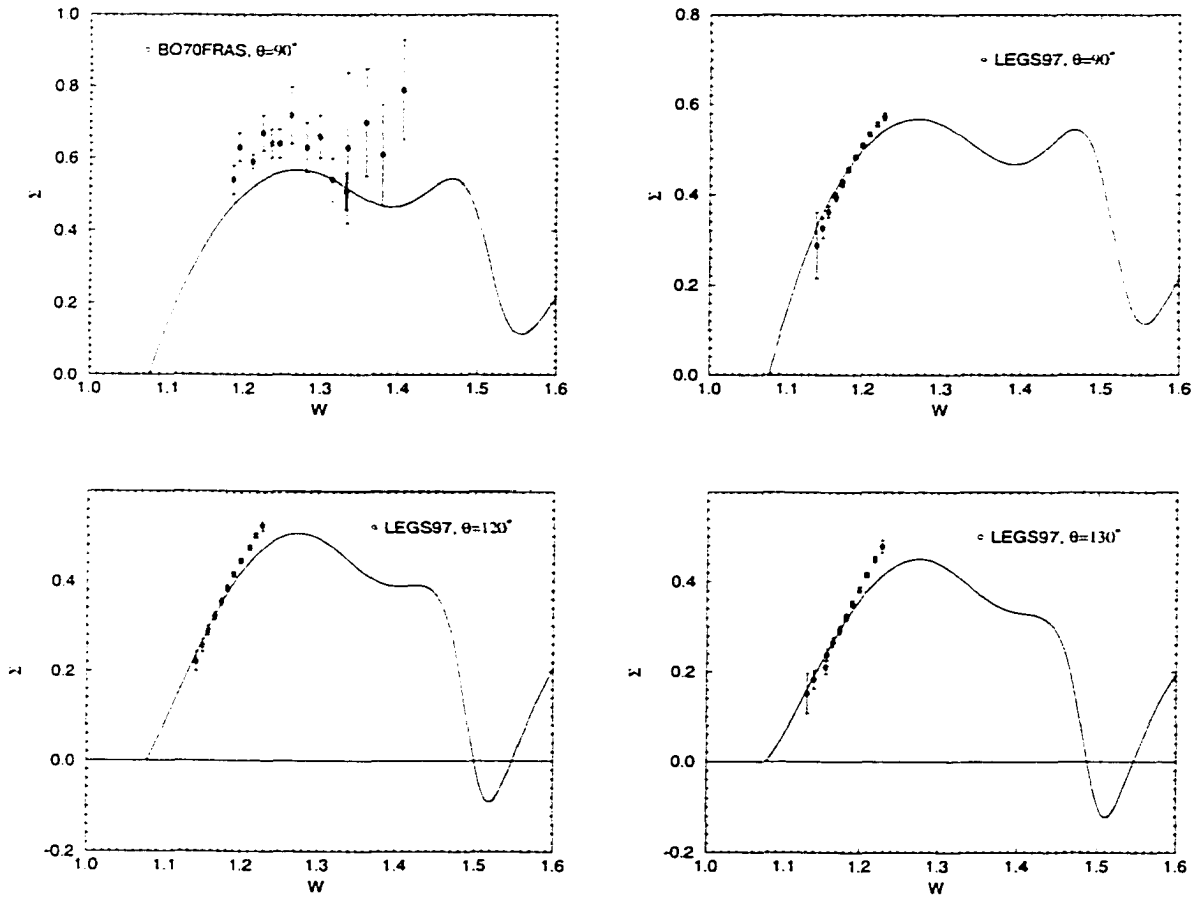

FIG. 8: Σ *vs.* total energy W(GeV) for the $\gamma p \to \pi^0 p$ process.

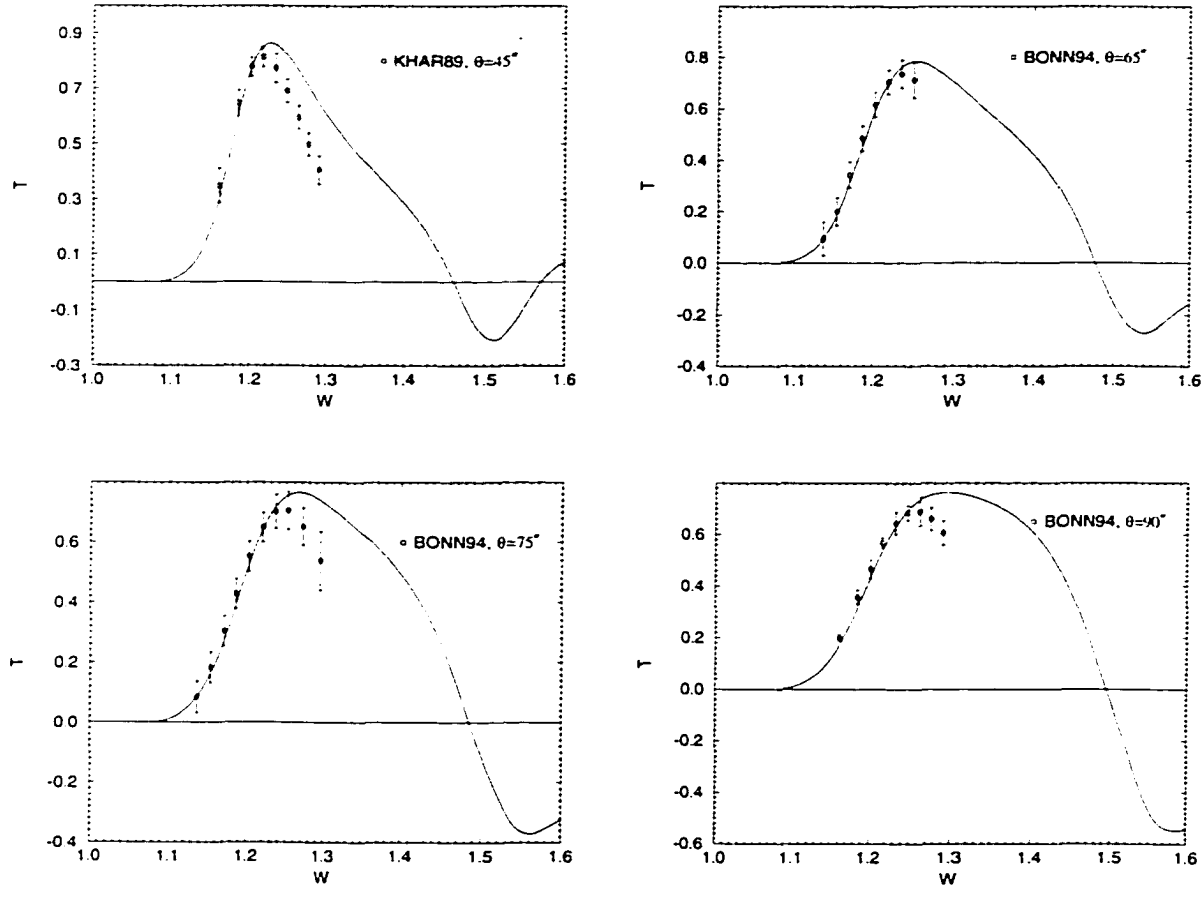

FIG. 9: T *vs.* total energy W(GeV) for the $\gamma p \to \pi^+ n$ process.

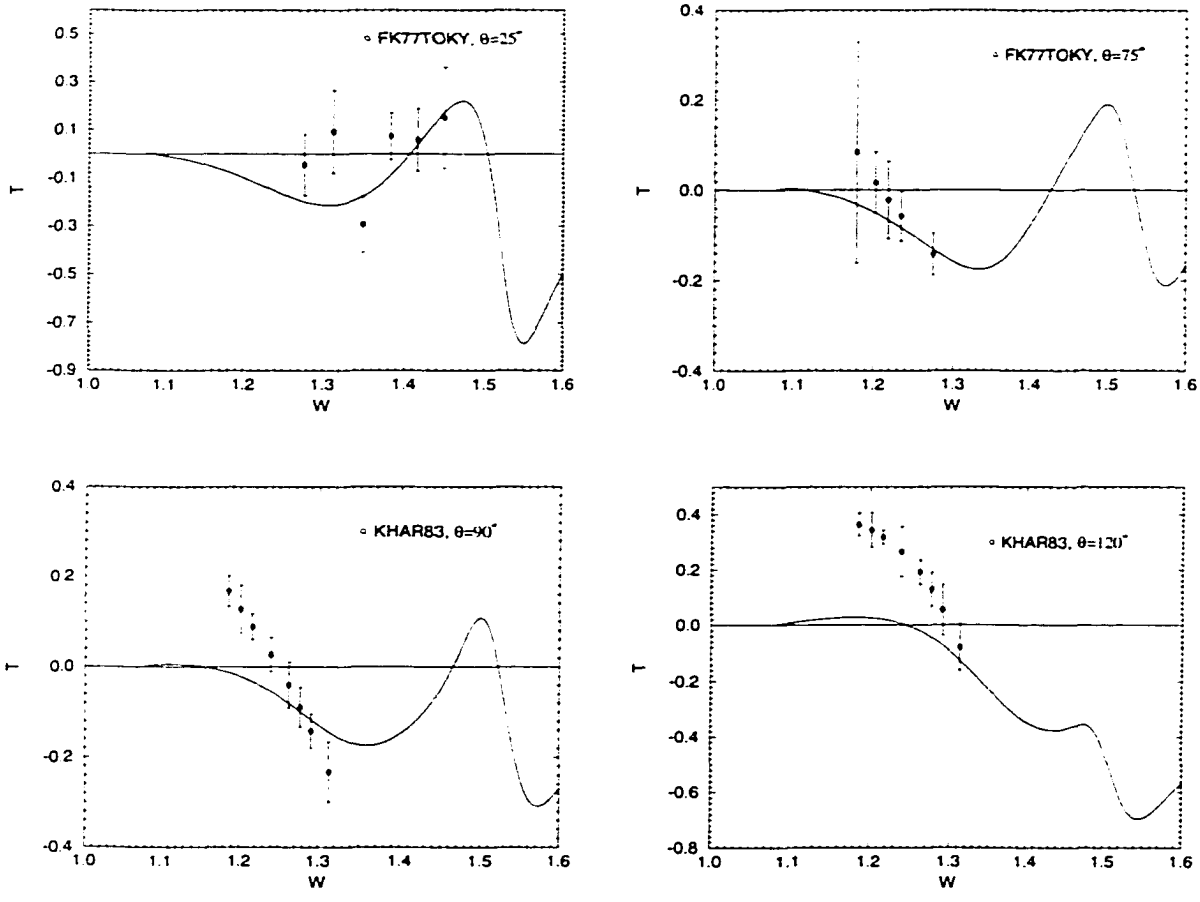

FIG. 10: T *vs.* total energy W(GeV) for the $\gamma p \to \pi^0 p$ process.

Chapter 4

DOUBLE PION PHOTOPRODUCTION

4.1 Kinematics

Before we present the amplitude for the process of interest, we first describe the kinematics of the process. The kinematics are shown schematically in figure 11. k is the momentum of the photon, p_1 is that of the target nucleon, p_2 is that of the scattered nucleon, and Q_1 and Q_2 are the pion momenta. Momentum conservation gives

$$k + p_1 = p_2 + Q_1 + Q_2. \tag{27}$$

Thus, when we construct the amplitude for the process using all the four-vectors at our disposal, we can eliminate one of these from consideration.

The total center-of-mass energy of the process is $\sqrt{s}$, where $s = (k + p_1)^2$. We may define a variable t as the square of the momentum transfered to the nucleon, which is related to the scattering angle of the nucleon in the c.o.m. frame. Thus, $t = (p_2 - p_1)^2 = 2M^2 - 2E_1E_2 - 2|\vec{p_1}||\vec{p_2}|\cos\theta$ where M, E_1 and E_2 are respectively the mass of the nucleon, energies of the incident and the outgoing nucleons and θ is the scattering angle.

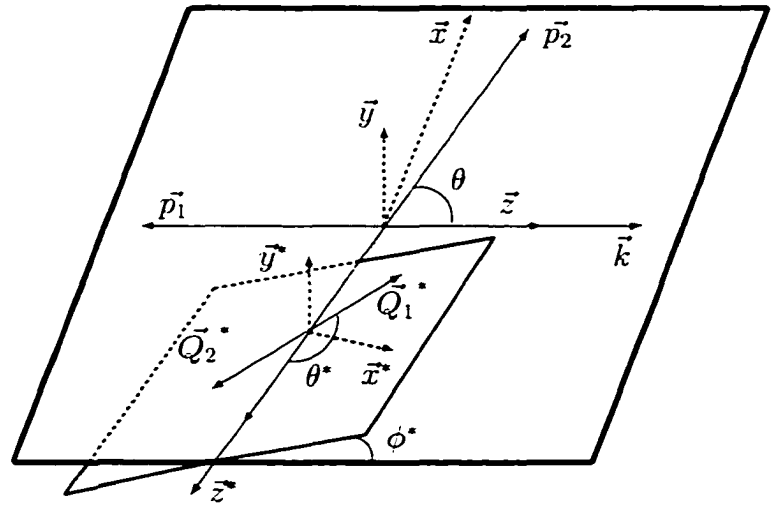

FIG. 11: Kinematics of the two-pion photoproduction process.

The differential cross section for this process is described in terms of 5 kinematic variables. These may be, for instance, two Lorentz invariants and three angles. One obvious choice for one of the invariants is s. The choice of the other four quantities can be fairly arbitrary, and will depend on what information is being presented. One choice is the scattering angle of the nucleon, θ, or equivalently, t. For the other three variables, we can choose, for example, $s_{\pi\pi} \equiv (Q_1 + Q_2)^2$ and $d\Omega^*_{\pi\pi} \equiv d\theta^*_{\pi\pi} d\phi^*_{\pi\pi}$, as illustrated in the figure. Another equally valid choice would be $s_{N\pi_1} \equiv (p_2 + Q_1)^2$ and $d\Omega^*_{N\pi_1}$, where the solid angle is defined in the rest frame of the nucleon-pion pair. In this work, we choose the kinematic variables s, t, $s_{\pi\pi}$ and $d\Omega^*_{\pi\pi}$. Detailed analysis of these variables is given in appendix A.

4.2 Invariant amplitude and cross section

The invariant matrix element $i\mathcal{M}_{fi}$ can be written as

$$i\mathcal{M}_{fi} = \bar{u}(p_2)O^{\mu}\epsilon_{\mu}u(p_1), \tag{28}$$

where $u(p_1)$ and $u(p_2)$ are respectively the Dirac spinors for the initial and final nucleons. O^{μ} is the hadronic current operator describing the hadronic strong interaction, and ϵ^{μ} the photon polarization vector.

The hadronic current can be expressed as

$$O^{\mu} = \sum_{j=1}^{16} B_j \mathcal{N}_j^{\mu}, \tag{29}$$

where the amplitude coefficients B_j are Lorentz invariant quantities depending on kinematic variables only. The $\mathcal{N}_j^{\mu}$ are chosen to be the sixteen covariant matrices

$$\begin{aligned}
\mathcal{N}_1^{\mu} &= \gamma.k\gamma^{\mu}, & \mathcal{N}_9^{\mu} &= \gamma.k\gamma.Q_1\gamma^{\mu},\\
\mathcal{N}_2^{\mu} &= p_1^{\mu}, & \mathcal{N}_{10}^{\mu} &= \gamma.Q_1 p_1^{\mu},\\
\mathcal{N}_3^{\mu} &= Q_1^{\mu}, & \mathcal{N}_{11}^{\mu} &= \gamma.Q_1 Q_1^{\mu},\\
\mathcal{N}_4^{\mu} &= Q_2^{\mu}, & \mathcal{N}_{12}^{\mu} &= \gamma.Q_1 Q_2^{\mu},\\
\mathcal{N}_5^{\mu} &= \gamma^{\mu}, & \mathcal{N}_{13}^{\mu} &= \gamma.Q_1\gamma^{\mu},\\
\mathcal{N}_6^{\mu} &= \gamma.kp_1^{\mu}, & \mathcal{N}_{14}^{\mu} &= \gamma.k\gamma.Q_1 p_1^{\mu},\\
\mathcal{N}_7^{\mu} &= \gamma.kQ_1^{\mu}, & \mathcal{N}_{15}^{\mu} &= \gamma.k\gamma.Q_1 Q_1^{\mu},\\
\mathcal{N}_8^{\mu} &= \gamma.kQ_2^{\mu}, & \mathcal{N}_{16}^{\mu} &= \gamma.k\gamma.Q_1 Q_2^{\mu}.
\end{aligned} \tag{30}$$

In equation (30), we have already taken into account the Dirac equations for the incoming and outgoing nucleons, both on shell, namely

$$\not{p}_1 u_1 = M u_1, \tag{31}$$

$$\not{p}_2 u_2 = M u_2, \tag{32}$$

as well as the conservation of four-momentum $p_1 + k = p_2 + Q_1 + Q_2$. Also, note that since we have an even number of pseudoscalar mesons (π_1 and π_2) with

unnatural parities, the matrices $\mathcal{N}_j^\mu$'s do not contain the pseudoscalar matrix γ_5. Furthermore, any other covariant matrix can be expressed in terms of a linear combination of these sixteen $\mathcal{N}_j^\mu$.

Conservation of current (gauge invariance) requires that

$$k_\mu O^\mu = 0, \tag{33}$$

which yields four conditions on the invariant scalars B_j, namely

$$\begin{aligned}
(k^2 B_1 + p_1.kB_2 + Q_1.kB_3 + Q_2.kB_4) &= 0, \\
\gamma.k(B_5 + p_1.kB_6 + Q_1.kB_7 + Q_2.kB_8) &= 0, \\
\gamma.Q_1(k^2 B_9 + p_1.kB_{10} + Q_1.kB_{11} + Q_2.kB_{12}) &= 0, \\
\gamma.Q_1\gamma.k(B_{13} + p_1.kB_{14} + Q_1.kB_{15} + Q_2.kB_{16}) &= 0.
\end{aligned} \tag{34}$$

From these equations, we can eliminate four of the amplitude coefficients, leaving us with twelve independent amplitude coefficients, or Lorentz-Dirac structures, to describe the amplitude. One choice would be to eliminate B_2, B_5, B_{10}, and B_{13}, giving

$$\begin{aligned}
i\mathcal{M}_{fi} = \bar{u}(p_2)\Big\{ & (B_1 + \not{Q}_1 B_9)(-\frac{1}{2}\gamma_\mu\gamma_\nu - \frac{p_{1\mu}k_\nu}{p_1.k}) + (B_3 + \not{Q}_1 B_{11})(-\frac{p_{1\mu}Q_{1\nu}}{p_1.k}) + \\
& (B_4 + \not{Q}_1 B_{12})(-\frac{p_{1\mu}Q_{2\nu}}{p_1.k}) + (B_6 + \not{Q}_1 B_{14})(\gamma_\nu p_{1\mu}) + \\
& (B_7 + \not{Q}_1 B_{15})(\gamma_\nu Q_{1\mu}) + (B_8 + \not{Q}_1 B_{16})(\gamma_\nu Q_{2\mu})\Big\} F^{\mu\nu} u(p_1),
\end{aligned} \tag{35}$$

where $F^{\mu\nu} = \epsilon^\mu k^\nu - \epsilon^\nu k^\mu$ is the electromagnetic field strength tensor. It is clear that another form of $\bar{u}(p_2)\epsilon_\mu O^\mu u(p_1)$ can be derived by eliminating a different set of four amplitude coefficients.

Another way to write down $i\mathcal{M}_{fi}$ is to use a different set of 4-momenta such as $q = Q_1 - Q_2$, $Q = Q_1 + Q_2$, k and p_1. By doing this, the 16 covariant matrices are

$$\mathcal{N}_1^\mu = \gamma.k\gamma^\mu, \qquad \mathcal{N}_9^\mu = \gamma.k\gamma.q\gamma^\mu,$$

$$\begin{aligned}
\mathcal{N}_2^\mu &= p_1^\mu, & \mathcal{N}_{10}^\mu &= \gamma.qp_1^\mu,\\
\mathcal{N}_3^\mu &= q^\mu, & \mathcal{N}_{11}^\mu &= \gamma.qq^\mu,\\
\mathcal{N}_4^\mu &= Q^\mu, & \mathcal{N}_{12}^\mu &= \gamma.qQ^\mu,\\
\mathcal{N}_5^\mu &= \gamma^\mu, & \mathcal{N}_{13}^\mu &= \gamma.q\gamma^\mu,\\
\mathcal{N}_6^\mu &= \gamma.kp_1^\mu, & \mathcal{N}_{14}^\mu &= \gamma.k\gamma.qp_1^\mu,\\
\mathcal{N}_7^\mu &= \gamma.kq^\mu, & \mathcal{N}_{15}^\mu &= \gamma.k\gamma.qq^\mu,\\
\mathcal{N}_8^\mu &= \gamma.kQ^\mu, & \mathcal{N}_{16}^\mu &= \gamma.k\gamma.qQ^\mu. \qquad (36)
\end{aligned}$$

Current conservation again yields four equations and by eliminating B_2, B_5, B_{10}, and B_{13}, we find

$$\begin{aligned}
i\mathcal{M}_{fi} = \bar{u}(p_2)\{&(B_1+ \not{q}B_9)(-\frac{1}{2}\gamma_\mu\gamma_\nu - \frac{p_{1\mu}k_\nu}{p_1.k}) + (B_3+ \not{q}B_{11})(-\frac{p_{1\mu}q_\nu}{p_1.k}) +\\
&(B_4+ \not{q}B_{12})(-\frac{p_{1\mu}Q_\nu}{p_1.k}) + (B_6+ \not{q}B_{14})(\gamma_\nu p_{1\mu}) +\\
&(B_7+ \not{q}B_{15})(\gamma_\nu q_\mu) + (B_8+ \not{q}B_{16})(\gamma_\nu Q_\mu)\}F^{\mu\nu}u(p_1). \qquad (37)
\end{aligned}$$

Even though the 16 covariant matrices look independent from each other, we claim that, by using the so-called 'equivalence theorems', they can be related to each other. These theorems can be established by equating the result obtained by saturating the indices α, β, γ, δ, ν, η and σ in $\epsilon^{\alpha\beta\gamma\delta}\epsilon^{\nu\eta\sigma\mu}$ with the 4-vectors of the process, and contracting them using on one hand the expression [53]

$$\epsilon^{\alpha\beta\gamma\delta}\epsilon^{\nu\eta\sigma\mu} = \begin{vmatrix} g^{\alpha\nu} & g^{\alpha\eta} & g^{\alpha\rho} & g^{\alpha\mu}\\ g^{\beta\nu} & g^{\beta\eta} & g^{\beta\rho} & g^{\beta\mu}\\ g^{\gamma\nu} & g^{\gamma\eta} & g^{\gamma\rho} & g^{\gamma\mu}\\ g^{\delta\nu} & g^{\delta\eta} & g^{\delta\rho} & g^{\delta\mu} \end{vmatrix}, \qquad (38)$$

and on the other hand

$$\begin{aligned}
\epsilon^{\alpha\beta\gamma\delta}\epsilon^{\nu\eta\sigma\mu} &= \gamma_5\epsilon^{\alpha\beta\gamma\delta}\gamma_5\epsilon^{\nu\eta\sigma\mu}\\
&= \left(\frac{-i}{4!}\epsilon^{\rho\lambda\tau\kappa}\gamma_\rho\gamma_\lambda\gamma_\tau\gamma_\kappa\right)\epsilon^{\alpha\beta\gamma\delta}\left(\frac{-i}{4!}\epsilon^{\rho'\lambda'\tau'\kappa'}\gamma_{\rho'}\gamma_{\lambda'}\gamma_{\tau'}\gamma_{\kappa'}\right)\epsilon^{\nu\eta\sigma\mu}
\end{aligned}$$

$$= \frac{-1}{(4!)^2}\gamma_\rho\gamma_\lambda\gamma_\tau\gamma_\kappa \begin{vmatrix} g^{\rho\alpha} & g^{\rho\beta} & g^{\rho\gamma} & g^{\rho\delta} \\ g^{\lambda\alpha} & g^{\lambda\beta} & g^{\lambda\gamma} & g^{\lambda\delta} \\ g^{\tau\alpha} & g^{\tau\beta} & g^{\tau\gamma} & g^{\tau\delta} \\ g^{\kappa\alpha} & g^{\kappa\beta} & g^{\kappa\gamma} & g^{\kappa\delta} \end{vmatrix} \times$$

$$\gamma_{\rho'}\gamma_{\lambda'}\gamma_{\tau'}\gamma_{\kappa'} \begin{vmatrix} g^{\rho'\nu} & g^{\rho'\eta} & g^{\rho'\sigma} & g^{\rho\mu} \\ g^{\lambda'\nu} & g^{\lambda'\eta} & g^{\lambda'\sigma} & g^{\lambda\mu} \\ g^{\tau'\nu} & g^{\tau'\eta} & g^{\tau'\sigma} & g^{\tau\mu} \\ g^{\kappa'\nu} & g^{\kappa'\eta} & g^{\kappa'\sigma} & g^{\kappa\mu} \end{vmatrix}. \qquad (39)$$

By this technique, we find four equivalence equations. They are

$$\begin{aligned}
\mathcal{N}_4^\mu &= \frac{-1}{2b_{16}}\,(2b_{28}\mathcal{N}_3^\mu + 2m_N b_{34}\mathcal{N}_7^\mu - 2m_N b_{31}\mathcal{N}_{11}^\mu + 2b_{33}\mathcal{N}_{15}^\mu + 2b_{13}\mathcal{N}_2^\mu \\
&\quad +2m_N b_{25}\mathcal{N}_6^\mu + 2m_N b_{38}\mathcal{N}_{10}^\mu + 2b_{36}\mathcal{N}_{14}^\mu - m_N b_8\mathcal{N}_5^\mu - b_7\mathcal{N}_1^\mu - b_{19}\mathcal{N}_{13}^\mu), \\
\mathcal{N}_8^\mu &= \frac{1}{2b_{16}}\,(2m_N b_{23}\mathcal{N}_3^\mu + 2b_{21}\mathcal{N}_7^\mu - 2b_{18}\mathcal{N}_{11}^\mu + 2m_N b_{32}\mathcal{N}_{15}^\mu + 2m_N b_{17}\mathcal{N}_2^\mu \\
&\quad +2b_9\mathcal{N}_6^\mu + 2b_{26}\mathcal{N}_{10}^\mu - 8m_N k\cdot qk\cdot Q\mathcal{N}_{14}^\mu - b_3\mathcal{N}_5^\mu - m_N b_{12}\mathcal{N}_1^\mu - b_{19}\mathcal{N}_{13}^\mu), \\
\mathcal{N}_{12}^\mu &= \frac{1}{2b_{16}}\,(2m_N b_{11}\mathcal{N}_3^\mu + 2b_6\mathcal{N}_7^\mu + 2b_{20}\mathcal{N}_{11}^\mu + 2m_N b_{37}\mathcal{N}_{15}^\mu - 2m_N b_{22}\mathcal{N}_2^\mu \\
&\quad -2b_{14}\mathcal{N}_6^\mu - 2b_{15}\mathcal{N}_{10}^\mu + 2m_N b_{35}\mathcal{N}_{14}^\mu + b_2\mathcal{N}_5^\mu - m_N b_{12}\mathcal{N}_{13}^\mu + b_7\mathcal{N}_9^\mu), \\
\mathcal{N}_{16}^\mu &= \frac{1}{2b_{16}}\,(2b_1\mathcal{N}_3^\mu + 2m_N b_{10}\mathcal{N}_7^\mu - 2m_N b_{29}\mathcal{N}_{11}^\mu + 2b_{30}\mathcal{N}_{15}^\mu + 2b_4\mathcal{N}_2^\mu \\
&\quad -4m_N b_{27}k\cdot q\mathcal{N}_6^\mu - 2m_N b_{24}\mathcal{N}_{10}^\mu + 2b_5\mathcal{N}_{14}^\mu - b_2\mathcal{N}_5^\mu - b_3\mathcal{N}_{13}^\mu + m_N b_8\mathcal{N}_9^\mu),
\end{aligned}$$

where the b_i are lengthy kinematical functions. These equations allow us to drop the structures $\mathcal{N}_4^\mu$, $\mathcal{N}_8^\mu$, $\mathcal{N}_{12}$ and $\mathcal{N}_{16}$ from equation (30).

We may also rewrite $i\mathcal{M}_{fi}$ in a form that is similar to that written by Chew-Goldberger-Low-Nambu for the process $\gamma N \to N\pi$ [36]. Thus, we write the amplitude as [55]

$$i\mathcal{M}_{fi} = \chi_f^\dagger \frac{F}{2Mab}\chi_i, \qquad (40)$$

where the amplitude F is

$$\begin{aligned}
F = \quad & \vec{\epsilon}.\vec{Q}_1 F_1 + \vec{\epsilon}.\vec{p}_2 F_2 + \vec{\epsilon}.\vec{Q}_1\vec{\sigma}.\vec{p}_2\vec{\sigma}.\vec{Q}_1 F_3 + \vec{\epsilon}.\vec{p}_2\vec{\sigma}.\vec{p}_2\vec{\sigma}.\vec{Q}_1 F_4 + \\
& \vec{\epsilon}.\vec{Q}_1\vec{\sigma}.\vec{p}_2\vec{\sigma}.\vec{k}F_5 + \vec{\epsilon}.\vec{p}_2\vec{\sigma}.\vec{p}_2\vec{\sigma}.\vec{k}F_6 + \vec{\epsilon}.\vec{Q}_1\vec{\sigma}.\vec{Q}_1\vec{\sigma}.\vec{k}F_7 + \vec{\epsilon}.\vec{p}_2\vec{\sigma}.\vec{Q}_1\vec{\sigma}.\vec{k}F_8 +
\end{aligned}$$

$$\vec{\sigma}.\vec{Q}_1\vec{\sigma}.\vec{\epsilon}F_9 + \vec{\sigma}.\vec{p}_2\vec{\sigma}.\vec{\epsilon}F_{10} + i\vec{\sigma}.(\vec{\epsilon}\times\vec{k})F_{11} + i\vec{\sigma}.\vec{p}_2\vec{\sigma}.\vec{Q}_1\vec{\sigma}.(\vec{\epsilon}\times\vec{k})F_{12}, \quad (41)$$

or

$$\begin{aligned} F &= \vec{\epsilon}.\vec{Q}_1F_1' + \vec{\epsilon}.\vec{p}_2F_2' + \vec{\epsilon}.\vec{Q}_1\vec{\sigma}.\vec{p}_2\times\vec{Q}_1F_3' + \vec{\epsilon}.\vec{p}_2\vec{\sigma}.\vec{p}_2\times\vec{Q}_1F_4' + \\ &\quad \vec{\epsilon}.\vec{Q}_1\vec{\sigma}.\vec{p}_2\times\vec{k}F_5' + \vec{\epsilon}.\vec{p}_2\vec{\sigma}.\vec{p}_2\times\vec{k}F_6' + \vec{\epsilon}.\vec{Q}_1\vec{\sigma}.\vec{Q}_1\times\vec{k}F_7' + \vec{\epsilon}.\vec{p}_2\vec{\sigma}.\vec{Q}_1\times\vec{k}F_8' + \\ &\quad \vec{\sigma}.\vec{Q}_1\times\vec{\epsilon}F_9' + \vec{\sigma}.\vec{p}_2\times\vec{\epsilon}F_{10}' + i\vec{\sigma}.(\vec{\epsilon}\times\vec{k})F_{11}' + i\vec{\sigma}.\vec{p}_2\times\vec{Q}_1\vec{\sigma}.(\vec{\epsilon}\times\vec{k})F_{12}'. \quad (42) \end{aligned}$$

The constants a and b are respectively, $p_1^0 + M$ and $p_2^0 + M$ and the F_i and F_i' are linear combinations of the B_i. We note that the second form of F is obtained by writing $\vec{\sigma}.\vec{Q}_1\vec{\sigma}.\vec{\epsilon} = \vec{Q}_1.\vec{\epsilon} + i\vec{\sigma}.\vec{Q}_1\times\vec{\epsilon}$.

Neither of these equations may be the optimal forms, as we are yet to explore which choice of structures will lead to the simplest representation of helicity amplitudes, differential cross sections, etc. Thus, these forms are the most general that can be written for this amplitude. All quantities of interest can now be calculated in terms of the coefficients, the B_j. Thus, up to this point, everything has been completely model independent. All that is now left to be done is to construct a model for the B_j. In this section, we discuss the model that we choose to calculate the single and double pion photoproduction cross sections.

Finally, the square of the amplitude $|i\mathcal{M}_{fi}|^2$ or the cross section now looks like

$$|i\mathcal{M}_{fi}|^2 = \sum_{i,j=1}^{12} B_iB_j^*F_{ij},$$

where F_{ij} are quantities depending on scalar products only. We note that expressions of these F_{ij} are long and complicated, and are not shown here. However, the full expression for the cross section is given in appendix B.

4.3 EFFECTIVE LAGRANGIAN FOR DOUBLE PION PHOTOPRODUCTION

An approach similar to what we have used for the single pion photoproduction is used to calculate the amplitude coefficients for the double pion photoproduction.

It should be pointed out that the extractions of these amplitude coefficients B_j are done with the help of Mathematica. Some of the amplitudes are very complicated and create several thousands of output lines. For this reason, we do not write down here the expressions for these lengthy amplitude coefficients, but we show all the 'Feynman' diagrams that we need for the process of interest. In all of the diagrams, solid lines correspond to the ground state nucleons, thick solid lines represent baryon resonances, wavy lines are photons, dashed lines are pions, and curly lines are vector mesons.

The diagrams in figure 12 are the Born terms. These are the diagrams in which the only intermediate particles are ground state nucleons and pions. Diagrams (c) and (f) contain, respectively, the gauge term $NN\pi\gamma$ or Kroll-Ruderman term and the $NN\pi\pi\gamma$ term which arise from minimal substitution in the $NN\pi$ vertex and the $NN\pi\pi$ vertex. Diagram (g) contains the $\gamma\pi\pi\pi$ chiral anomaly vertex, which will be the object of study of at least one experiment at Jefferson Lab [58]. In addition, the set of diagrams (a), (b) and (c) together satisfies gauge invariance and so does each diagram of (d), (e), (f) and (g). Finally, we point out that each diagram shown actually corresponds to a set of contributions, as we do not show all of the permutations that arise. For example, figure (12a) represents six different diagrams, the other five arising from attaching the photon and pion lines to the nucleon line in all possible ways.

Figure 13 shows the diagrams that involve vector mesons. For this work, we consider only the ρ meson. The $\rho\pi\pi$ decay does not exist with two identical pions, so most of these diagrams do not contribute to the process $\gamma N \to N\pi^0\pi^0$. Diagram (b) contains the gauge term $\rho\pi\pi\gamma$ arising from minimal coupling in the $\rho\pi\pi$ vertex. Similarly, the $NN\rho\gamma$ vertex arises from minimal substitution in $NN\rho$. As before, these diagrams can be divided into two sets of diagrams (a)-(e) and (f)-(h) which separately satisfy gauge invariance.

Figure 14 represents the diagrams which contain a single nucleon resonance. In our case, these resonances can be either the $\Delta(1232)$, Roper $N^*(1440)$, the $N^*(1520)$ or the $N^*(1535)$. The combined set of diagrams (a)-(d) is gauge invariant whereas each one of the rest of the diagrams satisfies gauge invarince on its

own.

In figure 15, we present the diagrams that contain both a baryon resonance and a vector meson and in figure 16, we show diagrams with two baryonic resonances. The diagrams of figures 15 and 16 depend on some new couplings, in general. For instance, diagrams in figure 15 are proportional to the set of couplings $g_{N^*N\rho}$ while diagrams 16(a) and 16(b) depend respectively on the couplings $g_{N_1^*N_2^*\pi}$ and $g_{N_1^*N_2^*\gamma}$. Neither of these sets of couplings are known, in general

In addition to the vertices shown in chapter 3, a few more vertices are needed for this calculation. They are presented in the next sections. The corresponding vertices along with the propagators are shown in appendix C.

4.4 Born terms

The Lagrangians for the Born terms shown in figure 12 are

$$\begin{aligned}
\mathcal{L}_{NN\pi\pi} &= \bar{N}(-\frac{4\pi\lambda_1}{m_\pi}\phi_i\phi_i - \frac{1}{4F_\pi^2}\gamma_\mu\epsilon_{ijk}\tau_i\phi_j(\partial^\mu\phi_k))N + H.c., \\
\mathcal{L}_{NN\gamma\pi\pi} &= \bar{N}\frac{-e}{4F_\pi^2}\gamma_\mu(\tau_i\delta_{3j} - \tau_3\delta_{ij})\phi_i\phi_j A^\mu N + H.c., \\
\mathcal{L}_{\gamma\pi\pi\pi} &= \frac{F^{3\pi}}{6}\epsilon^{\mu\nu\alpha\beta}\epsilon^{ijk}A_\mu(\partial_\nu\phi_i)(\partial_\alpha\phi_j)(\partial_\beta\phi_k) + H.c.,
\end{aligned}$$

where $F^{\nu\lambda} = \partial^\nu A^\lambda - \partial^\lambda A^\nu$ is the electromagnetic field strength tensor. N is a generic notation for the nucleon and ϕ for the pion. q_π is the charge of the pion and τ_i the isospin operator for $I = \frac{1}{2}$. λ_1 and F_π are coupling constants and $F^{3\pi}$ is the $\gamma \to 3\pi$ structure function that we are going to discuss in chapter 6.

We note that as $\mathcal{L}_{NN\gamma\pi\pi}$ is proportional to $\gamma.\epsilon$ (given the fact that A^μ is proportional to ϵ^μ) and our general amplitude, equation (37) does not depend on the amplitude coefficient B_5, diagram (f) in figure 12 contributes in the born terms through gauge invariance. In addition, for the $NN\pi\pi$ vertex, we take into account both the isoscalar part and the isovector part [54] of the amplitude. However, the isovector part does not contribute in the coupling involving two identical pions $(\pi^0\pi^0)$.

4.5 Vector meson couplings

The Lagrangians with the ρ-meson are

$$\begin{aligned}
\mathcal{L}_{\rho\pi\pi} &= f_\rho \epsilon_{ikj} \phi_i \partial_\mu \phi_j A^\nu_{\rho k} + H.c., \\
\mathcal{L}_{\rho\pi\pi\gamma} &= e_j f_\rho \epsilon_{ikj} A^\mu_{\rho k} A_{\gamma\mu} \phi_i \phi_j + H.c., \\
\mathcal{L}_{\rho\gamma NN} &= \frac{G^t}{2M} q_\rho \bar{N} (\gamma . A^*_\rho \gamma . A_\gamma - A^*_\rho . A_\gamma) N + H.c.,
\end{aligned} \tag{43}$$

where φ represents a meson field and N the nucleon field. f_ρ is a coupling constant and e_j is the charge of the pion 'j'.

4.6 Spin-$\frac{1}{2}$ resonance couplings

The Lagrangians involving the N^* are

$$\begin{aligned}
\mathcal{L}_{N^* N\gamma\pi} &= \bar{N}^* \frac{f_{N^* N\pi}}{m_\pi} I_5 \tau_i \epsilon_{ij3} \gamma_\mu . A^\mu \phi_j N + H.c., \\
\mathcal{L}_{N^* N\pi\pi} &= \bar{N}^* I_5 (-\frac{4\pi\lambda^*_1}{m_\pi} \phi_i \phi_i - \frac{1}{4F^{*2}_\pi} \gamma_\mu \epsilon_{ijk} \tau_i \phi_j (\partial^\mu \phi_k)) N + H.c., \\
\mathcal{L}_{N^* N\rho} &= \bar{N}^* I_5 \tau_j \left\{ - G^{*v} \gamma^\mu (A_{\rho j}{}^*)_\mu + \frac{G^{*t}}{M^* + M} \gamma^\mu \gamma^\nu \partial_\mu (A_{\rho j}{}^*)_\nu \right\} N + H.c.
\end{aligned} \tag{44}$$

where N^* represents a generic notation for the spin-$\frac{1}{2}$ resonance, N is the nucleon field and ϕ is the pion field. The operator I_5 is either 1 or γ_5 depending on the parity of the resonance. M_{N^*} is the mass of the the resonance and M the mass of the nucleon. $f_{N^* N\pi}$, λ^*_1, F^*_π, G^{*v} and G^{*t} are coupling constants.

4.7 Spin-$\frac{3}{2}$ resonance couplings

As we mentioned earlier, the spin-$\frac{3}{2}$ resonant states involved in this energy range (E_γ = 800 MeV) are the $\Delta(1232)$ and the isospin-$\frac{1}{2}$ $N^*(1520)$ resonances. The effective Lagrangians for the $RN\pi\gamma$ and $RN\rho$ interactions are

$$\begin{aligned}
\mathcal{L}_{RN\pi\gamma} &= \bar{R}^{\mu}\frac{f_{RN\pi}}{m_{\pi}}I_5T_j\Theta_{\mu\nu}(Z)A^{\nu}\phi_j N + H.c.,\\
\mathcal{L}_{RN\rho} &= \bar{R}^{\mu}_{\Delta}I_5T_j\{a_1(A_{\rho j}{}^{\star})_{\mu} + a_2\gamma^{\nu}\partial_{\mu}(A^{\star}_{\rho j})_{\nu} + a_3p^{\nu}_{\Delta}\partial_{\mu}(A^{\star}_{\rho j})_{\nu}\}N + H.c.,
\end{aligned} \tag{45}$$

where R^{μ} is the vector spinor of the resonance, N is the nucleon field and ϕ the pion field. $f_{RN\pi}$, a_1, a_2, and a_3 are coupling constants.

As seen in figure 16, two pion photoproduction contains also the double resonant vertices such as $R'R\pi$ and $R'R\gamma$. The corresponding effective Lagrangians are

$$\begin{aligned}
\mathcal{L}^1_{R'R\pi} &= \bar{R}'^{\mu}I_5T_jT^1_{R'R\pi}\partial_{\mu}\partial_{\nu}\phi_jR^{\nu} + H.c.,\\
\mathcal{L}^2_{R'R\pi} &= \bar{R}'^{\mu}I_5T_jT^2_{R'R\pi}g_{\mu\nu}\phi_jR^{\nu} + H.c.,\\
\mathcal{L}^1_{RR\gamma} &= \bar{R}^{\mu}I_5(-e\frac{1+T_3}{2})[\gamma_{\lambda}g_{\mu\nu} - (\gamma_{\mu}g_{\nu\lambda} + \gamma_{\nu}g_{\mu\lambda}) + \gamma_{\mu}\gamma_{\lambda}\gamma_{\nu}]A^{\lambda}R^{\nu} + H.c.,\\
\mathcal{L}^2_{RR\gamma} &= \bar{R}'^{\mu}I_5T^2_{RR}\gamma_{\alpha}\gamma_{\beta}F^{\alpha\beta}R^{\mu} + H.c.,\\
\mathcal{L}^3_{RR\gamma} &= \bar{R}'^{\mu}I_5k_{\mu}\gamma_{\alpha}A^{\alpha}k_{\nu}R^{\nu} + H.c.,\\
\mathcal{L}^4_{RR\gamma} &= \bar{R}'^{\mu}I_5k_{\mu}\gamma_{\alpha}\gamma_{\beta}F^{\alpha\beta}k_{\nu}R^{\nu} + H.c.,
\end{aligned} \tag{46}$$

where the off-shell terms have already been ignored in writing the above equations. We note that predictions by Oset *et. al* [30] conclude that the off-shell contribution of the $\Delta(1232)$ to the total cross section is very small and can be neglected everywhere in our energy range, threshold to $E_{\gamma} = 800$ MeV. The first Lagrangian $\mathcal{L}^1_{RR\gamma}$ arises from the interaction between the photon field A^{ν} and the resonance (for instance the Δ) via its charge. Thus, this term vanishes with a chargeless resonance. The second term $\mathcal{L}^2_{RR\gamma}$ corresponds to the interaction due to the magnetic moment of the resonance. We remark that in the $\Delta\Delta\gamma$ coupling, the photon can be either isoscalar or isovector. Consequently, the coupling T_{RR} is written as $T_{RR} = (k^{\star}_s + T_3k^{\star}_v)$ where $k^{\star}_s$ and $k^{\star}_v$ are respectively the isoscalar and isovector anomalous magnetic moments of the Δ. $\mathcal{L}^3_{RR\gamma}$ and $\mathcal{L}^4_{RR\gamma}$ arise respectively from the interaction between the photon field A^{ν} and the resonance via its quadrupole and octupole moments. In this work, we use only the $\mathcal{L}^{1,2}_{RR\gamma}$

Lagrangians for the $\Delta\Delta\gamma$ coupling . The $\mathcal{L}^{3,4}_{RR\gamma}$ terms are not well-known in the literature and we ignore them here.

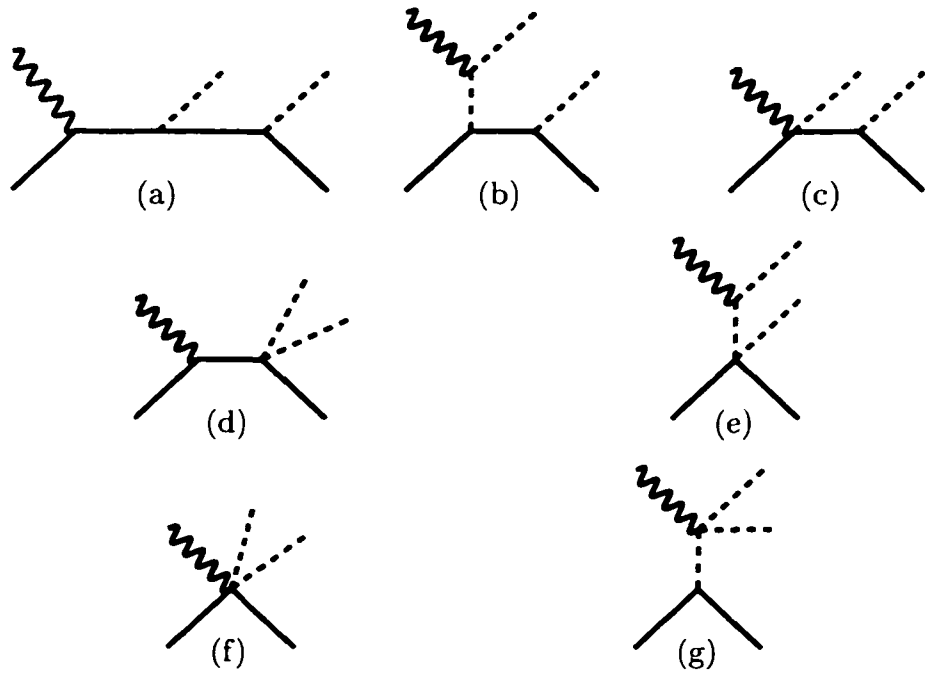

FIG. 12: Born diagrams: continuous straight lines are nucleons. Dashed lines are pions and wavy curves are photons. All intermediate particles are ground-state nucleons and pions.

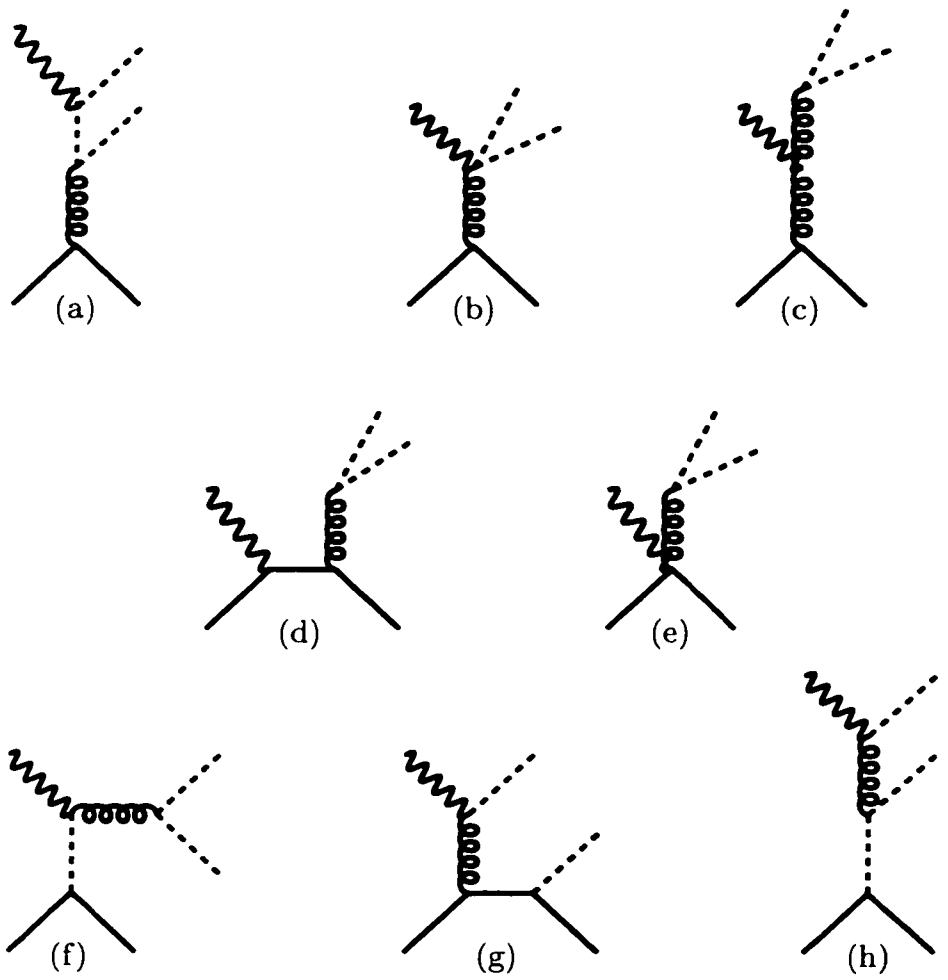

FIG. 13: Diagrams containing vector mesons. The curly lines represent the mesons.

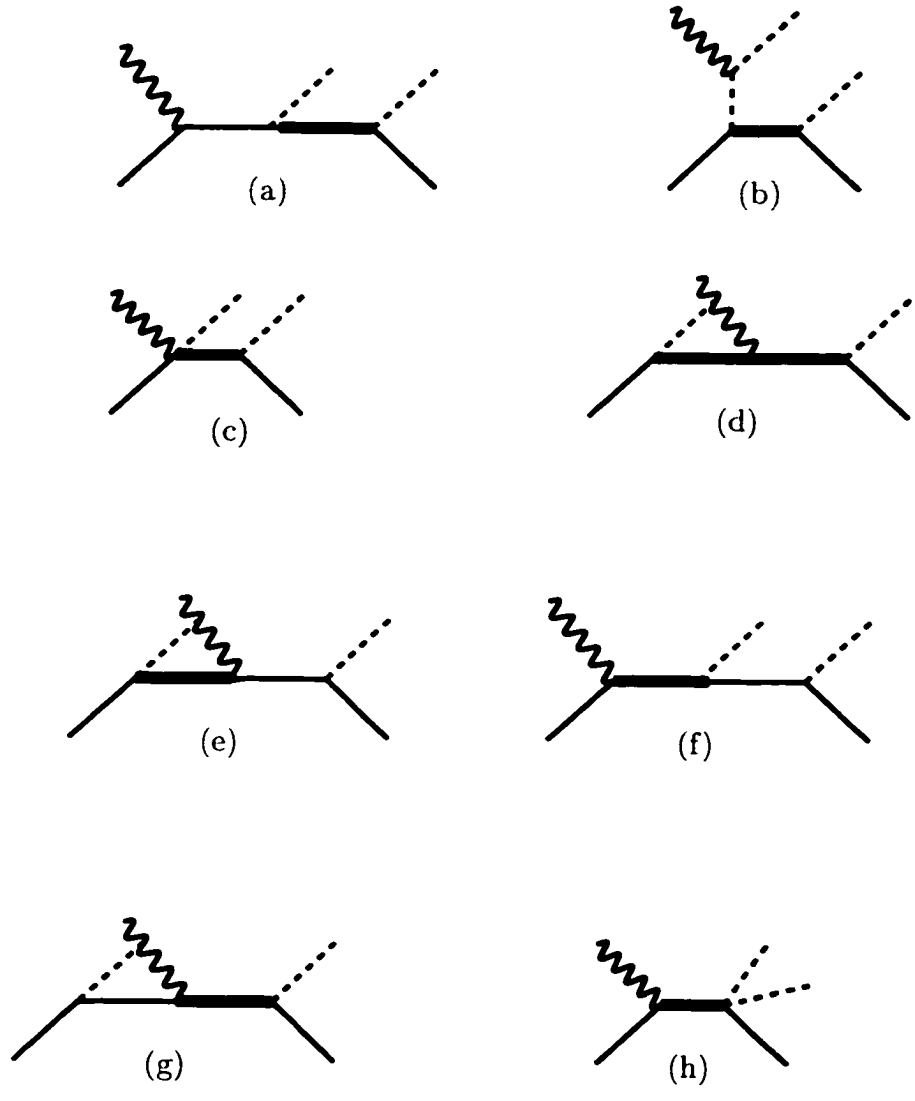

FIG. 14: Diagrams containing resonances. The thick solid lines are the nucleon resonances.

FIG. 15: Diagrams containing a nucleon resonance and a vector meson.

FIG. 16: Diagrams containing two resonances.

4.8 Coupling constants and fitting procedure

We note that some of the parameters that are used in this work are already well-known in the literature, so we do not discuss them here. They are presented in appendix F. However, we calculate some of the necessary coupling constants by using the properties of the helicity amplitudes, partial-wave amplitudes and decay widths obtained from experimental measurements (PDG) [34]. They are the coupling constants of the following decay processes:

$$\begin{aligned} N^*(1520, J^P = \frac{3^-}{2}) &\rightarrow \Delta(J^P = \frac{3^+}{2}) + \pi(J^P = 0^-), \\ \Delta(1232, J^P = \frac{3^+}{2}) &\rightarrow N(J^P = \frac{1^+}{2}) + \gamma(J^P = 1^-), \\ N^*(1520, J^P = \frac{3^-}{2}) &\rightarrow N(J^P = \frac{1^+}{2}) + \gamma(J^P = 1^-). \end{aligned}$$

Detailed calculations of the corresponding coupling constants are presented in appendices G and H. On the other hand, we fit our theoretical cross section to the experimental data and extract some previously unknown coupling constants. These fitted coupling constants are $T^1_{\Delta\pi\Delta}$, $T^2_{\Delta\pi\Delta}$ in the $\Delta\pi\Delta$ coupling, k^*_s, k^*_v in the magnetic moment term of the $\Delta\gamma\Delta$ coupling and a_1, a_2, a_3 in the $\Delta\rho N$ coupling. The corresponding amplitudes and vertices are shown in figure 17.

$$\mathcal{M}_{\Delta\gamma\Delta} = \bar{u}_\lambda(p_f)[-eq_\Delta \not{\epsilon} + (k_s^* + T_\Delta k_v^*)\gamma_\mu\gamma_\nu F^{\mu\nu}]u^\lambda(p_i),$$

$$\mathcal{M}_{\Delta\pi\Delta} = \bar{u}_\mu(p_f)\gamma_5 T_j(T^1_{\Delta\pi\Delta}Q^\mu_j Q^\nu_j + T^2_{\Delta\pi\Delta}g^{\mu\nu})u_\nu(p_i),$$

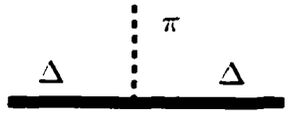

$$\mathcal{M}_{\Delta N\rho} = \bar{u}(p_f)\gamma_5 T_j(a_1\epsilon^\mu_\rho + a_2\gamma.\epsilon_\rho Q^\mu_j + a_3\epsilon_\rho.p_\Delta Q^\mu_j)u(p_i).$$

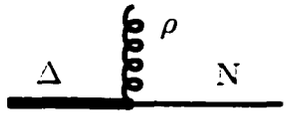

FIG. 17: Parameters extracted from fit.

Chapter 5

RESULTS AND DISCUSSION

In figure 19, we present for the $\gamma p \rightarrow \pi^+\pi^- p$ isospin channel, contributions to the total cross section of four sets of diagrams. One of these contributions is the Born terms shown in figure 12. Another is the $\Delta(1232)$-terms (figure 14, diagrams (a), (b), (c) and (d) but not including the magnetic moment term of the $\Delta\gamma\Delta$ interaction as its corresponding coupling constants are still to be extracted from a fit). The third contribution is that of the $N^*(1440)$ and the fourth contribution is that of the diagrams with $N^*(1520)\Delta\pi$ coupling shown in figure 16. We note that the seagull terms (diagrams (d) and (e)) in the Born diagrams are relatively small compared to the other diagrams. In addition, for the $\Delta(1232)$-terms, diagrams (e), (f), (g) and (h) are not included for the same reason. However, we find that, in general the $\Delta(1232)$-terms contribute significantly at all the energies for this particular isospin channel. To be precise, the Kroll-Ruderman terms (diagram (b)), the pion-exchange terms (diagram (c)) and the $\Delta\gamma\Delta$ coupling terms (diagram (d)) with a Δ^{++} are the most important. This is due to the fact that the Δ^{++} states have an isospin coefficient 1 whereas for the Δ^0 states, this isospin coefficient is $\frac{1}{\sqrt{3}}$. In addition, we observe that the contributions of the $N^*(1520)$ are small compared to that of the $\Delta(1232)$ but present a peak at about 730 MeV which is the source of the peak of the total cross section. We also note that the main contribution for $N^*(1520)$ arises from the S-wave $\Delta^{++}\pi^-$ final state, but not the D-wave part.

We note that in producing the contribution of the $\Delta(1232)$-terms (figure 14) in the $\gamma p \to \pi^+\pi^- p$ channel, an absorptive factor has been attached to each vertex of diagrams containing the Δ^{++} state in order to reduce the Δ-contribution. Figure 18 shows the contributions of the $\Delta(1232)$-terms with and without the absorptive effect. In this calculation, we use the Eikonal [56, 57] model in which the absorptive factor is

$$C_\Delta = \left(1 - \zeta_\Delta e^{-\frac{(J-\frac{1}{2})^2}{2A_\Delta \vec{P_\Delta}^2}}\right)^{\frac{1}{2}}, \tag{47}$$

where $J = \frac{3}{2}$ and $\vec{P_\Delta}$ are respectively the spin and the three-momentum of the Δ. ζ_Δ and A_Δ are some parameters that we choose to obtain the best fit for our calculation. In this work, we choose $\zeta_\Delta = 0.45$ and $A_\Delta = 50$ GeV^{-2}. We remark that this type of factor has not been introduced in the calculation of the single pion photoproduction because the Δ^{++} does not appear in that process. For the same reason, we do not use this factor for the $\gamma p \to \pi^0\pi^0 p$ and $\gamma p \to \pi^+\pi^0 n$ channels.

The ρ-terms (figure 13), as well as the $N^*(1440)$ contribution are very small for the $\pi^+\pi^- p$ isospin channel. However, the $N^*(1440)$ is expected to give a larger relative contribution for the $\pi^0\pi^0 p$ channel. $N^*(1535)\frac{1}{2}^-$ which decays almost equally into πN and ηN does not affect the cross section significantly. Resonances such as $N^*(1600)\frac{3}{2}^+$ and $N^*(1620)\frac{1}{2}^-$, both with isospin $I = \frac{3}{2}$, and higher resonances are not included as their contributions are thought to be irrelevant at this energy range (E_γ=0-800 MeV) and should not modify the total cross section significantly. However, this hypothesis must be tested. The experimental data presented in this work are taken from [26], the DAPHNE data obtained in 1995.

In figure 20, Born, Δ and $N^*(1520)\Delta\pi$-terms contributions are shown for the double neutral pion channel. All Δ-Kroll-Ruderman terms and the pion-exchange terms vanish as photons do not couple to neutral pions. Indeed, Δ terms are relatively small. On the other hand, the $N^*(1520)$-terms contribute significantly in this channel and the $N^*(1440)$-terms present a peak at about 650 MeV.

For the $\gamma p \to \pi^+\pi^0 n$ isospin channel, we plot in figure 21 the contributions

of the Born terms, Δ, $N^*(1440)$ and $N^*(1520)$ terms. We claim that there is a decrease of Δ contribution compared to the $\gamma p \to \pi^+\pi^- p$. This is due to the fact that the neutral pions do not couple with photons and that a few significant Feynman diagrams do vanish. However, we still see the peak of $N^*(1520)$ terms at about 730 MeV.

Figures 22 to 36 present total cross sections of $\gamma p \to \pi^+\pi^- p$, $\gamma p \to \pi^0\pi^0 p$ and $\gamma p \to \pi^+\pi^0 n$ processes. All terms that we previously mentioned are included. In addition, diagram (d) of figure 14 with the magnetic moment vertex $\bar{u}_\lambda(p_f)(k_s^* + T_\Delta k_v^*)\gamma_\mu\gamma_\nu F^{\mu\nu}u^\lambda(p_i)$ is taken into account. Diagrams (a) and (b) of both figures 15 and 16 are also included where the thick solid lines are the $\Delta(1232)$ resonances.

In table VIII, we show parameters extracted from individual fits of the three processes. $T^1_{\Delta\pi\Delta}$ and $T^2_{\Delta\pi\Delta}$ are the parameters describing the $\Delta\pi\Delta$ coupling. k_s^* and k_v^* are respectively the isoscalar and isovector anomalous magnetic moments of the $\Delta\gamma\Delta$ coupling and a_1, a_2 and a_3 are the parameters for the $\Delta\rho N$ coupling. In addition, values of χ^2 and N(number of data points) are given. The first row corresponds to the $\gamma p \to \pi^+\pi^- p$ process. Total cross section and several contributions are shown in figure 22. χ^2 per degree of freedom is $\chi^2_{DOF} = 2.90$. We observe that we obtain good agreement with the experimental data up to $E_\gamma = 800$ MeV. The second row corresponds to the $\gamma p \to \pi^0\pi^0 p$ process and the fit is presented in figure 23 with $\chi^2_{DOF} = 5.32$. Our calculation fits quite well the experimental data. For the $\gamma p \to \pi^+\pi^0 n$ process, parameters are given in the third row and calculation is given in figure 24. We reproduce pretty well the total cross section up to $E_\gamma = 750$ MeV, but there is a significant discrepancy above that energy. χ^2 per degree of freedom is $\chi^2_{DOF} = 20.43$ which is much higher compared to the those of the previous processes. We note that a pretty good fit usually gives a χ^2 per degree of freedom about 1 to 3 (see for instance figure 2). Consequently, our model fails to fit the $\gamma p \to \pi^+\pi^0 n$ process with a reasonable value of χ^2_{DOF}. Thus, we will consider giving different weight to the χ^2 corresponding to this process when simultaneously fitting these three processes.

In table IX, we present different values of coupling constants extracted from simultaneous fits. Parameters in the first row are derived by simultaneously fitting

the total cross sections of $\gamma p \to \pi^+\pi^- p$, $\gamma p \to \pi^0\pi^0 p$ and $\gamma p \to \pi^+\pi^0 n$ processes with equal weight. This means that $\chi^2 = \chi_1^2 + \chi_2^2 + \chi_3^2$. The fits are shown in figures 25, 26 and 27, and $\chi^2_{DOF} = 12.91$. Consequently, we reproduce pretty well the total cross section of the $\pi^+\pi^0 n$ channel up to $E_\gamma = 760$ MeV. After that, our fit keeps rising instead of decreasing with the data points. On the other hand, we poorly reproduce the total cross sections of both $\pi^+\pi^- p$ and $\pi^0\pi^0 p$ channels.

Parameters in the second and third rows are obtained by simultaneously fitting the three total cross sections and by giving different weight to χ_3^2. For the second row, we take $\chi^2 = \chi_1^2 + \chi_2^2 + 0.50\chi_3^2$ and the value of χ^2 per degree of freedom is $\chi^2_{DOF} = 9.32$. The fits are presented in figures 28, 29 and 30. For the third row, we choose $\chi^2 = \chi_1^2 + \chi_2^2 + 0.10\chi_3^2$ which yields $\chi^2_{DOF} = 5.39$ and the fits are shown in figures 31, 32 and 33.

Next, we drop the $\pi^+\pi^0 n$ channel and simultaneously fit only the total cross sections of $\gamma p \to \pi^+\pi^- p$ and $\gamma p \to \pi^0\pi^0 p$. Extracted parameters are shown in the fourth row. We note that these two processes form the pair that yields the lowest value of χ^2_{DOF} among the other pairs. The fits are presented in figures 34 and 35, and figure 36 is then plotted by using the same parameters. The value of χ^2 per degree of freedom is $\chi^2_{DOF} = 3.67$.

We remark that for the $N(1440)$, we choose $\Gamma_{1440} = 140$ MeV. With this choice, contribution of diagrams in figure 14, except the seagull terms (the last diagram and its cross term) are irrelevent to the total cross sections. For the $\gamma p \to \pi^+\pi^- p$ and $\gamma p \to \pi^+\pi^0 n$ processes, the isoscalar seagull term almost cancels the isovector one with our choice of parameters ($\lambda_1^\star = 4.75$ and $F_\pi^\star = 0.053$). As a result, their contributions to both total cross sections are very small. However, for the $\gamma p \to \pi^0\pi^0 p$ process, the isovector part does not contribute. The isoscalar term presents a peak around $E_\gamma = 650$ MeV, contributes significantly (figure 20) to the total cross section and plays a major role in fitting the experimental data.

TABLE VIII: Table of parameters; these parameters are obtained by respectively fitting the $\pi^+\pi^-p$, $\pi^0\pi^0p$ and $\pi^+\pi^0n$ channels.

$T^1_{\Delta\pi\Delta}$	$T^2_{\Delta\pi\Delta}$	$k^\star_s$	$k^\star_v$	a_1	a_2	a_3	χ^2	N
-2.012	-0.511	0.816	-0.145	3.869	-0.579	66.412	98.66	41
-6.071	-0.360	1.807	-1.596	3.727	4.824	-31.676	26.63	12
1.196	-0.874	0.476	-0.250	-10.828	0.316	42.146	102.15	12

TABLE IX: Table of parameters; the first three rows are obtained by simultaneously fitting all three processes, and parameters in the fourth row are extracted by simultaneously fitting only the $\pi^+\pi^-p$ and $\pi^+\pi^0n$ channels.

$T^1_{\Delta\pi\Delta}$	$T^2_{\Delta\pi\Delta}$	$k^\star_s$	$k^\star_v$	a_1	a_2	a_3	χ^2	N
-1.350	-.0406	0.638	-0.168	2.645	6.105	22.168	749.626	65
-1.741	-0.285	0.567	-0.130	2.881	6.093	25.495	541.022	65
-2.726	0.194	0.396	-0.042	2.312	4.116	37.105	313.023	65
-4.176	0.703	0.307	-0.069	1.672	1.897	47.182	213.496	53

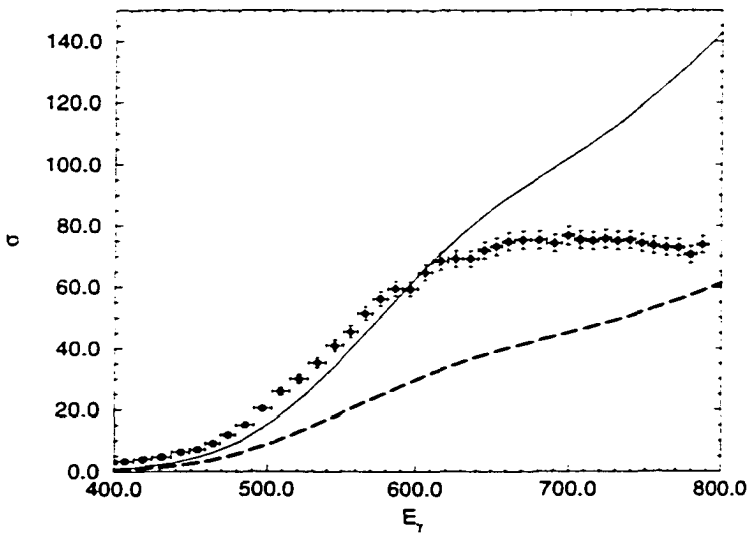

FIG. 18: Contribution of the $\Delta(1232)$-terms. The solid line represents the Δ-contribution without the absorptive factor. The long-dashed line is the contribution with the factor. The experimental data are taken from [26]

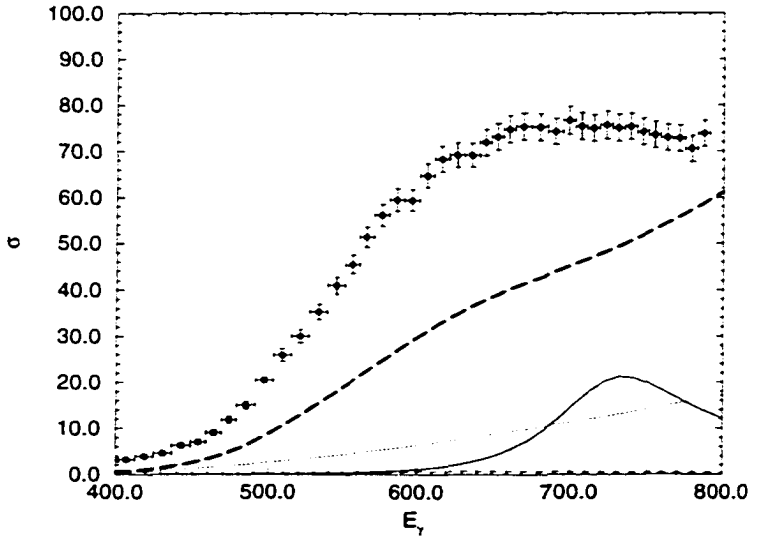

FIG. 19: Cross section (μb) of $\gamma p \to \pi^+\pi^- p$. The dotted line is the Born contribution, the thick long-dashed line corresponds to the Δ, the dashed line to the $N^*(1440)$ and the solid line to the $N^*(1520)$ contribution.

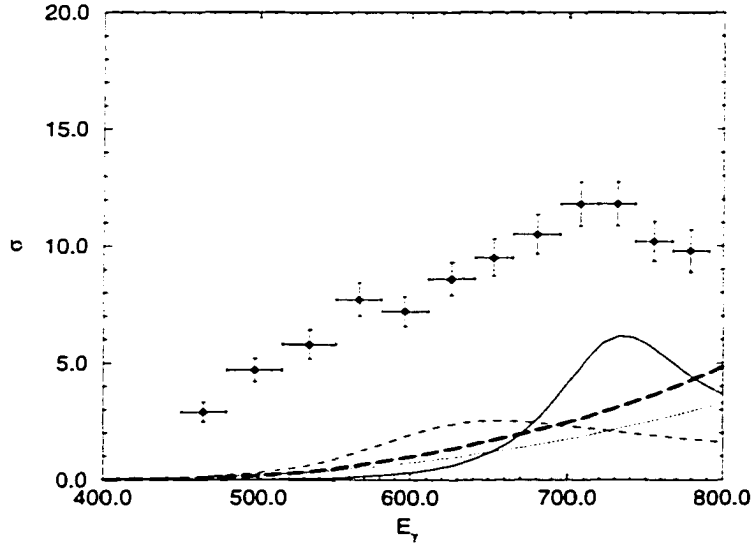

FIG. 20: Cross section (μb) of $\gamma p \rightarrow \pi^0\pi^0 p$ *vs.* Lab photon kinetic energy E_γ(MeV). The key of this figure is as in figure 19.

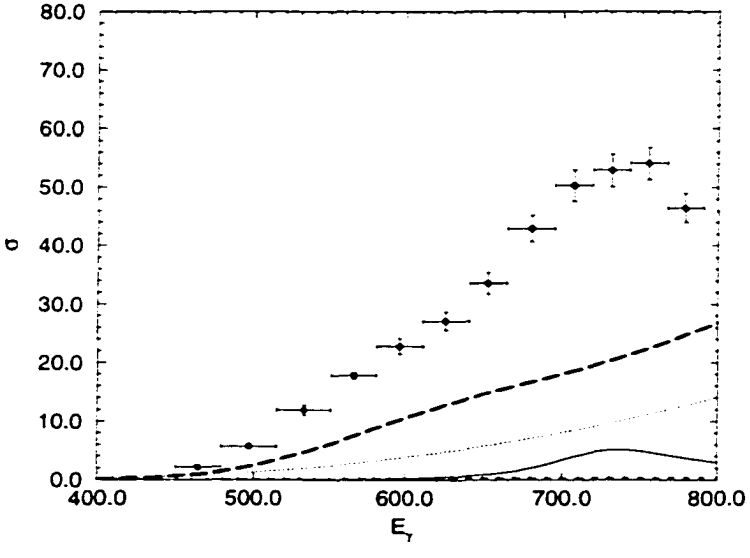

FIG. 21: Cross section (μb) of $\gamma p \rightarrow \pi^+\pi^0 n$ *vs.* Lab photon kinetic energy E_γ(MeV). The key of this figure is as in figure 19.

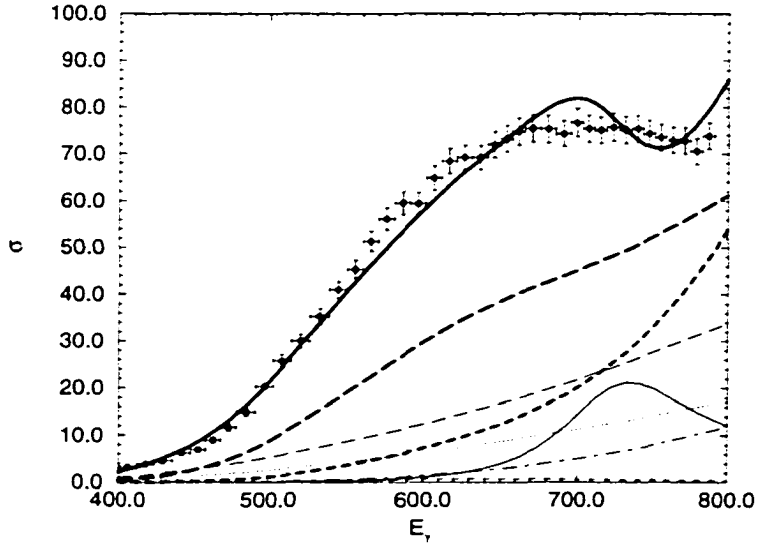

FIG. 22: Total cross section (μb) of $\gamma p \to \pi^+\pi^- p$ *vs.* Lab photon kinetic energy E_γ(MeV). The thick continuous line corresponds to the total cross section, the thick long-dashed line to the Δ contribution, the long-dash-dotted line to the contribution of diagrams with the magnetic moment $\Delta\gamma\Delta$ vertices, the thick dashed line to the contribution of diagrams with $\Delta\rho N$ vertices, the long-dashed line to the contribution of diagrams with $\Delta\pi\Delta$ vertices, the solid line to the contribution of diagrams with $N(1520)\pi\Delta$ vertices, the dotted line to the Born terms and the dashed line to the N(1440) contribution. The N(1535) contribution is very small and does not appear in the figure. The data sets are taken from Daphne 1995. This fit is obtained by fitting only the $\gamma p \to \pi^+\pi^- p$ reaction data to our calculation.

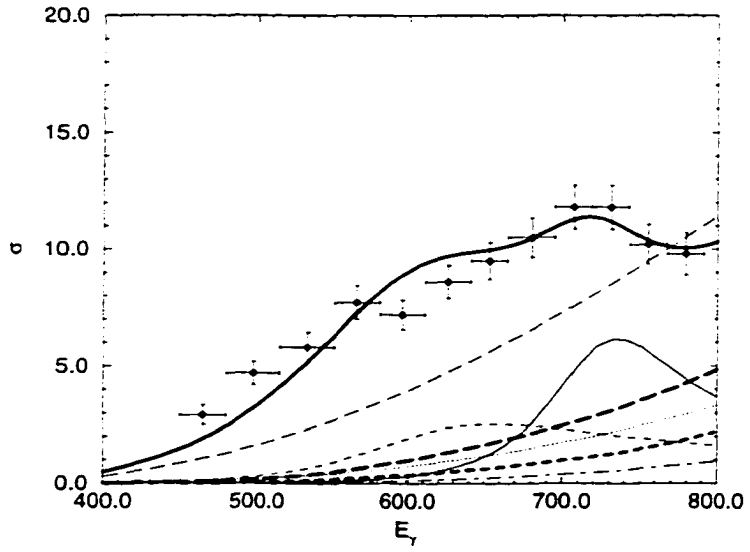

FIG. 23: Total cross section (μb) of $\gamma p \to \pi^0\pi^0 p$ *vs.* Lab photon kinetic energy E_γ(MeV). The key of this figure is as in figure 22. This fit is obtained by fitting only the $\gamma p \to \pi^0\pi^0 p$ reaction data to our calculation.

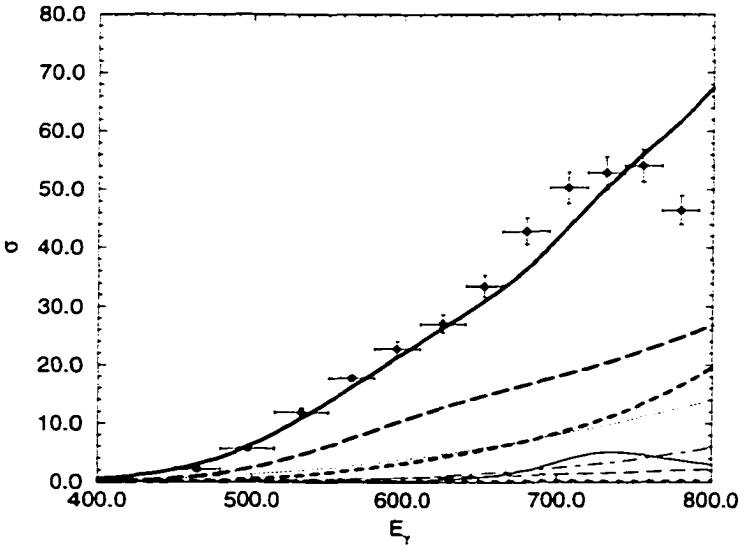

FIG. 24: Total cross section (μb) of $\gamma p \to \pi^+\pi^0 n$ *vs.* Lab photon kinetic energy E_γ(MeV). The key of this figure is as in figure 22. This fit is obtained by fitting only the $\gamma p \to \pi^+\pi^0 n$ reaction data to our calculation.

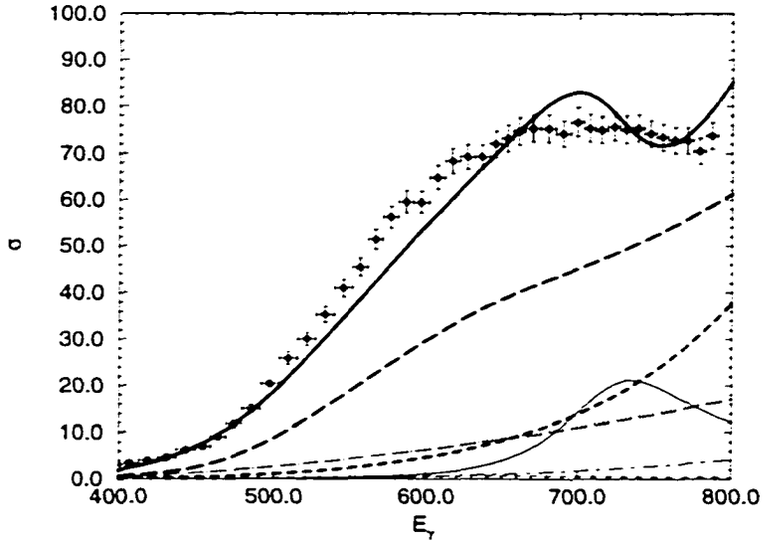

FIG. 25: Total cross section (μb) of $\gamma p \rightarrow \pi^+\pi^- p$ *vs.* Laboratory kinetic energy E_γ(MeV). The key of this figure is as in figure 22. This fit is obtained by simultaneously fitting the three processes with $\chi^2 = \chi_1^2 + \chi_2^2 + \chi_3^2$.

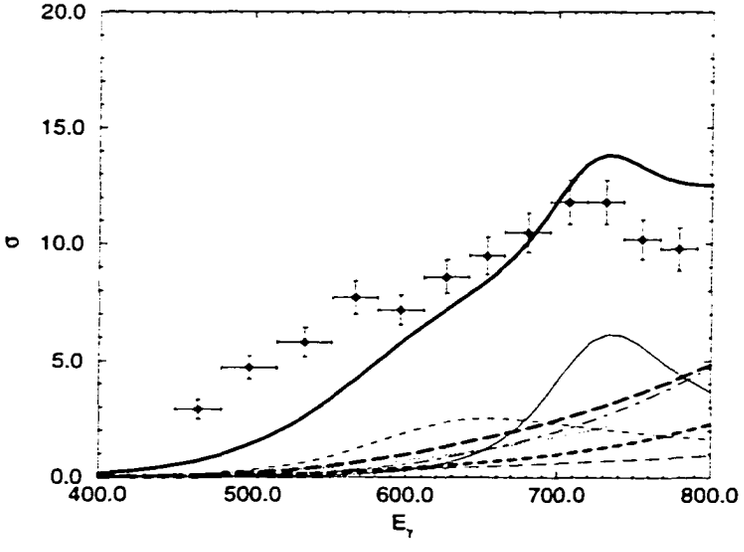

FIG. 26: Total cross section (μb) of $\gamma p \rightarrow \pi^0\pi^0 p$ *vs.* Laboratory kinetic energy E_γ(MeV). The key of this figure is as in figure 22. This fit is obtained by simultaneously fitting the three processes with $\chi^2 = \chi_1^2 + \chi_2^2 + \chi_3^2$.

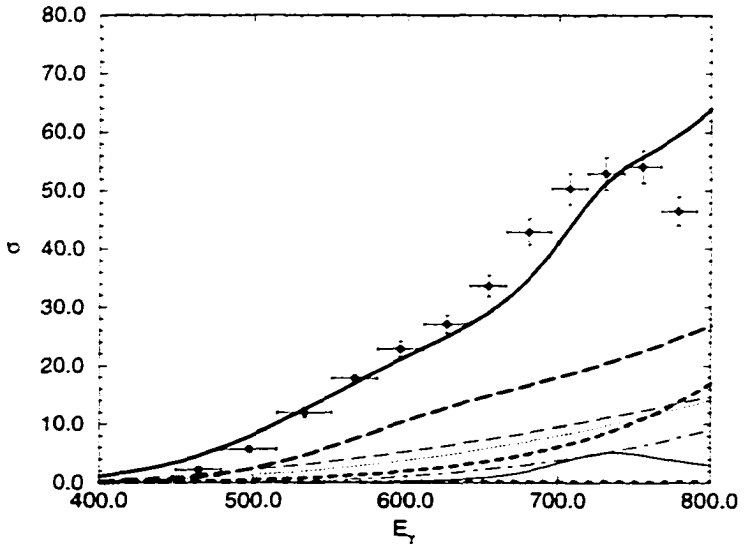

FIG. 27: Total cross section (μb) of $\gamma p \to \pi^+\pi^0 n$. The key of this figure is as in figure 22. This fit is obtained by simultaneously fitting the three processes to our theoretical calculation with $\chi^2 = \chi_1^2 + \chi_2^2 + \chi_3^2$.

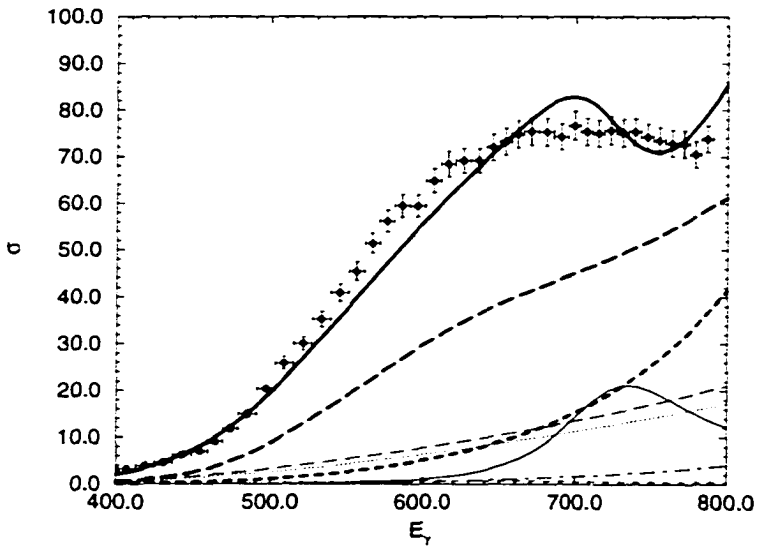

FIG. 28: Total cross section (μb) of $\gamma p \to \pi^+\pi^- p$. The key of this figure is as in figure 22. This fit is obtained by simultaneously fitting the three processes to our theoretical calculation with $\chi^2 = \chi_1^2 + \chi_2^2 + 0.50\chi_3^2$.

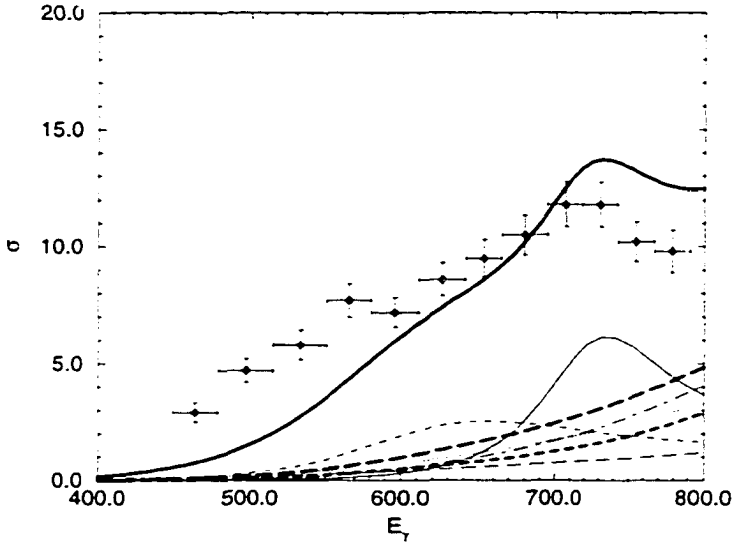

FIG. 29: Total cross section (μb) of $\gamma p \to \pi^0\pi^0 p$. The key of this figure is as in figure 22. This fit is obtained by simultaneously fitting the three processes to our theoretical calculation with $\chi^2 = \chi_1^2 + \chi_2^2 + 0.50\chi_3^2$.

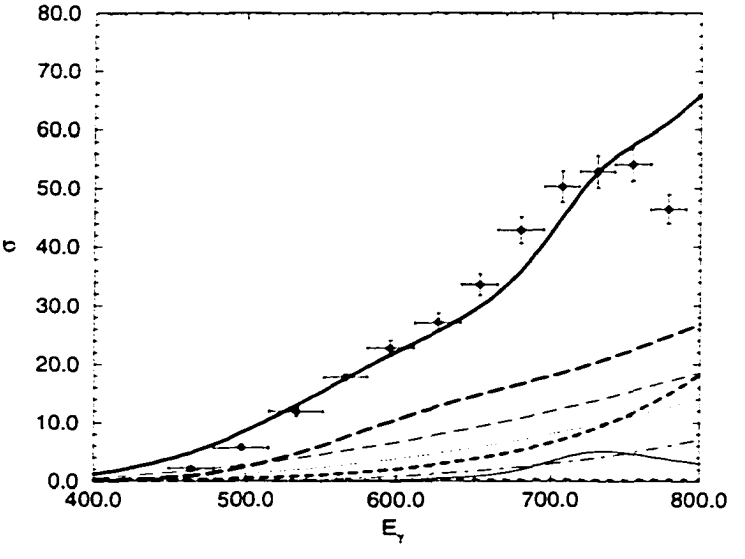

FIG. 30: Total cross section (μb) of $\gamma p \to \pi^+\pi^0 n$. The key of this figure is as in figure 22. This fit is obtained by simultaneously fitting the three processes to our theoretical calculation with $\chi^2 = \chi_1^2 + \chi_2^2 + 0.50\chi_3^2$.

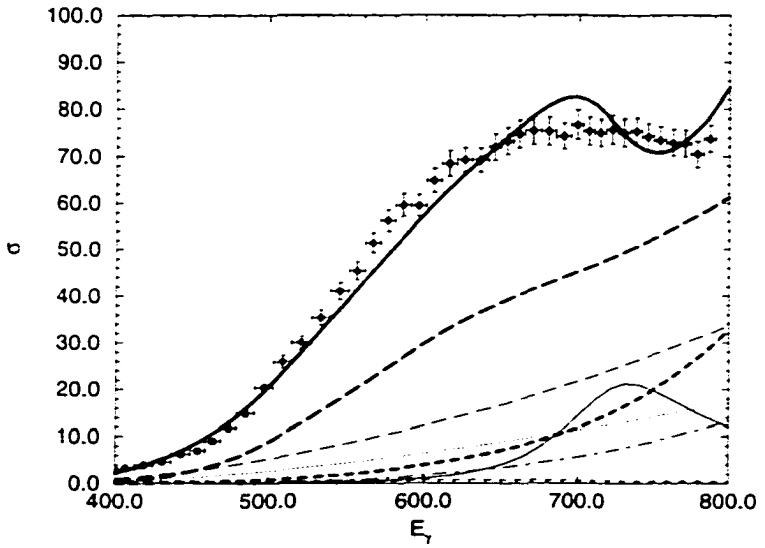

FIG. 31: Total cross section (μb) of $\gamma p \to \pi^+\pi^- p$. The key of this figure is as in figure 22. This fit is obtained by simultaneously fitting the three processes to our theoretical calculation with $\chi^2 = \chi_1^2 + \chi_2^2 + 0.10\chi_3^2$.

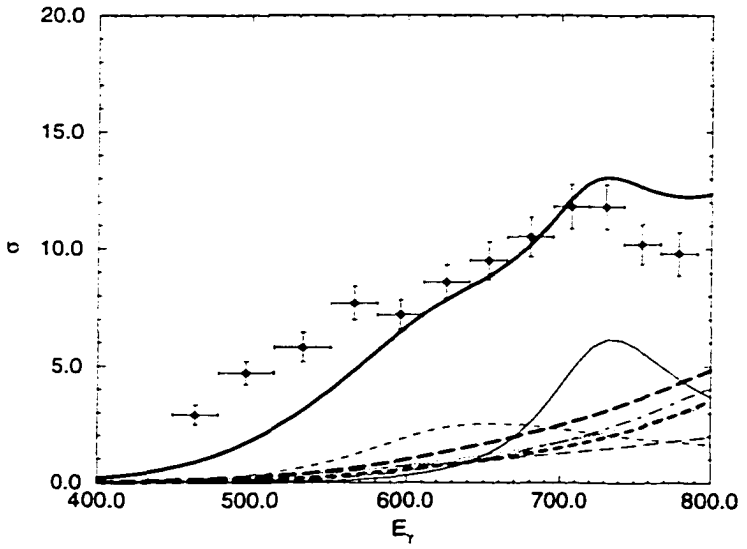

FIG. 32: Total cross section (μb) of $\gamma p \to \pi^0\pi^0 p$. The key of this figure is as in figure 22. This fit is obtained by simultaneously fitting the three processes to our theoretical calculation with $\chi^2 = \chi_1^2 + \chi_2^2 + 0.10\chi_3^2$.

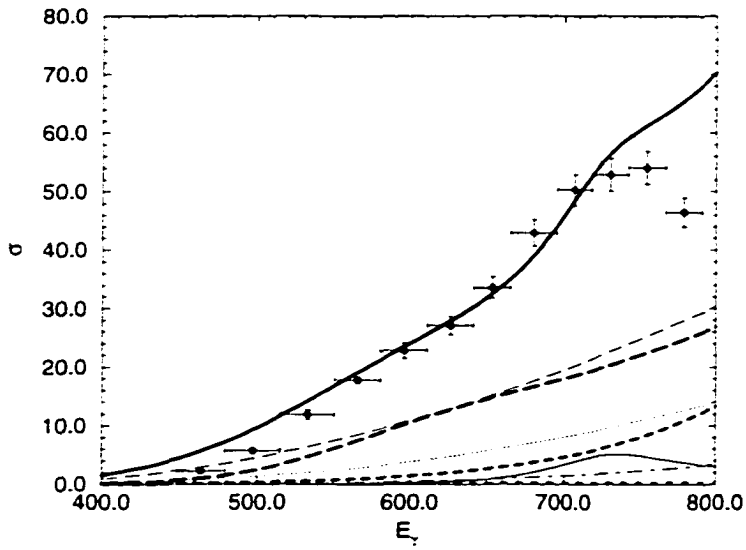

FIG. 33: Total cross section (μb) of $\gamma p \to \pi^+\pi^0 n$. The key of this figure is as in figure 22. This fit is obtained by simultaneously fitting the three processes to our theoretical calculation with $\chi^2 = \chi_1^2 + \chi_2^2 + 0.10\chi_3^2$.

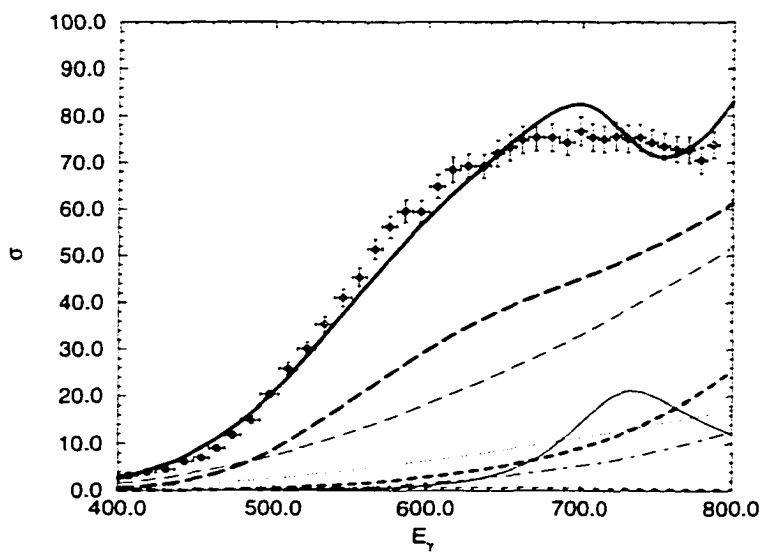

FIG. 34: Total cross section (μb) of $\gamma p \to \pi^+\pi^- p$. The key of this figure is as in figure 22. This fit is obtained by simultaneously fitting the $\gamma p \to \pi^+\pi^- p$ and $\gamma p \to \pi^0\pi^0 p$ processes to our theoretical calculation with $\chi^2 = \chi_1^2 + \chi_2^2$.

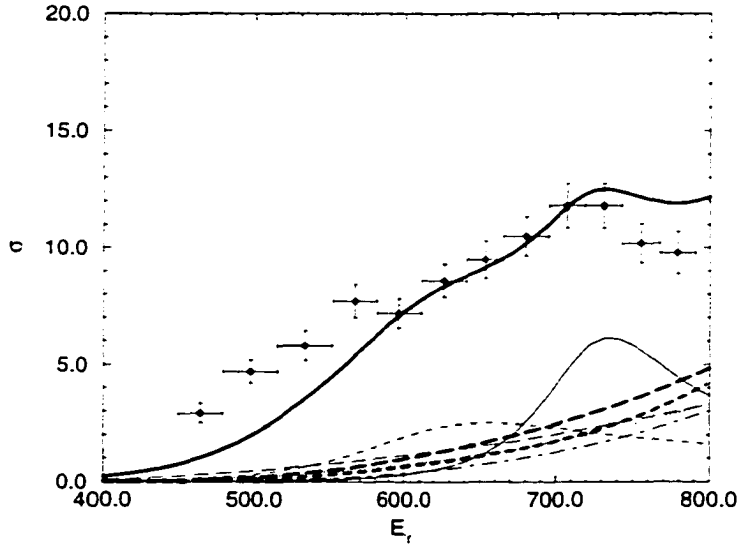

FIG. 35: Total cross section (μb) of $\gamma p \to \pi^0\pi^0 p$ *vs.* Laboratory kinetic energy E_γ(MeV). The key of this figure is as in figure 22. This fit is obtained by simultaneously fitting the $\gamma p \to \pi^+\pi^- p$ and $\gamma p \to \pi^0\pi^0 p$ processes to our theoretical calculation with $\chi^2 = \chi_1^2 + \chi_2^2$.

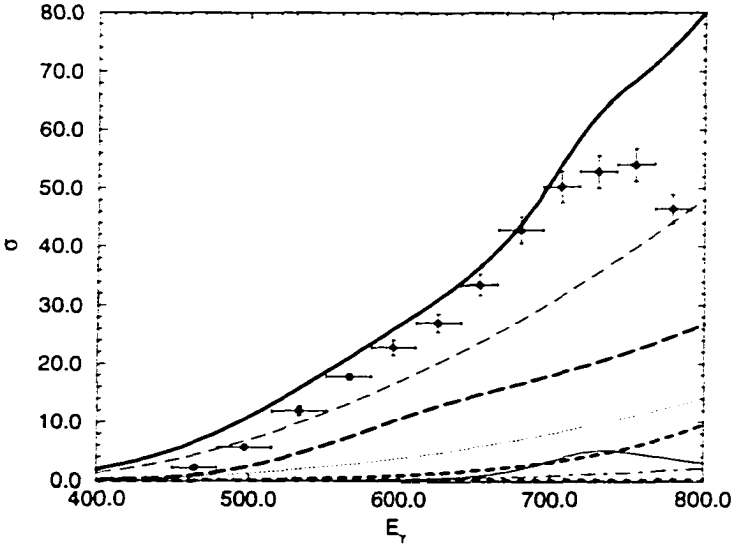

FIG. 36: Total cross section (μb) of $\gamma p \to \pi^+\pi^0 n$ *vs.* Laboratory kinetic energy E_γ(MeV). The key of this figure is as in figure 22. This fit is obtained by using the parameters extracted from the previous fit.

Chapter 6

STUDY OF THE AXIAL ANOMALY

6.1 The axial anomaly and the vertex $\gamma \to 3\pi$

Symmetry breaking in physics can occur through several different mechanisms. These mechanisms include explicit, spontaneous, dynamical, and quantum mechanical symmetry breaking terms. Quantum mechanical symmetry breaking occurs when a symmetry that is present in a classical Lagrangian is broken when the theory is quantized. This leads to the occurence of an 'anomaly'. In early theoretical investigations of π^0 decay through two methods, namely the partially conserved axial current (PCAC) and current algebra, it was discovered that an anomalous axial current is needed to explain the π^0 decay rate [59, 60]. Later, with the development of effective chiral Lagrangians, it was clear that the symmetry properties of these Lagrangians forbade the transition between an even and odd number of mesons, although these transitions are allowed by QCD and are observed in reactions such as $\pi^0 \to \gamma\gamma$ and $K\bar{K} \to \pi^+\pi^-\pi^0$. To amend this problem, the Wess-Zumino-Witten effective Lagrangian was constructed [61, 62]. While we do not reproduce here the structure of the axial anomaly in the Lagrangian, it is important to note that the expression has a known coefficient that depends only on the number of colors N_c and on the pion decay constant $F_\pi = 93.1 \pm 0.1$ MeV.

Thus, the axial anomaly allows the $\pi^0 \to \gamma\gamma$ process to proceed and to provide one of the widely noted methods for measuring the number of colors. The predicted amplitude for the $\pi^0 \to \gamma\gamma$ process is

$$A_{\pi\gamma\gamma} = \frac{\alpha N_c}{3\pi F_\pi} = 0.025 \text{ GeV}^{-1}. \quad (48)$$

For $N_c = 3$. The experimental result [63] yields $A_{\pi\gamma\gamma} = (0.0240 \pm 0.0003)$ GeV^{-1} which is in a good agreement with the predicted amplitude. This is generally regarded as an important triumph of QCD, both as a test of $N_c = 3$ and of the symmetries and anomalies of the theory.

The axial anomaly also predicts amplitudes for the reactions $\gamma \to \pi^+\pi^-\pi^0$, $\gamma \to K^+K^-\pi^0$ and $\gamma \to \pi^+\pi^-\eta_8$, where η_8 is the octet component of the η meson. The coupling constant $F^{3\pi}$ for the amplitude $\gamma \to 3\pi$ was first derived from $\pi^0 \to \gamma\gamma$ using PCAC [64, 65, 66], and later from the Wess-Zumino-Witten effective chiral Lagrangian. The coupling constant, given by

$$F^{3\pi} = \frac{eN_c}{12\pi^2 F_\pi^3} = 9.5 \text{ GeV}^{-3} \quad (49)$$

is similar to the π^0 decay amplitude and it depends only on N_c and the pion decay constant.

R. A. Miskimen [58] *et al.*, have proposed to study the axial anomaly and measure $F^{3\pi}$ using the $\gamma\pi^+ \to \pi^+\pi^0$ reaction near threshold. Cross sections for the $\gamma\pi^+ \to \pi^+\pi^0$ will be obtained from measurement of $\gamma p \to \pi^+\pi^0 n$ near $t \approx -m_\pi^2$ where t is the square of the momentum transfered of the intermediate pion. In fact, preliminary cross sections for the $\gamma p \to \pi^+\pi^0 n$ process have been measured using the CEBAF Large Acceptance Spectrometer (CLAS) with tagged photon energies between 0.5 and 2.4 GeV. The π^+ is detected using the time-of-flight and tracking system. The π^0 is detected via reconstruction of the invariant mass of its two decay photons, which are detected by an electromagnetic calorimeter. From the cross section measurement, the $\gamma \to 3\pi$ structure function ($F^{3\pi}$) can be extracted at low t, and its momentum dependence can be evaluated. In the chiral limit, $F^{3\pi}$ is related to the $\pi^0 \to 2\gamma$ amplitude. Within the context of the chiral

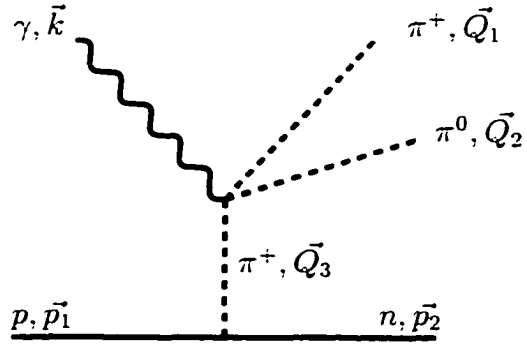

FIG. 37: Feynman diagram showing the anomalous vertex $\gamma 3\pi$. The continuous straight lines are baryons. Dashed lines are pions and the wavy curve is the photon.

anomaly, which successfully predicts the decay of the π^0, the $\gamma \to 3\pi$ vertex can be used to evaluate the validity of chiral symmetry in QCD.

Figure (37) shows the t-channel pion exchange diagram for the reaction and how it is related to $\gamma\pi^+ \to \pi^+\pi^0$.

Using the kinematics of figure (37), we define $t' = (k - Q_1)^2$, $u = (k - Q_2)^2$ and the already defined $s_{\pi\pi} = (Q_1 + Q_2)^2$. The constant chiral value for $F^{3\pi}$ is strictly valid in the limit where all pairs of invariant masses are zero, $k^2 = s_{\pi\pi} = t' = u = 0$. In the physical region, where $s_{\pi\pi} > 4m_\pi^2$ and $t = Q_3^2 = (p_2 - p_1)^2 < 0$, $F^{3\pi}$ acquires momentum dependence on k^2, $s_{\pi\pi}$, t' and u.

6.2 Differential cross section

The differential cross section for the process is given by

$$d\sigma = \frac{1}{(2j+1)} \frac{|\mathcal{M}|^2 \, ds_{\pi\pi} d\Omega^*_{\pi\pi} d\cos\theta_2}{256(2\pi)^4 (W^2 - M^2) W^2 \sqrt{s_{\pi\pi}}} \lambda^{\frac{1}{2}}(s_{\pi\pi}, m_\pi^2, m_\pi^2) \lambda^{\frac{1}{2}}(W^2, s_{\pi\pi}, M^2), \tag{50}$$

where j is the spin of the incoming nucleon and θ_2 is the angle between the incoming photon and the outgoing nucleon.

Writing t in term of θ_2, we obtain

$t = (p_1 - p_2)^2 = p_1^2 + p_2^2 - 2p_1.p_2 = 2M^2 - 2(E_1E_2 - \vec{p_1}.\vec{p_2}) = 2M^2 - 2(E_1E_2 - 2|\vec{p_1}||\vec{p_2}|\cos\theta_{12})$, where θ_{12} is the angle between $\vec{p_1}$ and $\vec{p_2}$. Now, using $\theta_{12} = \pi - \theta_2$ and $d\cos\theta_2 = -dt/(2|\vec{p_1}||\vec{p_2}|)$ the cross section can be rewritten as

$$\frac{d\sigma}{dtds_{\pi\pi}} = \frac{1}{2(2j+1)} \frac{d\Omega^*_{\pi\pi}\,|\mathcal{M}|^2\,\lambda^{\frac{1}{2}}(s_{\pi\pi}, m_\pi^2, m_\pi^2)\lambda^{\frac{1}{2}}(W^2, s_{\pi\pi}, M^2)}{256(2\pi)^4(W^2 - M^2)W^2\sqrt{s_{\pi\pi}}|\vec{p_1}||\vec{p_2}|}, \qquad (51)$$

where $\lambda(a,b,c) = (a^2 + b^2 + c^2 - 2ab - 2ac - 2bc)$ is the Källen function.

In figure 38, we present two different sets of differential cross sections $d\sigma/dtds_{\pi\pi}$ (nb/m_π^4) *vs.* $s_{\pi\pi} = (Q_1 + Q_2)^2$ (m_π^2) for the $\gamma p \to \pi^+\pi^0 n$ process. The solid lines correspond to the contribution of all the Born terms whereas the long-dashed lines are the Born terms without the anomaly contribution. The first set of curves (the one with higher cross section at higher $s_{\pi\pi}$) corresponds to $t = -m_\pi^2$ and the second one to $t = -5m_\pi^2$. These curves are plotted at photon energy $E_\gamma = 1.0$ GeV and the coupling constant $F^{3\pi}$ is taken to be 9.5 GeV^3. Both sets show that the effects of the anomaly terms in the Born terms are more perceptible at lower t and at higher $s_{\pi\pi}$. Figures 39 and 40 show similar sets of curves with photon energies respectively $E_\gamma = 1.5$ GeV and $E_\gamma = 2.0$ GeV.

Figure 41 presents the contributions of the anomaly terms for different energies and near threshold. These curves show that for a given kinematically allowed value of $s_{\pi\pi}$, the contribution of the anomaly term is less relevent for higher energy E_γ. However, its contribution is more significant at higher energy with higher $s_{\pi\pi}$.

In figure 42, we show differential cross sections $d\sigma/dtds_{\pi\pi}$ (nb/m_π^4) *vs.* t (m_π^2) for the $\gamma p \to \pi^+\pi^0 n$ process for different values of the photon energies $E_\gamma = 1.0$ GeV, $E_\gamma = 1.5$ GeV, and $E_\gamma = 2.$ GeV, with $s_{\pi\pi} = 10m_\pi^2$ and $F^{3\pi} = 9.5$ GeV^3. We note that as the energy E_γ increases, the contribution of the anomaly term (figure 37) decreases and the difference between the two curves (solid and long-dashed) becomes imperceptible. This decrease of the anomaly term is also shown in figure 43. Thus, we remark that the anomaly contribution is more likely to be separated from the Born terms at lower energy and near threshold $t \approx -m_\pi^2$.

In figure 44, we include the Born term, the ρ and the Δ, and plot the differential cross sections $d\sigma/dtds_{\pi\pi}$ (nb/m_π^4) *vs.* $s_{\pi\pi} = (Q_1 + Q_2)^2$ (m_π^2) for $E_\gamma = 1.5$ GeV

and $t = -m_\pi^2$. The solid line represents the contribution of the Born, ρ and Δ terms together whereas the long-dashed line represents those without the anomaly term. We again observe that the effect of the anomaly term is relevant at threshold and at higher $s_{\pi\pi}$. Furthermore, comparing figure 39 and figure 44 we remark that the main contribution to the differential cross section comes from the Born term but not from the ρ or the Δ term. The thick dot-dashed line corresponds to the anomaly alone whereas the thick long-dashed line corresponds to the difference between the full calculation and the calculation without the anomaly. In other words, the thick long-dashed line contains the interference term between the two calculations. Figure 45 shows the differential cross section $d\sigma/dtds_{\pi\pi}$ (nb/m_π^4) *vs.* t (m_π^2) with $E_\gamma = 1.5$ GeV and $s = 15\ m_\pi^2$. This again shows the relevance of the anomaly term at threshold.

We note that in these calculations, we have not introduced any type of form factors, and we have not taken into account the effect of the unitarity. Additionally, at this energy range ($E_\gamma = 1-2$ GeV), higher resonances such as the $\Delta(1600)$, $N(1620)$ $N(1650)$, and many more should be taken into consideration. For these reasons, our differential cross section results may not be valid in this high energy region. However, we have seen from figure 44 that the Born term is the most relevant contribution, and therefore inclusion of these higher resonances may not significantly affect the differential cross sections. Hence, we hope to observe the significance of the anomaly term in the process.

Another issue that may arise in extracting the anomaly term is to determine whether the contribution of the terms with the anomaly term is largely separated from the contribution of the terms without the anomaly one so that the extraction is feasible. This problem may occur if we need to take into account the uncertainties of the Δ term, for instance. To look at this, we present in each of the figures 46 and 47 two sets of curves. The first set (thick solid and thick dashed lines) corresponds to $f_{\pi\Delta N} = 2.22$ and the second set (non-thick lines) corresponds to $f_{\pi\Delta N} = 2.10$. The calculated value of $f_{\pi\Delta N}$ is 2.16 ± 0.06. The solid lines are the contribution of the Born term (including the anomaly), the ρ and Δ term, and the long-dashed lines represent the contribution without the anomaly term.

Thus, figure 46 shows that the contribution of the terms with the anomaly overlaps with that of the terms without the anomaly for all values of $s_{\pi\pi}$, and therefore extraction of the anomaly term may be difficult. On the other hand, we observe in figure 47 that both contributions start to separate at about $s_{\pi\pi} = 21\ m_\pi^2$ and the extraction becomes more feasible. The effect of this overlap can be minimized if we have a more precise value of $f_{\pi\Delta N}$.

We close this chapter by stating that we have examined a technique that examines the anomalous vertex $\gamma 3\pi$ and extracts the structure function $F^{3\pi}$through the measurement of the cross section of the $\gamma p \to \pi^+\pi^0 n$ process near $t \approx -m_\pi^2$ where t is the momentum transfer squared of the intermediate pion. We note that there is still much to be done in the framework of this model, such as the question of unitarity and the inclusion of more higher resonances, if we are to obtain a more reliable result from our calculation. In addition, precise physical properties of the other couplings should be used to be able to examine the small effect of the anomaly term. However, we remark that extraction of the structure function $F^{3\pi}$ is more realistic at higher energy and higher $s_{\pi\pi}$.

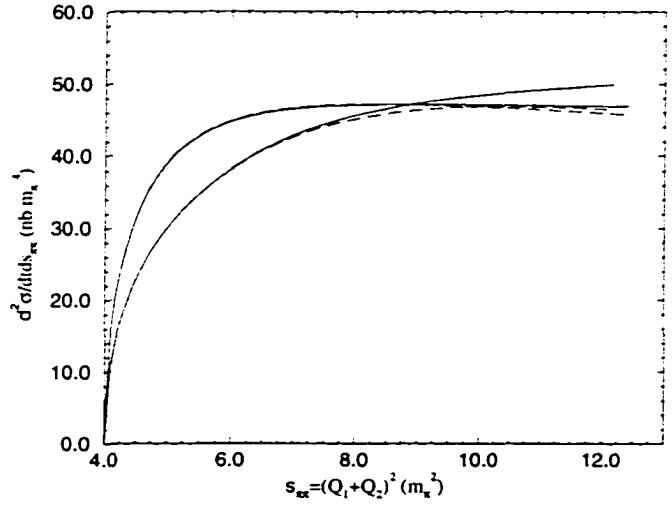

FIG. 38: Differential cross section $d\sigma/dtds_{\pi\pi}$ (nb/m_π^4) of $\gamma p \to \pi^+\pi^0 n$ *vs.* $s = (Q_1 + Q_2)^2$ (m_π^2) for $E_\gamma = 1.$ GeV and $F^{3\pi} = 9.5$ GeV^3. The solid line corresponds to the contribution of all the Born terms. The long-dashed line represents the Born terms without the anomaly term. The first set of curves (the one with higher cross section at higher s) corresponds to $t = -m_\pi^2$ and the second one to $t = -5m_\pi^2$.

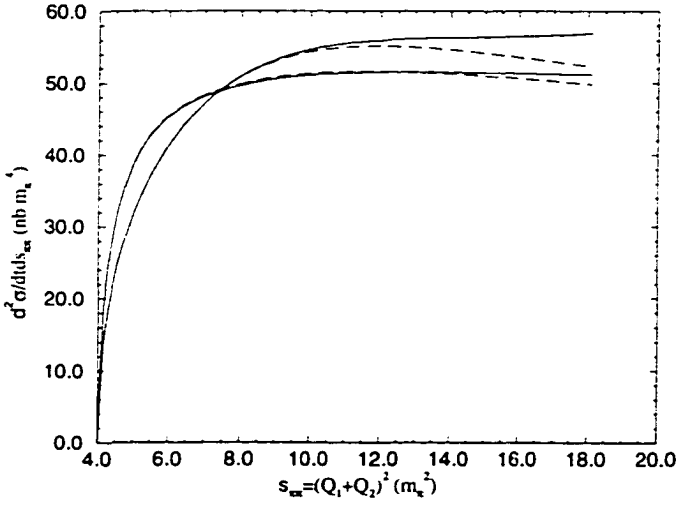

FIG. 39: Differential cross section $d\sigma/dtds_{\pi\pi}$ (nb/m_π^4) of $\gamma p \to \pi^+\pi^0 n$ *vs.* $s = (Q_1 + Q_2)^2$ (m_π^2) for $E_\gamma = 1.5$ GeV and $F^{3\pi} = 9.5$ GeV^3. The key of the figure is that of figure 38.

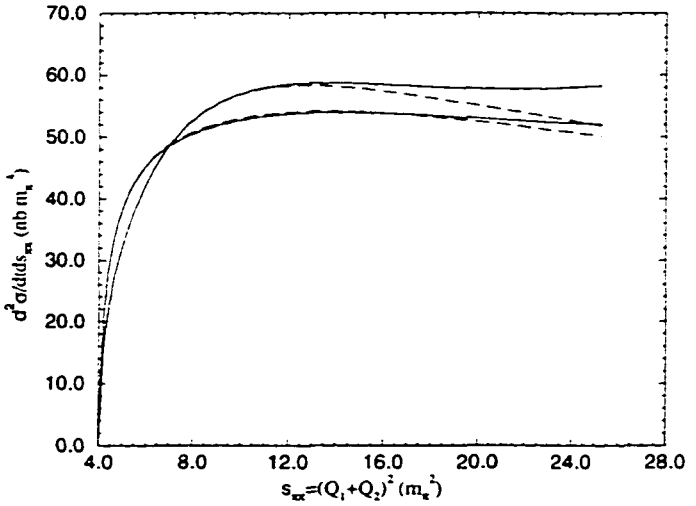

FIG. 40: Differential cross section $d\sigma/dtds_{\pi\pi}$ (nb/m_π^4) of $\gamma p \to \pi^+\pi^0 n$ *vs.* $s = (Q_1+Q_2)^2$ (m_π^2) for $E_\gamma = 2.$ GeV and $F^{3\pi} = 9.5$ GeV^3. The key of the figure is that of figure 38 .

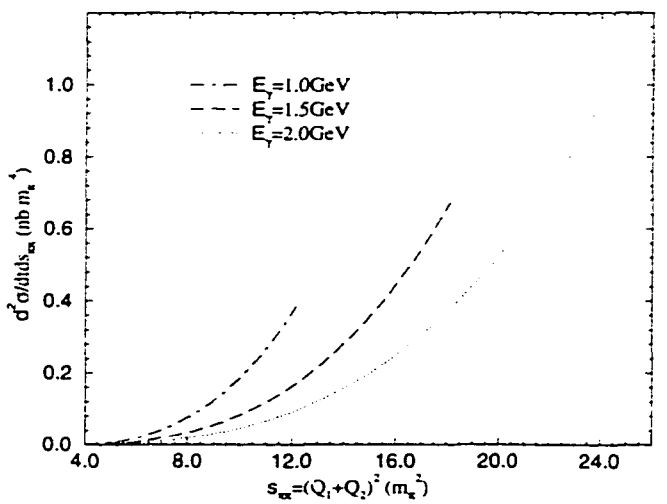

FIG. 41: Differential cross section $d\sigma/dtds_{\pi\pi}$ (nb/m_π^4) of $\gamma p \to \pi^+\pi^0 n$ *vs.* $s = (Q_1+Q_2)^2$ (m_π^2). Theses curves are the contributions of the anomaly terms alone for different energies. $t = -m_\pi^2$ and $F^{3\pi} = 9.5$ GeV^3.

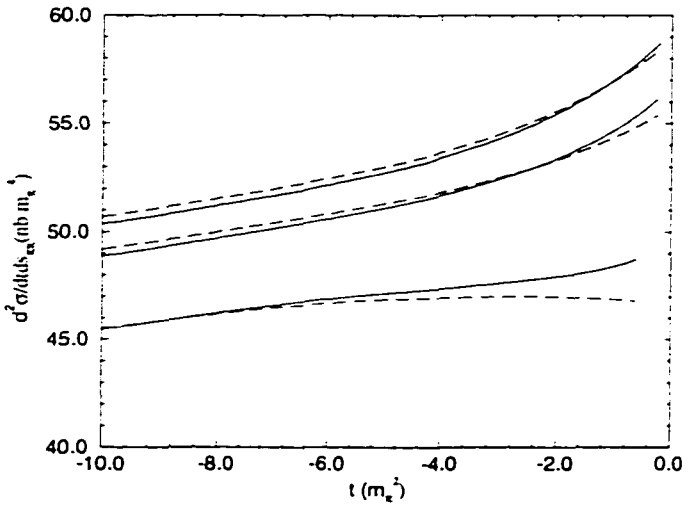

FIG. 42: Differential cross section $d\sigma/dtds_{\pi\pi}$ (nb/m_π^4) of $\gamma p \to \pi^+\pi^0 n$ *vs.* t (m_π^2). The solid curves are the contributions of all the Born terms and the long-dashed curves are those of the Born terms without the anomaly terms. These three sets of curves correspond respectively to $E_\gamma = 1.$ GeV, $E_\gamma = 1.5$ GeV, and $E_\gamma = 2.$ GeV where the lowest set corresponds to the lowest energy and so on. $s = 10m_\pi^2$ and $F^{3\pi} = 9.5$ GeV^3.

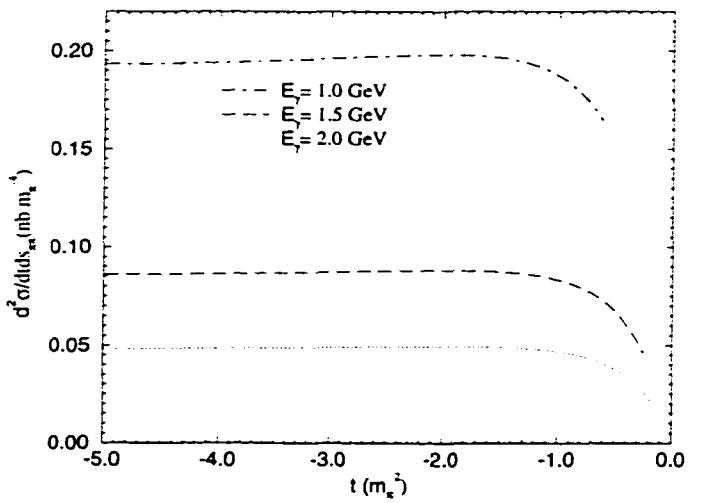

FIG. 43: Differential cross section $d\sigma/dtds_{\pi\pi}$ (nb/m_π^4) of $\gamma p \to \pi^+\pi^0 n$ *vs.* t (m_π^2). These curves are the contributions of the anomaly terms alone for different energies. $s = 10m_\pi^2$ and $F^{3\pi} = 9.5$ GeV^3.

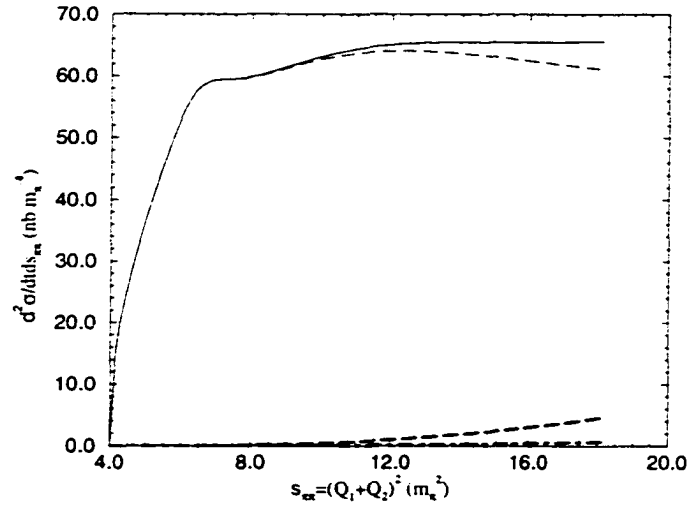

FIG. 44: Differential cross section $d\sigma/dtds_{\pi\pi}$ (nb/m_π^4) of $\gamma p \to \pi^+\pi^0 n$ *vs.* $s = (Q_1 + Q_2)^2$ (m_π^2) for $E_\gamma = 1.5$ GeV, $t = -m_\pi^2$ and $F^{3\pi} = 9.5$ GeV^3. The solid line corresponds to the contribution of the Born term, the ρ and Δ term. The long-dashed line represents all contributions without the anomaly term. The thick long-dashed line is the difference between the full calculation and the calculation without the anomaly, and the thick dot-dashed line corresponds to the anomaly term alone.

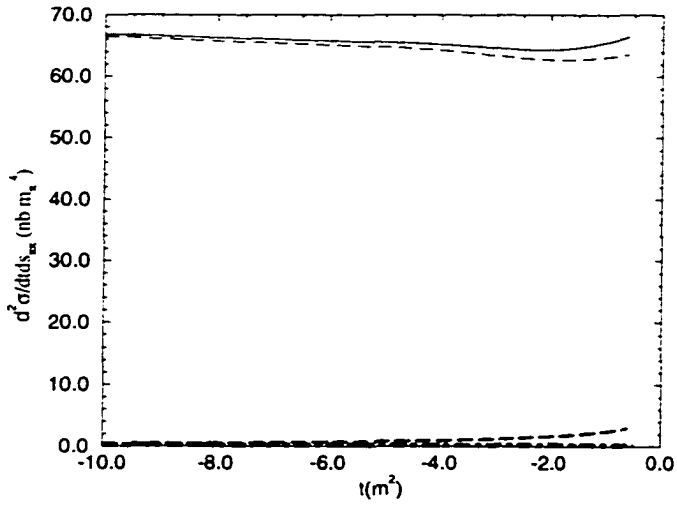

FIG. 45: Differential cross section $d\sigma/dtds_{\pi\pi}$ (nb/m_π^4) of $\gamma p \to \pi^+\pi^0 n$ *vs.* t (m_π^2). $E_\gamma = 1.5$ GeV. $s = 15m_\pi^2$ and $F^{3\pi} = 9.5$ GeV^3. The key of the figure is that of figure 44 .

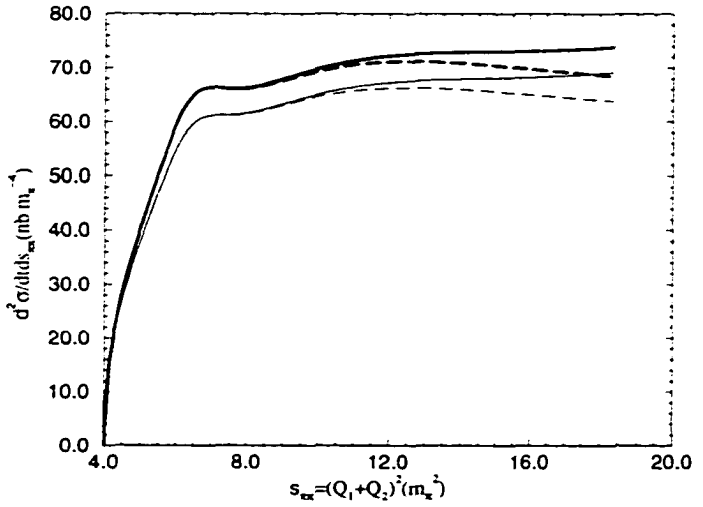

FIG. 46: Differential cross section $d\sigma/dtds_{\pi\pi}$ (nb/m_π^4) of $\gamma p \to \pi^+\pi^0 n$ *vs.* $s = (Q_1+Q_2)^2$ (m_π^2) for $E_\gamma = 1.5$ GeV, $t = -m_\pi^2$ and $F^{3\pi} = 9.5$ GeV^3. The solid lines are the contribution of the Born term (including the anomaly term), the ρ and Δ term, and the long-dashed lines represent the contribution without the anomaly term. In addition, both thick solid and thick long-dashed lines correspond to $f_{\pi\Delta N} = 2.22$ and the non-thick lines correspond to $f_{\pi\Delta N} = 2.10$.

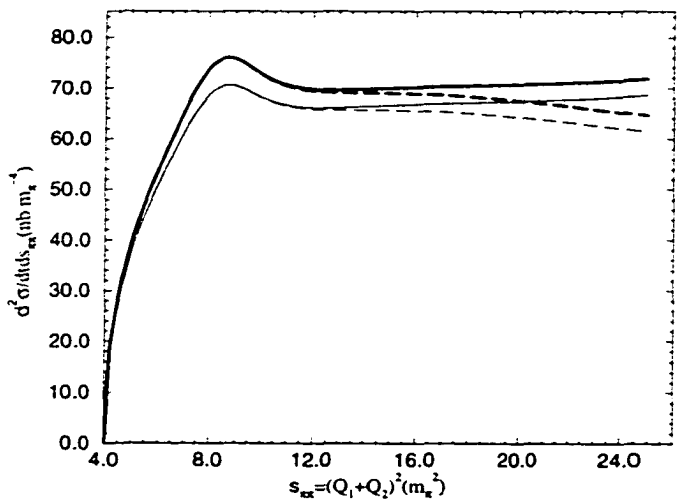

FIG. 47: Differential cross section $d\sigma/dtds_{\pi\pi}$ (nb/m_π^4) of $\gamma p \to \pi^+\pi^0 n$ *vs.* $s = (Q_1 + Q_2)^2$ (m_π^2) for $E_\gamma = 2.$ GeV, $t = -m_\pi^2$ and $F^{3\pi} = 9.5$ GeV^3. The key of this fugure is that of the figure 46.

Chapter 7

CONCLUSIONS

The model that we proposed for the single pion photoproduction reproduces quite well the cross sections for the $\gamma p \to \pi^+\pi^- p$ and $\gamma p \to \pi^0\pi^0 p$ isospin channels from threshold to the $N^*(1520)\frac{3}{2}^-$ resonance region. This confirms that vertices such as $\Delta\pi\Delta$, $\Delta N\rho$ and $\Delta\gamma\Delta$ are essential ingredients in fitting the cross sections and enhance the agreement between our calculation and the experimental data. We also note that the seagull terms with the $N(1440)$ resonance plays a key role in fitting the experimental data for the $\gamma p \to \pi^0\pi^0 p$ process.

Additionally, if further improvement should be made in this work, there are a few important points that we may have to examine carefully. The first is the validity of the effective Lagrangian approach for particles with size and structure. It is thought that any structure in these particles can be accounted for by the introduction of appropriate form factors at the vertices. However, in this work, we have not yet introduced these forms factors since they do not preserve gauge invariance.

Another very important issue is that of unitarity in the amplitude we calculate. Unitarity for three particles in the final state is rather a difficult problem and no attempt as far as we know has been successful in solving this particular problem. In our case, we ignore unitarity as it may not significantly affect the total cross section in our energy range. Furthermore, estimates made by Oset *et al.*[30] confirms that below 800 MeV, the unitarity correction is very small. On

the other hand, this problem could be solved by including the appropriate loops in the calculation, but the inclusion of loop diagrams would make this calculation intractable (there would be far too many possible diagrams for a meaningful analysis to be done). In some sense, the inclusion of form factors at the vertices would partially address this problem. Perhaps a better approach would be to use these amplitudes as input to a coupled-channel treatment.

Appendix A

KINEMATICS

The kinematics of the process are shown schematically in figure 11 in chapter 3. Choosing the photon 3-momentum to follow the $+z$ direction, the four-vector momenta are

$k = (k_0, 0, 0, k_0)$,

$p_1 = (E_1, 0, 0, -k_0)$,

$p_2 = (E_2, p_2 \sin\theta, 0, p_2 \cos\theta)$,

$Q_1 = (Q_{10}, Q_{11}, Q_{12}, Q_{13})$,

$Q_2 = (Q_{20}, Q_{21}, Q_{22}, Q_{23})$ where $k_0 = \frac{s-M^2}{2\sqrt{s}}$, $E_1 = \frac{s+M^2}{2\sqrt{s}}$, $E_2 = \frac{s+M^2-s_{\pi\pi}}{2\sqrt{s}}$, $p_2 = \frac{\lambda^{\frac{1}{2}}(s,s_{\pi\pi},M^2)}{2\sqrt{s}}$ and $\lambda(a,b,c) = (a^2+b^2+c^2-2ab-2ac-2bc)$ is the Källen function.

To obtain the components of Q_1 and Q_2, we start by writing their components in the center of mass frame of the two pions, then make a boost to express them in the final state center of mass frame of the system and finally, perform a rotation to evaluate them in the initial state center of mass frame of the reaction.

In the center of mass frame of the two pions, the four-momenta are

$$Q_1^\star = \{\tfrac{\sqrt{s_{\pi\pi}}}{2}, |\vec{Q}_1^\star|(\sin\theta^\star\cos\phi^\star, \sin\theta^\star\sin\phi^\star, \cos\theta^\star)\},$$

and

$$Q_2^\star = \{\tfrac{\sqrt{s_{\pi\pi}}}{2}, -|\vec{Q}_1^\star|(\sin\theta^\star\cos\phi^\star, \sin\theta^\star\sin\phi^\star, \cos\theta^\star)\},$$

where $|\vec{Q}_1^\star| = |\vec{Q}_2^\star| = \frac{\lambda^{\frac{1}{2}}(s_{\pi\pi}, m_\pi^2, m_\pi^2)}{2\sqrt{s_{\pi\pi}}}$ so that $Q_1^\star + Q_2^\star = (\sqrt{s_{\pi\pi}}, 0, 0, 0)$.

In the reaction center of mass frame, we can express $Q_1 + Q_2$ as

$$Q_1 + Q_2 = \{\tfrac{s+s_{\pi\pi}-M^2}{2\sqrt{s}}, -\tfrac{\lambda^{\frac{1}{2}}(s,s_{\pi\pi},M^2)}{2\sqrt{s}}(\sin\theta, 0, \cos\theta)\},$$

and using the Lorentz transformation

$$P'_{||} = \gamma(P^\star_{||} + \beta E^\star),$$

$$E' = \gamma(E^\star + \beta P^\star_{||}),$$

$$P^\star_\perp = P'_\perp,$$

where $||$ and $\perp$ respectively mean parallel and perpendicular to the boost direction, we obtain

$$\begin{aligned} \frac{\lambda^{\frac{1}{2}}(s, s_{\pi\pi}, M^2)}{2\sqrt{s}} &= \gamma\beta\sqrt{s_{\pi\pi}}, \\ \frac{s + s_{\pi\pi} - M^2}{2\sqrt{s}} &= \gamma\sqrt{s_{\pi\pi}}. \end{aligned}$$

Solving for γ and β, we get

$$\begin{aligned} \gamma &= \frac{s + s_{\pi\pi} - M^2}{2\sqrt{s s_{\pi\pi}}}, \\ \beta &= \frac{\lambda^{\frac{1}{2}}(s, s_{\pi\pi}, M^2)}{(s + s_{\pi\pi} - M^2)}. \end{aligned}$$

The components of the four-momenta $Q_1^\star$ and $Q_2^\star$ in the center of mass frame of the two pions are

$E_1^\star = \frac{\sqrt{s_{\pi\pi}}}{2}$,

$Q_{11}^\star = Q^\star \sin\theta^\star \cos\phi^\star = (Q_{11}^\star)_\perp$,

$Q_{12}^\star = Q^\star \sin\theta^\star \sin\phi^\star = (Q_{12}^\star)_\perp$,

$Q_{13}^\star = Q^\star \cos\theta^\star = (Q_{13}^\star)_{||}$,

$E_2^\star = \frac{\sqrt{s_{\pi\pi}}}{2}$,

$Q^*_{21} = -Q^* \sin\theta^* \cos\phi^* = -(Q^*_{21})_\perp$,
$Q^*_{22} = -Q^* \sin\theta^* \sin\phi^* = -(Q^*_{22})_\perp$,
$Q^*_{23} = -Q^* \cos\theta^* = -(Q^*_{23})_{||}$ where $Q^* = |\vec{Q}^*_1| = |\vec{Q}^*_2|$.

Now, expressing these components in the final state center of the mass frame where $\vec{p_2} + \vec{Q}_1 + \vec{Q}_2 = \vec{0}$, we have

$E'_1 = \gamma(E^*_1 + \beta Q^*_{13})$,
$Q'_{13} = \gamma(Q^*_{13} + \beta E^*_1)$,
$Q'_{11} = Q^*_{11}$,
$Q'_{12} = Q^*_{12}$,
$E'_2 = \gamma(E^*_2 + \beta Q^*_{23})$,
$Q'_{23} = \gamma(Q^*_{23} + \beta E^*_2)$,
$Q'_{21} = Q^*_{21}$,
$Q'_{22} = Q^*_{22}$.

Finally, a rotation about the y-axis is needed to obtain these components written in the initial center of mass frame of the system which are

$Q_{11} = -Q'_{11} \cos\theta - Q'_{13} \sin\theta$,
$Q_{12} = Q'_{12}$,
$Q_{13} = Q'_{11} \sin\theta - Q'_{13} \cos\theta$,

$Q_{21} = -Q'_{21} \cos\theta - Q'_{23} \sin\theta$,
$Q_{22} = Q'_{22}$,
$Q_{23} = Q'_{21} \sin\theta - Q'_{23} \cos\theta$.

Appendix B

CROSS SECTION

The cross section for the $\gamma(k) + N(p_1) \rightarrow \pi(Q_1) + \pi(Q_2) + N(p_2)$ process is

$$\sigma = \int \frac{|\mathcal{M}|^2}{4\sqrt{(k.p_1)^2 - M^2k^2}} d\phi_3,$$

where $k^\mu, p_1^\mu, Q_1^\mu, Q_2^\mu, p_2^\mu$ are respectively the four-momenta of the incident photon and incident nucleon, the outgoing pions and outgoing nucleon. $\mathcal{M}$ is the amplitude for the transition which is to be Lorentz invariant to ensure the independence of the choice of the frame. $d\phi_3$ is the phase space which is given by

$$d\phi_3 = (2\pi)^4 \delta^4(p_1 + k - p_2 - Q_1 - Q_2) \frac{d^3\vec{p}_2}{(2\pi)^3 2E_2} \frac{d^3\vec{Q}_1}{(2\pi)^3 2w_1} \frac{d^3\vec{Q}_2}{(2\pi)^3 2w_2}, \quad (52)$$

where E_2, w_1 and w_2 are respectively the energies of the outgoing nucleon, and the two pions.

Using the property of the δ-function

$$\delta^4(p_1 + k - p_2 - Q_1 - Q_2) = \int dQ^4 \delta^4(Q - Q_1 - Q_2) \delta^4(p_1 + k - p_2 - Q) \quad (53)$$

we can write the total cross section as

$$\sigma = \int \frac{(2\pi)^4 |\mathcal{M}|^2}{4\sqrt{(k.p_1)^2 - M^2k^2}} d^4Q \delta^4(Q - Q_1 - Q_2) \delta^4(p_1 + k - p_2 - Q) \times$$

$$\frac{d^3\vec{p}_2}{(2\pi)^3 2E_2}\frac{d^3\vec{Q}_1}{(2\pi)^3 2w_1}\frac{d^3\vec{Q}_2}{(2\pi)^3 2w_2}.$$

Writing $s_{\pi\pi} = Q^2 = Q_0^2 - Q_2^2$, which yields $ds_{\pi\pi} = dQ_0^2 = 2Q_0 dQ_0$, or $dQ_0 = \frac{ds_{\pi\pi}}{2Q_0}$, and replacing d^4Q by $dQ_0 d^3\vec{Q}$ where Q_0 is the total energy of the $\pi\pi$ system, we obtain

$$\sigma = \int \frac{(2\pi)^4 |\mathcal{M}|^2}{(2\pi)^9 4\sqrt{(k.p_1)^2 - M^2k^2}} ds_{\pi\pi}\delta^4(Q - Q_1 - Q_2)\frac{d^3\vec{Q}_1}{2w_1}\frac{d^3\vec{Q}_2}{2w_2}\times$$

$$\delta^4(p_1 + k - p_2 - Q)\frac{d^3\vec{p}_2}{2E_2}\frac{d^3\vec{Q}}{2Q_0}.$$

Since the quantity $\frac{d\vec{p}^3}{p^0}$ is a Lorentz scalar, we can evaluate the integrals

$$\int \delta^4(Q - Q_1 - Q_2)\frac{d^3\vec{Q}_1}{2w_1}\frac{d^3\vec{Q}_2}{2w_2} \tag{54}$$

and

$$\int \delta^4(p_1 + k - p_2 - Q)\frac{d^3\vec{p}_2}{2E_2}\frac{d^3\vec{Q}}{2Q_0} \tag{55}$$

in any reference frame that we choose. Using the fact that

$$\int \delta^4(P - P_1 - P_2)\frac{d^3\vec{P}_1}{2E_1}\frac{d^3\vec{P}_2}{2E_2} = \int \frac{d\Omega_{p_1}}{8P^2}\lambda^{\frac{1}{2}}(P^2, P_1^2, P_2^2), \tag{56}$$

where $\lambda(a,b,c) = (a^2 + b^2 + c^2 - 2ab - 2ac - 2bc)$ is the Källen function, and evaluating the integral given in equations (54) in the center of mass of the two pions, we obtain

$$\int \delta^4(Q - Q_1 - Q_2)\frac{d^3\vec{Q}_1}{2w_1}\frac{d^3\vec{Q}_2}{2w_2} = \int \frac{\lambda^{\frac{1}{2}}(Q^2, Q_1^2, Q_2^2)}{8s_{\pi\pi}} d\Omega^\star_{\pi\pi},$$

where $|\vec{Q}_1^\star|$ is the magnitude of the three-momentum of the first pion in the c.o.m frame of the two pions and $\Omega^\star_{p_1}$ its solid angle. Similarly, the second integral yields

$$\int \delta^4(p_1 + k - p_2 - Q)\frac{d^3\vec{p}_2}{2E_2}\frac{d^3\vec{Q}}{2Q_0} = \int \frac{\lambda^{\frac{1}{2}}(s, s_{\pi\pi}, p_2^2)}{8s} d\Omega_2,$$

where $|\vec{p}_2|$ is the magnitude of the three-momentum of the outgoing nucleon in the c.o.m of the reaction, Ω_2 its solid angle and s is the square of the total energy of the system.

Finally, integrating over the azimutal angle ϕ_2 of the outgoing nucleon, averaging over the initial spin of the nucleon and initial photon polarization, and summing over the spin of the final nucleon, we obtain the final expression of the total cross section

$$\sigma = \frac{1}{2(2j+1)} \int \frac{ds_{\pi\pi} d\Omega^*_{\pi\pi} d\cos\theta_2}{128(2\pi)^4 (s-M^2) s\sqrt{s_{\pi\pi}}} |\mathcal{M}|^2 \lambda^{\frac{1}{2}}(s_{\pi\pi}, m_\pi^2, m_\pi^2) \lambda^{\frac{1}{2}}(s, s_{\pi\pi}, M^2), \tag{57}$$

where j is the spin of the nucleon and $\lambda(a,b,c)$ is the Källen function and $4m_\pi^2 \leq s_{\pi\pi} \leq (W-M)^2$.

Appendix C

VERTICES

Different vertices corresponding to the Lagrangians given in chapters 2 and 4 are given below. N denotes a nucleon and N^* the $N(1440)\frac{1}{2}^+$ or any $\frac{1}{2}^+$ resonance. N^o represents the $N(1520)\frac{3}{2}^-$ or any $\frac{3}{2}^-$ nucleon resonance.

$$\mathcal{M}_{\gamma NN} = \bar{u}(p_f)(-e\frac{1+\tau_3}{2}\not{\epsilon} + e\frac{k_s+\tau_3 k_v}{4M}\gamma_\mu\gamma_\nu F^{\mu\nu})u(p_i)$$

$$\mathcal{M}_{\pi NN} = \bar{u}(p_f)(\frac{f_{\pi NN}}{m_\pi}\tau_j\gamma_5 \not{Q}_j)u(p_i)$$

$$\mathcal{M}_{\pi\gamma NN} = \bar{u}(p_f)\gamma_5\frac{f_{\pi NN}}{m_\pi}\epsilon_{ij3}\tau_i \not{\epsilon}_j u(p_i)$$

$$\mathcal{M}_{\pi\pi NN} = \bar{u}(p_f)(-\frac{4\pi\lambda_1}{m_\pi} + \frac{-1}{4F_\pi^2}\epsilon_{abc}\tau_c \not{Q}_b)u(p_i)$$

$$\mathcal{M}_{\pi\pi\gamma NN} = \bar{u}(p_f)\frac{-e}{4F_\pi^2}(\tau_i\delta_{3j} - \tau_3\delta_{ij}) \not{\epsilon} u(p_i)$$

$$\mathcal{M}_{\gamma\pi\pi} = -2q_\pi\epsilon.Q$$

$$\mathcal{M}_{\gamma\pi\pi\pi} = \frac{F^{3\pi}}{6}\epsilon^{\mu\nu\alpha\beta}\epsilon^{ijk}\epsilon_\mu Q_{i\nu}Q_{j\alpha}Q_{k\beta}$$

$$\mathcal{M}_{\pi\Delta N} = \bar{u}(p_f)\frac{f_{\pi\Delta N}}{m_\pi}T_j\Theta_{\mu\nu}(Z)Q_j^\nu u^\mu(p_i)$$

$$\mathcal{M}_{N^*N\gamma} = \bar{u}(p_f)e\frac{k_s^R+\tau_3 k_v^R}{2(M_{N^*}+M)}\gamma_\mu\gamma_\nu F^{\mu\nu}u(p_i)$$

$$\mathcal{M}_{N^*N\pi} = \bar{u}(p_f)\frac{f_{N^*N\pi}}{m_\pi}\tau_j\gamma_5 \not{Q}_j u(p_i)$$

$$\mathcal{M}_{N^*N\gamma\pi} = \bar{u}(p_f)\frac{f_{N^*N\pi}}{m_\pi}\gamma_5\epsilon_{ij3}\tau_i \not{\epsilon}_j u(p_i)$$

$$\mathcal{M}_{N^*N\pi\pi} = \bar{u}(p_f)(-\frac{4\pi\lambda_1^*}{m_\pi} - \frac{1}{4F_\pi^{*2}}\epsilon_{ijk}\tau_k \not{Q}_j)u(p_i)$$

$$\mathcal{M}_{\pi N^\circ N} = \bar{u}(p_f)\gamma_5\frac{f_{\pi N^\circ N}}{m_\pi}\tau_j\Theta_{\mu\nu}(Z)Q_j^\nu u^\mu(p_i)$$

$$\mathcal{M}^1_{\gamma\Delta N} = \bar{u}^\mu(p_f)T_3 k_v^{\Delta(1)}\gamma_5\Theta_{\mu\nu}(Y)\gamma_\lambda F^{\lambda\nu}u(p_i)$$

$$\mathcal{M}^2_{\gamma\Delta N} = \bar{u}^\mu(p_f)T_3 k_v^{\Delta(2)}\gamma_5\Theta_{\mu\nu}(X)p_{N\lambda}F^{\nu\lambda}u(p_i)$$

$$\mathcal{M}^1_{\gamma N^\circ N} = \bar{u}^\mu(p_f)(k_s^{N^\circ(1)} + \tau_3 k_v^{N^\circ(1)})\Theta_{\mu\nu}(Y)\gamma_\lambda F^{\lambda\nu}u(p_i)$$

$$\mathcal{M}^2_{\gamma N^\circ N} = \bar{u}^\mu(p_f)(k_s^{N^\circ(2)} + \tau_3 k_v^{N^\circ(2)})\Theta_{\mu\nu}(X)p_{N\lambda}F^{\nu\lambda}u(p_i)$$

$$\mathcal{M}_{N^\circ\pi\Delta} = \bar{u}_\mu(p_f)T_j(T^1_{N^\circ\pi\Delta}Q_j^\mu Q_j^\nu + T^2_{N^\circ\pi\Delta}g^{\mu\nu})u_\nu(p_f)$$

$$\mathcal{M}_{\Delta\gamma\Delta} = \bar{u}_\mu(p_f)[-e\frac{1+T_3}{2}[\gamma_\lambda g_{\mu\nu} - (\gamma_\mu g_{\nu\lambda} + \gamma_\nu g_{\mu\lambda}) + \gamma_\mu\gamma_\lambda\gamma_\nu]\epsilon^\lambda u^\nu(p_i) +$$

$$\bar{u}_\lambda(p_f)(k_s^* + T_\Delta k_v^*)\gamma_\mu\gamma_\nu F^{\mu\nu}]u^\lambda(p_i)$$

$$\mathcal{M}_{\Delta\pi\Delta} = \bar{u}_\mu(p_f)\gamma_5 T_j(T^1_{\Delta\pi\Delta}Q_j^\mu Q_j^\nu + T^2_{\Delta\pi\Delta}g^{\mu\nu})u_\nu(p_i)$$

$$\mathcal{M}_{\Delta N\rho} = \bar{u}(p_f)\gamma_5 T_j(a_1\epsilon^\mu_{\rho j} + a_2 \not{\epsilon}_\rho Q_j^\mu + a_3\epsilon_\rho . p_\Delta Q_j^\mu)u_\mu(p_i)$$

$$\mathcal{M}_{\rho\pi\pi} = -f_\rho\epsilon_\rho{}^\nu(Q_1 - Q_2)_\nu$$

$$\mathcal{M}_{\rho NN} = \bar{u}(p_f)\tau_j(-G^v \not{\epsilon}^*_{\rho j} + \frac{G^t}{2M} \not{\epsilon}^*_{\rho j} \not{Q})u(p_i)$$

$$\mathcal{M}_{\rho_o\pi\pi\gamma} = -(q_1 - q_2)f_\rho\epsilon_\rho{}^\mu\epsilon^*_\mu$$

$$\mathcal{M}_{\rho\pi\gamma} = \frac{g_{\rho\pi\gamma}}{m_\pi}\epsilon^{\alpha\beta\mu\nu}(\epsilon_\rho)_\alpha\epsilon_\beta(Q_\rho)_\mu(Q_\pi)_\nu$$

$$\mathcal{M}_{\rho\rho\gamma} = q_\rho[(Q_1 + Q_2)_\mu g_{\nu\alpha} - (Q_2 + k)_\nu g_{\mu\alpha} - (Q_1 - k)_\alpha g_{\mu\nu}]\epsilon^\mu\epsilon_1^\nu\epsilon_2^{*\alpha}$$

$\mathcal{M}_{\rho\gamma NN} = \frac{G'}{2M} q_\rho \bar{u}(p_f)\tau_i \epsilon_{j3i}(\not{\epsilon}^*_{\rho i}\not{\epsilon} - \epsilon^*_{\rho i}.\epsilon)u(p_i)$.

In these expressions, q_π, q_ρ and q_Δ are respectively the charges of the π, the ρ and the Δ, and values of different coupling constants are given in the appendix E. τ_j is the isospin operator for $I = \frac{1}{2}$ and T_j are the $I = \frac{1}{2}$ to $I = \frac{3}{2}$ operators. ϵ^μ_j is the photon polarization where the isospin index 'j' arises from the index 'j' in the term $A^\mu\phi_j$. The $Q's$ are 4-momenta of the ρ or π-mesons, the $p's$ are 4-momenta of the baryons and $F^{\mu\nu} = \epsilon^\mu k^\nu - \epsilon^\nu k^\mu$ is the electromagnetic field strength tensor.

$\Theta_{\mu\nu}(V)$ is given by $\Theta_{\mu\nu}(V) = g_{\mu\nu} + [\frac{1}{2}(1+4V)A + V]\gamma_\mu\gamma_\nu$ where A is an arbitrary parameter defining the so called 'point transformation'. V is also arbitrary and is called an 'off-shell parameter'.

Spin-$\frac{1}{2}$ and spin-1 Propagators

For spin $\frac{1}{2}$ resonances, the propagator is

$$\frac{i(\gamma.p + M)}{p^2 - M^2 + iM\Gamma},$$

whereas for a ground-state nucleon, the term $+iM\Gamma$ is replaced by the usual $+i\epsilon$.

For the π and ρ-mesons, the propagators are respectively,

$$\frac{i}{Q^2 - m^2 + i\epsilon}$$

and

$$Q^{\mu\nu} = i\frac{g^{\mu\nu} - \frac{Q^\mu Q^\nu}{Q^2}}{Q^2 - m^2 + im\Gamma}.$$

Energy-dependent decay widths

We use the following energy dependent widths for the decays $\Delta(1232) \to N\pi$, $N^*(1440) \to N\pi$, $N^*(1520) \to N\pi$ and $\rho \to \pi\pi$.

They are

$$\Gamma(\sqrt{s_\Delta}) = \Gamma(M_\Delta)\frac{|\vec{p}_{cm}(\sqrt{s_\Delta})|^3}{|\vec{p}_{cm}(M_\Delta)|^3}\theta(\sqrt{s_\Delta} - M - m_\pi),$$

$$\Gamma(\sqrt{s_{N^*_{1440}}}) = \Gamma(M_{N^*_{1440}})\frac{|\vec{p}_{cm}(\sqrt{s_{N^*_{1440}}})|^3}{|\vec{p}_{cm}(M_{N^*_{1440}})|^3}\theta(\sqrt{s_{N^*_{1440}}} - M - m_\pi),$$

$$\Gamma(\sqrt{s_{N^*_{1520}}}) = \Gamma(M_{N^*_{1520}})\frac{|\vec{p}_{cm}(\sqrt{s_{N^*_{1520}}})|^5}{|\vec{p}_{cm}(M_{N^*_{1520}})|^5}\theta(\sqrt{s_{N^*_{1520}}} - M - m_\pi),$$

$$\Gamma(\sqrt{s}) = \Gamma(m_\rho)\frac{|\vec{Q}_{cm}(\sqrt{s})|^3}{|\vec{Q}_{cm}(m_\rho)|^3}\theta(\sqrt{s_\rho} - 2m_\pi),$$

where $\vec{p}_{cm}(M_i)$ is the three momentum of the decaying particle i into two particles j and k, written in the rest frame of the particle i. $\vec{p}_{cm}(\sqrt{s_i})$ is the three momentum of the decaying particle i in which its mass is taken to be equal to $M_i = \sqrt{s_i} = \sqrt{p_i^2}$ where p_i is the four momentum of the particle i, written in the center the mass of the double pion photoproduction reaction.

The magnitudes of these momenta are

$$|\vec{p}_{cm}(M_i)| = \frac{\sqrt{\lambda(M_i^2, M_j^2, M_k^2)}}{2M_i},$$

$$|\vec{p}_{cm}(\sqrt{s_i})| = \frac{\sqrt{\lambda(s_i, M_j^2, M_k^2)}}{2\sqrt{s_i}}.$$

Appendix D

SPIN-$\frac{3}{2}$ FIELD

The Lagrangian for particles with spin-$\frac{3}{2}$ is not unique but depends on some arbitrary real parameters [67]. However, it can be shown that physical quantities such as energy, momentum and canonical commutation relations do not depend on these parameters.

For a free massive particle with spin-$\frac{3}{2}$, the field is described by the Lagrangian [68, 69]

$$L_{free} = \bar{\Psi}^{\mu} \Lambda_{\mu\nu} \Psi^{\nu}, \tag{58}$$

where

$$\begin{aligned} \Lambda_{\mu\nu} = \quad & [(-i\partial_{\lambda}\gamma^{\lambda} + M_R)g_{\mu\nu} - iA(\gamma_{\mu}\partial_{\nu} + \gamma_{\nu}\partial_{\mu}) \\ - \quad & \frac{i}{2}(3A^2 + 2A + 1)\gamma_{\mu}\partial^{\lambda}\gamma_{\lambda}\gamma_{\nu} \\ - \quad & M_R(3A^2 + 3A + 1)\gamma_{\mu}\gamma_{\nu}]. \end{aligned} \tag{59}$$

Ψ^{ν} is the Rarita-Schwinger vector spinor, M_R the mass of the spin-$\frac{3}{2}$ baryon and A an arbitrary parameter which differs from -$\frac{1}{2}$.

The propagator for the massive spin-$\frac{3}{2}$ baryon can be derived from the equation of motion $\Lambda_{\mu\nu}\Psi^{\nu} = 0$ known as the Rarita-Schwinger equation with the subsidiary conditions [70, 71]

$$\gamma_\mu \Psi^\mu = 0, \tag{60}$$

and

$$\partial_\mu \Psi^\mu = 0 \tag{61}$$

which are valid for all values of A.

The propagator $G^\lambda_\nu(x,y)$ satisfies the equation

$$\Lambda_{\mu\lambda} G^\lambda_\nu(x,y) = \delta^4(x,y) g_{\mu\nu}, \tag{62}$$

where $g_{\mu\nu}$ is the metric tensor. Working in momentum space, we have

$$G^\lambda_\nu(x,y) = \int \frac{d^4p}{(2\pi)^4} G^\lambda_\nu(p) e^{-i(x-y).p} \tag{63}$$

with

$$\Lambda_{\mu\lambda}(p) G^\lambda_\nu(p) = g_{\mu\nu}. \tag{64}$$

Solving for G, we can derive the propagator

$$\begin{aligned} G_{\mu\nu}(p) = \quad & \frac{\gamma.p + M_R}{p^2 - M_R^2} \left[g_{\mu\nu} - \frac{1}{3}\gamma_\mu\gamma_\nu - \frac{1}{3M_R}(\gamma_\mu p_\nu - \gamma_\nu p_\mu) - \frac{2}{3M_R^2} p_\mu p_\nu \right] + \\ & \frac{1}{3M_R^2} \frac{A+1}{2A+1} \left[\gamma_\mu p_\nu + \frac{A}{2A+1}\gamma_\nu p_\mu + \right. \\ & \left. \left\{ \frac{1}{2}\frac{A+1}{2A+1}\gamma.p - \frac{AM_R}{2A+1} \right\} \gamma_\mu\gamma_\nu \right]. \end{aligned} \tag{65}$$

It should be pointed out here that the free-field Lagrangian $\bar{\Psi}^\mu \Lambda_{\mu\nu} \Psi^\nu$ is invariant under the point transformation [72]

$$\Psi^\mu \to \Psi^\mu + a\gamma^\mu\gamma^\nu\Psi_\nu, \tag{66}$$

and

$$A \to \frac{A - 2a}{1 + 4a}, \tag{67}$$

where a is an arbitrary parameter $\neq -\frac{1}{4}$.

The meaning of the invariance of the free-field Lagrangian under point transformation is that physically interesting quantities are independent of the parameter A. Thus, we choose $A = -1$ and the spin-$\frac{3}{2}$ propagator becomes

$$P_{\mu\nu}(p) = \frac{\gamma.p + M_R}{p^2 - M_R^2}\left[\, g_{\mu\nu} - \frac{1}{3}\gamma_\mu\gamma_\nu - \frac{1}{3M_R}(\gamma_\mu p_\nu - \gamma_\nu p_\mu) - \frac{2}{3M_R^2}p_\mu p_\nu \,\right]. \quad (68)$$

We remark that in deriving this form of the propagator, we are ignoring the so-called off-shell contributions.

Setting $A = -1$, the Rarita-Schwinger equation becomes

$$\begin{aligned}\Lambda_{\mu\nu}\Psi^\nu = \quad & [(-i\partial_\lambda\gamma^\lambda + M_R)g_{\mu\nu} + i(\gamma_\mu\partial_\nu + \gamma_\nu\partial_\mu) \\ - \quad & i\gamma_\mu\partial^\lambda\gamma_\lambda\gamma_\nu - M_R\gamma_\mu\gamma_\nu]\Psi^\nu = 0. \end{aligned} \quad (69)$$

Multiplying this equation by ∂^μ yields

$$\partial^\mu\Lambda_{\mu\nu}\Psi^\nu = (M_R\partial_\nu - M_R\gamma.\partial\gamma_\nu)\Psi^\nu = 0,$$

or

$$\gamma.\partial\gamma.\Psi = \partial.\Psi. \quad (70)$$

Applying γ^ν into equation (69), we obtain

$$\gamma^\mu\Lambda_{\mu\nu}\Psi^\nu = [4i\partial_\nu - 4i\gamma.\partial\gamma_\nu - 3M_R\gamma_\nu]\Psi^\nu = 0, \quad (71)$$

and using equation (70), we derive

$$\gamma_\nu\Psi^\nu = 0, \quad (72)$$

and

$$\partial_\nu\Psi^\nu = 0. \quad (73)$$

Equations (72) and (73) are the subsidiary conditions that we mentioned before.

Now, looking at the interaction of a spin-$\frac{3}{2}$ field coupled with a nucleon field and a pseudoscalar meson field, the corresponding Lagrangian should be built in such a way that the Lagrangian is invariant under point transformations. The most general form of such an interaction Lagrangian containing only the first-order derivative of the pion-field is given [71, 73] by

$$L_{RN\pi} = f\bar{\psi}_\mu \Theta_{\mu\nu}(Z)\psi\partial_\nu\phi + H.c. \tag{74}$$

where $\Theta_{\mu\nu}(Z) = g_{\mu\nu} + [\frac{1}{2}(1+4Z)A + Z]\gamma_\mu\gamma_\nu$, and ψ and ϕ are respectively the nucleon field and the meson field.

The Lagrangian describing the interaction between the photon field A_λ and the resonance via its charge can be obtained from equation 58 through minimal substitution, namely by replacing ∂_λ by $-ie\frac{1+T_3}{2}A_\lambda$. As a result, we obtain

$$\mathcal{L}_{RR\gamma} = \bar{R}^\mu(-e)(\frac{1+T_3}{2})[\gamma_\lambda g_{\mu\nu} - (\gamma_\mu g_{\nu\lambda} + \gamma_\nu g_{\mu\lambda}) + \gamma_\mu\gamma_\lambda\gamma_\nu]A^\lambda R^\nu + H.c. \tag{75}$$

Appendix E

ISOSPIN OPERATORS AND ISOSPIN COEFFICIENTS

This appendix is devoted to studying the isospin operators and evaluating the isospin coefficients for the transtion $I_1 \longleftrightarrow I_2$ where I_1 and I_2 are isospin $\frac{1}{2}$ or $\frac{3}{2}$.

Isospin $\frac{1}{2}$ operator.

Isospin operators for $I = \frac{1}{2}$ systems can be constructed from Pauli spin matrices σ in the same way as angular momentum operators for spin-$\frac{1}{2}$ systems. These matrices are

$$\tau_1 = \begin{pmatrix} 0 & 1 \\ 1 & 0 \end{pmatrix}, \tau_2 = \begin{pmatrix} 0 & -i \\ i & 0 \end{pmatrix}, \text{ and } \tau_3 = \begin{pmatrix} 1 & 0 \\ 0 & -1 \end{pmatrix}$$

for the x-, y-, and z- components of the isospin operator τ.

From the form given in these matrices, we can build isospin raising τ_+ and lowering τ_- operators which transform respectively a neutron to a proton, and a proton to a neutron. They are

$$\tau_+ = \tfrac{1}{2}(\tau_1 + i\tau_2) = \begin{pmatrix} 0 & 1 \\ 0 & 0 \end{pmatrix}, \tau_- = \tfrac{1}{2}(\tau_1 - i\tau_2) = \begin{pmatrix} 0 & 0 \\ 1 & 0 \end{pmatrix}.$$

In the same way as for angular momentum raising and lowering operators, $\tau_\pm$ changes the third component I_3, without changing the isospin I itself. These operators are

$$\tau_{\pm}|I, I_3 >= \sqrt{I(I+1) - I_3(I_3 \pm 1)}|I, I_3 \pm 1 > . \tag{76}$$

For transitions involving pions, the operator responsible for the transitions can be written as $\vec{\phi}.\vec{\tau}$ where $\vec{\phi}$ is an isovector field representing the pions.

Writing $\phi_+ = -\frac{1}{\sqrt{2}}(\phi_1 - i\phi_2)$; destroys π^+, creates π^-,
$\phi_- = \frac{1}{\sqrt{2}}(\phi_1 + i\phi_2)$; destroys π^-, creates π^+,
$\phi_0 = \phi_3$; destroys π^0, creates π^0.

From these equations, we derive $\phi_1 = -\frac{1}{\sqrt{2}}(\phi_+ - \phi_-)$ and $\phi_2 = -\frac{i}{\sqrt{2}}(\phi_+ + \phi_-)$, and evaluating $\vec{\phi}.\vec{\tau}$, we obtain

$$\vec{\phi}.\vec{\tau} = \phi_1.\tau_1 + \phi_2.\tau_2 + \phi_3.\tau_3 = -\sqrt{2}(\phi_+\tau_+ - \phi_-\tau_-) + \phi_0\tau_0$$

or

$$\vec{\phi}.\vec{\tau} = \begin{pmatrix} \phi_0 & -\sqrt{2}\phi_+ \\ \sqrt{2}\phi_- & -\phi_0 \end{pmatrix}. \tag{77}$$

Now let's look at the coupling $NN\pi$ where the N's are nucleons and calculate the isospin coefficients associated with the coupling. In another words, let's calculate the matrix elements $\mathcal{M} = \chi^{\dagger}\vec{\phi}.\vec{\tau}\chi$ where $\chi = (p, n)$ and $\chi^{\dagger} = (p^*, n^*)$ represent respectively the incoming and outgoing nucleons.

This yields

$$\mathcal{M} = (p^*, n^*) \begin{pmatrix} \phi_0 & -\sqrt{2}\phi_+ \\ \sqrt{2}\phi_- & -\phi_0 \end{pmatrix} \begin{pmatrix} p \\ n \end{pmatrix}$$

or

$$\mathcal{M} = (p^*\phi_0 p - \sqrt{2}p^*\phi_+ n + \sqrt{2}n^*\phi_- p - \sqrt{2}n^*\phi_0 n) \tag{78}$$

This last expression of $\mathcal{M}$ gives the isospin coefficients of the coupling $NN\pi$. These coefficients are

$$\begin{cases} -\sqrt{2} & for \quad p \longleftrightarrow n\pi^+ \\ \sqrt{2} & for \quad n \longleftrightarrow p\pi^- \\ 1 & for \quad p \longleftrightarrow p\pi^0 \\ -1 & for \quad n \longleftrightarrow n\pi^0. \end{cases}$$

Now let's examine the transition $N^* \rightarrow N\pi$ where N^* is a nucleon resonance with isospin $I = \frac{1}{2}$. To better understand this, we look at a particular process where the N^{*+} decays into $n\pi^+$ or $p\pi^0$. Thus, let $\mathcal{M}_1$ and $\mathcal{M}_2$ respectively be the amplitude for the decays. Using the previous isospin-$\frac{1}{2}$ operator, $\mathcal{M}_1$ and $\mathcal{M}_2$ are written as $\mathcal{M}_1 = -\sqrt{2}N\mathcal{M}$ and $\mathcal{M}_2 = N\mathcal{M}$ where N is some normalization constant that we have to evaluate. The total decay looks like

$$\Gamma\alpha\{|\mathcal{M}_1|^2 + |\mathcal{M}_2|^2\} = \{2|N|^2|\mathcal{M}|^2 + |N|^2|\mathcal{M}_2|^2\} = 3|N|^2|\mathcal{M}|^2 = |\mathcal{M}|^2$$

and this yields in turn $N = \sqrt{\frac{1}{3}}$.

Therefore, the isospin coefficients for the process $N^*(I = \frac{1}{2}) \rightarrow N\pi$ are

$$\begin{cases} -\sqrt{\frac{2}{3}} & for \quad p^* \longleftrightarrow n\pi^+ \\ \sqrt{\frac{2}{3}} & for \quad n^* \longleftrightarrow p\pi^- \\ \frac{1}{\sqrt{3}} & for \quad p^* \longleftrightarrow p\pi^0 \\ -\frac{1}{\sqrt{3}} & for \quad n^* \longleftrightarrow n\pi^0. \end{cases}$$

We remark that these isospin coefficients are exactly the Glebsch-Gordan coefficients $< \frac{1}{2}, I_{3_N}; 1, I_{3_\pi} | \frac{1}{2}, I_{3_N^*} >$ where I_{3_N}, I_{3_π} and $I_{3_N^*}$ are respectively the third components of the isospins of the nucleon, the pion and the resonance. We also note that this normalization constant $\sqrt{\frac{1}{3}}$ can be included in the coupling constant of the $N^*N\pi$ coupling.

Isospin $\frac{3}{2}$ operator.

Using the properties of the raising operators shown in equation (76) and the fact that $\tau_+ = \tau_-^\dagger$, we write

$$\tau_+ \left| \frac{3}{2}, -\frac{3}{2} \right\rangle = \sqrt{3} \left| \frac{3}{2}, -\frac{1}{2} \right\rangle$$

$$\tau_+ \left| \frac{3}{2}, -\frac{1}{2} \right\rangle = 2 \left| \frac{3}{2}, +\frac{1}{2} \right\rangle$$

$$\tau_+ \left| \frac{3}{2}, +\frac{1}{2} \right\rangle = \sqrt{3} \left| \frac{3}{2}, +\frac{3}{2} \right\rangle.$$

Thus, in terms of matrices, τ_+ and τ_- become

$$\tau_+ = \begin{pmatrix} 0 & \sqrt{3} & 0 & 0 \\ 0 & 0 & 2 & 0 \\ 0 & 0 & 0 & \sqrt{3} \\ 0 & 0 & 0 & 0 \end{pmatrix}, \qquad \tau_- = \begin{pmatrix} 0 & 0 & 0 & 0 \\ \sqrt{3} & 0 & 0 & 0 \\ 0 & 2 & 0 & 0 \\ 0 & 0 & \sqrt{3} & 0 \end{pmatrix}.$$

For the transition $\Delta_1 \rightarrow \Delta_2\pi$, the transition operator $\vec{\phi}.\vec{\tau}$ given in equation (77) is

$$\vec{\phi}.\vec{\tau} = \begin{pmatrix} \frac{3}{2}\phi_0 & -\sqrt{\frac{3}{2}}\phi_+ & 0 & 0 \\ \sqrt{\frac{3}{2}}\phi_- & \frac{1}{2}\phi_0 & -\sqrt{2}\phi_+ & 0 \\ 0 & \sqrt{2}\phi_- & -\frac{1}{2}\phi_0 & -\sqrt{\frac{3}{2}}\phi_+ \\ 0 & 0 & \sqrt{\frac{3}{2}}\phi_- & -\frac{3}{2}\phi_0 \end{pmatrix},$$

and the matrix elements $\mathcal{M}_\Delta = \chi^\dagger_{\Delta_2}\vec{\phi}.\vec{\tau}\chi_{\Delta_1}$ where $\chi_{\Delta_1} = (\Delta_1^{++}, \Delta_1^{+}, \Delta_1^{0}, \Delta_1^{-})$ and $\chi^\dagger_{\Delta_2} = (\Delta_2^{*++}, \Delta_2^{*+}, \Delta_2^{*0}, \Delta_2^{*-})$ represent respectively the incoming and outgoing Δ become

$$\begin{aligned} \mathcal{M}_\Delta = \sqrt{\frac{3}{2}} \Big\{ & \sqrt{\frac{3}{2}}(\Delta_2^{*++}\phi_0\Delta_1^{++} - \Delta_2^{*-}\phi_0\Delta_1^{-}) + \sqrt{\frac{1}{6}}(\Delta_2^{*+}\phi_0\Delta_1^{+} - \Delta_2^{*0}\phi_0\Delta_1^{0}) + \\ & \frac{2}{\sqrt{3}}(\Delta_2^{*0}\phi_-\Delta_1^{+} - \Delta_2^{*+}\phi_+\Delta_1^{0}) + (\Delta_2^{*+}\phi_-\Delta_1^{++} - \Delta_2^{*++}\phi_+\Delta_1^{+}) \\ & (\Delta_2^{*-}\phi_-\Delta_1^{0} - \Delta_2^{*0}\phi_+\Delta_1^{-}) \Big\}. \end{aligned} \tag{79}$$

To demonstrate that these coefficients in front of each term are related to Glebsch-Gordan coefficients, we evaluate them. They are,

for $\Delta^{++} \rightarrow \pi^0\Delta^{++}$, $< \frac{3}{2}, \frac{3}{2}; 1, 0|\frac{3}{2}, \frac{3}{2} >= \sqrt{\frac{3}{5}} = \sqrt{\frac{3}{2}}\sqrt{\frac{2}{5}}$,

$\Delta^{+} \rightarrow \pi^0\Delta^{+}$, $< \frac{3}{2}, \frac{1}{2}; 1, 0|\frac{3}{2}, \frac{1}{2} >= \sqrt{\frac{1}{15}} = \sqrt{\frac{1}{6}}\sqrt{\frac{2}{5}}$,

$\Delta^{0} \rightarrow \pi^0\Delta^{0}$, $< \frac{3}{2}, -\frac{1}{2}; 1, 0|\frac{3}{2}, -\frac{1}{2} >= -\sqrt{\frac{1}{15}} = -\sqrt{\frac{1}{6}}\sqrt{\frac{2}{5}}$,

$\Delta^{-} \rightarrow \pi^0\Delta^{-}$, $< \frac{3}{2}, -\frac{3}{2}; 1, 0|\frac{3}{2}, -\frac{3}{2} >= -\sqrt{\frac{3}{5}} = -\sqrt{\frac{3}{2}}\sqrt{\frac{2}{5}}$,

$\Delta^{0} \rightarrow \pi^-\Delta^{+}$, $< \frac{3}{2}, \frac{1}{2}; 1, -1|\frac{3}{2}, -\frac{1}{2} >= 2\sqrt{\frac{2}{15}} = \frac{2}{\sqrt{3}}\sqrt{\frac{2}{5}}$,

$\Delta^{0} \rightarrow \pi^+\Delta^{0}$, $< \frac{3}{2}, -\frac{1}{2}; 1, 1|\frac{3}{2}, \frac{1}{2} >= -2\sqrt{\frac{2}{15}} = -\frac{2}{\sqrt{3}}\sqrt{\frac{2}{5}}$,

$\Delta^{+} \rightarrow \pi^-\Delta^{++}$, $< \frac{3}{2}, \frac{3}{2}; 1, -1|\frac{3}{2}, \frac{1}{2} >= \sqrt{\frac{2}{5}}$,

$\Delta^{++} \to \pi^+\Delta^+, < \frac{3}{2}, \frac{1}{2}; 1, 1|\frac{3}{2}, \frac{3}{2} >= -\sqrt{\frac{2}{5}},$
$\Delta^{-} \to \pi^-\Delta^0, < \frac{3}{2}, -\frac{1}{2}; 1, -1|\frac{3}{2}, -\frac{3}{2} >= \sqrt{\frac{2}{5}},$
$\Delta^{0} \to \pi^+\Delta^-, < \frac{3}{2}, -\frac{3}{2}; 1, 1|\frac{3}{2}, -\frac{1}{2} >= -\sqrt{\frac{2}{5}}.$

Comparing both sets of coefficients, we again realize that these coefficients in equation (79) are nothing else but the Glebsch-Gordan coefficients with some overall appropriate normalization constants.

For the $I = \frac{1}{2}$ to $I = \frac{3}{2}$ transition, the matrices τ_+ and τ_- cannot be built through the use of the raising and lowering operators since this particular transition not only involves a change of the third component of the isospin but also a change of the isospin itself. This means that we will not be able to use the matrices τ_+ and τ_- to evaluate the transition operator $\vec{\phi}.\vec{\tau}$. Therefore, we do not extract the isospin coefficients of this transition through the matrix elements $\chi_N^\dagger \vec{\phi}.\vec{\tau}\chi_\Delta$. Since we have shown from the $I = \frac{1}{2}$ to $I = \frac{1}{2}$ and $I = \frac{3}{2}$ to $I = \frac{3}{2}$ transitions that these isospin coefficients are related to those of the Glebsch-Gordan coefficients, we just take the Glebsch-Gordan coefficients as the isospin coefficients of the $I = \frac{1}{2}$ to $I = \frac{3}{2}$ transition. We then assume that the normalization constant is included in the coupling constant of the $\Delta \to \pi N$ coupling.

Thus, to construct the $\vec{\phi}.\vec{\tau}$ operator, we first calculate the Glebsch-Gordan coefficients. They are,

for $\Delta^{++} \to \pi^+ p, < \frac{1}{2}, \frac{1}{2}; 1, 1|\frac{3}{2}, \frac{3}{2} >= 1,$
$\Delta^{+} \to \pi^0 p, < \frac{1}{2}, \frac{1}{2}; 1, 0|\frac{3}{2}, \frac{1}{2} >= \sqrt{\frac{2}{3}},$
$\Delta^{+} \to \pi^+ n, < \frac{1}{2}, -\frac{1}{2}; 1, 1|\frac{3}{2}, \frac{1}{2} >= \sqrt{\frac{1}{3}},$
$\Delta^{0} \to \pi^- p, < \frac{1}{2}, \frac{1}{2}; 1, -1|\frac{3}{2}, -\frac{1}{2} >= \sqrt{\frac{1}{3}},$
$\Delta^{0} \to \pi^0 n, < \frac{1}{2}, -\frac{1}{2}; 1, 0|\frac{3}{2}, -\frac{1}{2} >= \sqrt{\frac{2}{3}},$
$\Delta^{-} \to \pi^- n, < \frac{1}{2}, -\frac{1}{2}; 1, -1|\frac{3}{2}, -\frac{3}{2} >= 1.$

The matrix elements $\chi_N^\dagger \vec{\phi}.\vec{\tau}\chi_\Delta$ look like

$$\begin{aligned} \chi_\Delta^\dagger \vec{\phi}.\vec{\tau}\chi_N = \quad & \alpha(p\phi_-\Delta^{++}) + \beta(p\phi_0\Delta^+) + \gamma(n\phi_-\Delta^+) \\ + \quad & \delta(p\phi_+\Delta^0) + \epsilon(n\phi_0\Delta^0) + \theta(n\phi_+\Delta^-) \end{aligned} \tag{80}$$

where α, β, γ, δ, ϵ and θ are the previous Glebsch-Gordan coefficients such that

$\alpha = \theta = 1$, $\beta = \epsilon = \sqrt{\frac{2}{3}}$ and $\gamma = \delta = \sqrt{\frac{1}{3}}$.

Since $\chi_N^\dagger$ is a (1×2) matrix and χ_Δ is a (4×1) matrix, the $\vec{\phi}.\vec{\tau}$ operator is a (2×4) matrix.

Let $\vec{\phi}.\vec{\tau} = \begin{pmatrix} a_1 & a_2 & a_3 & a_4 \\ b_1 & b_2 & b_3 & b_4 \end{pmatrix}$, the matrix elements $\chi_N^\dagger \vec{\phi}.\vec{\tau}\chi_\Delta$ becomes

$$\chi_N^\dagger \vec{\phi}.\vec{\tau}\chi_\Delta = (p^*, n^*) \begin{pmatrix} a_1 & a_2 & a_3 & a_4 \\ b_1 & b_2 & b_3 & b_4 \end{pmatrix} \begin{pmatrix} \Delta^{++} \\ \Delta^{+} \\ \Delta^{0} \\ \Delta^{-} \end{pmatrix},$$

or

$$\begin{aligned} \chi_N^\dagger \vec{\phi}.\vec{\tau}\chi_\Delta = \quad & p^* a_1 \Delta^{++} + n^* b_1 \Delta^{++} + p^* a_2 \Delta^{+} + n^* b_2 \Delta^{+} \\ + \quad & p^* a_3 \Delta^{0} + n^* b_3 \Delta^{0} + p^* a_4 \Delta^{-} + n^* b_4 \Delta^{-}. \end{aligned} \tag{81}$$

Comparing equations (80) and (81), we find $a_1 = \alpha\phi_- = \phi_-$, $b_1 = 0$, $a_2 = \beta\phi_- = \sqrt{\frac{2}{3}}\phi_-$, $b_2 = \gamma\phi_- = \sqrt{\frac{1}{3}}\phi_-$, $a_3 = \delta\phi_+ = \sqrt{\frac{1}{3}}\phi_+$, $b_3 = \epsilon\phi_0 = \sqrt{\frac{2}{3}}\phi_0$, $a_4 = 0$, $b_4 = \theta\phi_+ = \phi_+$. Therefore, we write

$$\vec{\phi}.\vec{\tau} = \sqrt{\frac{1}{3}} \begin{pmatrix} \sqrt{3}\phi_- & \sqrt{2}\phi_0 & \phi_+ & 0 \\ 0 & \phi_- & \sqrt{2}\phi_0 & \sqrt{3}\phi_+ \end{pmatrix},$$

or

$$\vec{\phi}.\vec{\tau} = \sqrt{\frac{1}{3}} \left\{ \phi_+ \begin{pmatrix} 0 & 0 & 1 & 0 \\ 0 & 0 & 0 & \sqrt{3} \end{pmatrix} + \phi_- \begin{pmatrix} \sqrt{3} & 0 & 0 & 0 \\ 0 & 1 & 0 & 0 \end{pmatrix} + \phi_0 \begin{pmatrix} 0 & \sqrt{2} & 0 & 0 \\ 0 & 0 & \sqrt{2} & 0 \end{pmatrix} \right\}.$$

Since $\vec{\phi}.\vec{\tau} = -\sqrt{2}(\phi_+\tau_+ - \phi_-\tau_-) + \phi_0\tau_0$, we obtain

$$\tau_+ = -\sqrt{\frac{1}{6}} \begin{pmatrix} 0 & 0 & 1 & 0 \\ 0 & 0 & 0 & \sqrt{3} \end{pmatrix},$$

$$\tau_- = \sqrt{\frac{1}{6}} \begin{pmatrix} \sqrt{3} & 0 & 0 & 0 \\ 0 & 1 & 0 & 0 \end{pmatrix},$$

and

$$\tau_0 = \sqrt{\frac{1}{3}} \begin{pmatrix} 0 & \sqrt{2} & 0 & 0 \\ 0 & 0 & \sqrt{2} & 0 \end{pmatrix}.$$

Finally, we note that all the coefficients and operators in all the transitions described above are the same for transitions involving ρ-meson such as the $\Delta N\rho$ and ρNN transitions since ρ-mesons have the same isospin as the pions.

Appendix F

COUPLING CONSTANTS

Values of coupling constants which are used in chapter 4 and in appendix C are given in this appendix. They are

$e = 0.302862$

$k_s = \frac{1}{2}(\kappa_p + \kappa_n)$

$k_v = \frac{1}{2}(\kappa_p - \kappa_n)$ where κ_p=1.79 nuclear magnetons (nm) and κ_n=-1.91 nm

$f_{\pi NN} = 1$

$\lambda_1 = 0.0075$

$F_\pi = 0.093$

$F^{3\pi} = 9.64$

$f_{\pi\Delta N} = 2.13$

$f_{\pi N^\circ N} = 2.58$

$k_v^{\Delta(1)} = 0.668$

$k_v^{\Delta(2)} = -0.305$

$$T_1 = k_s^{N^o(1)} + \tau_3 k_v^{N^o(1)} = \begin{cases} 0.620 & \text{for } \gamma N^o p \\ -0.110 & \text{for } \gamma N^o n, \end{cases}$$

$$T_2 = k_s^{N^o(2)} + \tau_3 k_v^{N^o(2)} = \begin{cases} 0.350 & \text{for } \gamma N^o p \\ 0.039 & \text{for } \gamma N^o n. \end{cases}$$

$f_\rho = 6.2$

$G^v = 2.66$

$G^t = 9.86$

$g_{\rho^0\pi^0\gamma} = 0.0444$, $g_{\rho\pi\gamma} = 0.0346$

$T^1_{N^o\pi\Delta} = -8.25$

$T^2_{N^o\pi\Delta} = -0.33.$

Appendix G

THE $N^{\star}(\frac{3}{2}^{\pm}) \rightarrow \gamma(1^{-})N(\frac{1}{2}^{+})$ DECAY

Since the values of the helicity amplitudes of the processes are given in the Particle Data Group [34], we will extract the corresponding coupling constants by the use of these helicity amplitudes.

The amplitude for the $\Delta N\gamma$ transition is

$$\mathcal{M}_{\Delta N\gamma} = \bar{u}_N \gamma_5 (T_{1\Delta} g_{\mu\nu}\gamma_\lambda F^{\star\lambda\nu} - T_{2\Delta} g_{\mu\nu} p_\Delta^\lambda F^{\star\lambda\nu}) u_\mu, \tag{82}$$

where in the c.o.m. of the Δ-particle, the momenta of the Δ, N and γ are respectively, $p_\Delta = (M_\Delta, \vec{0})$, $p_N = (E_N, |\vec{k}|\sin\theta, 0, |\vec{k}|\cos\theta)$ and $k = (k_0, -|\vec{k}|\sin\theta, 0, -|\vec{k}|\cos\theta)$. $T_{1\Delta}$ and $T_{2\Delta}$ are the coupling constants and $F^{\star\lambda\nu} = \epsilon_\gamma^{\star\lambda} k^\nu - \epsilon_\gamma^{\star\nu} k^\lambda$ is the electromagnetic field tensor, where $\epsilon_\gamma^{\star\nu}$ is the out-going photon polarization. u_N is the nucleon spinor and u_μ the Δ-vector spinor.

The spinor u_μ can be expressed in terms of a Dirac spinor for a spin-$\frac{1}{2}$-particle and a polarization vector of a spin-1 particle. However, the combination of a spin-$\frac{1}{2}$ and a spin-1 gives total spin-$\frac{1}{2}$ or $\frac{3}{2}$, but since we are dealing with a Δ particle, then we take only the spin-$\frac{3}{2}$.

As a result, the Dirac vectors corresponding to different helicities for the Δ particle are represented by

$$
\begin{aligned}
\left|\frac{3}{2};\frac{3}{2}\right\rangle &= \left|1,1;\frac{1}{2},\frac{1}{2}\right\rangle, \\
\left|\frac{3}{2};\frac{1}{2}\right\rangle &= C_1\left|1,0;\frac{1}{2},\frac{1}{2}\right\rangle + C_2\left|1,1;\frac{1}{2},-\frac{1}{2}\right\rangle, \\
\left|\frac{3}{2};-\frac{1}{2}\right\rangle &= C_3\left|1,0;\frac{1}{2},-\frac{1}{2}\right\rangle + C_4\left|1,-1;\frac{1}{2},\frac{1}{2}\right\rangle, \\
\left|\frac{3}{2};-\frac{3}{2}\right\rangle &= \left|1,-1;\frac{1}{2},-\frac{1}{2}\right\rangle,
\end{aligned}
$$

where the C_i's are the usual Clebsch-Gordan coefficients given by

$C_1 =< \frac{3}{2},\frac{1}{2}|1,0;\frac{1}{2},\frac{1}{2} >= \sqrt{\frac{2}{3}}$, $C_2 =< \frac{3}{2},\frac{1}{2}|1,1;\frac{1}{2},-\frac{1}{2} >= \sqrt{\frac{1}{3}}$,
$C_3 =< \frac{3}{2},\frac{1}{2}|1,1;\frac{1}{2},-\frac{1}{2} >= \sqrt{\frac{2}{3}}$ and $C_4 =< \frac{3}{2},-\frac{1}{2}|1,-1;\frac{1}{2},\frac{1}{2} >= \sqrt{\frac{1}{3}}$.
Thus, the Dirac spinors are

$$
\begin{aligned}
u_\mu(\lambda=\frac{3}{2}) &= u(\frac{1}{2})\epsilon_\mu(+1), \\
u_\mu(\lambda=\frac{1}{2}) &= \sqrt{\frac{2}{3}}u(\frac{1}{2})\epsilon_\mu(0) + \sqrt{\frac{1}{3}}u(-\frac{1}{2})\epsilon_\mu(+1), \\
u_\mu(\lambda=-\frac{1}{2}) &= \sqrt{\frac{2}{3}}u(-\frac{1}{2})\epsilon_\mu(0) + \sqrt{\frac{1}{3}}u(\frac{1}{2})\epsilon_\mu(-1), \\
u_\mu(\lambda=-\frac{3}{2}) &= u(-\frac{1}{2})\epsilon_\mu(-1). \qquad (83)
\end{aligned}
$$

In equation (83),

$$u(\pm\tfrac{1}{2}) = \sqrt{E_\Delta + M_\Delta}\begin{pmatrix}1\\0\end{pmatrix}\chi_{\pm\frac{1}{2}},$$

where

$$\chi_{+\frac{1}{2}} = \begin{pmatrix}1\\0\end{pmatrix} \quad \text{and} \quad \chi_{-\frac{1}{2}} = \begin{pmatrix}0\\1\end{pmatrix}$$

and

$$
\begin{aligned}
\epsilon_\mu(+1) &= -\tfrac{1}{\sqrt{2}}(0,1,i,0), \\
\epsilon_\mu(0) &= \tfrac{1}{M_\Delta}(0,0,0,M_\Delta), \\
\epsilon_\mu(-1) &= \tfrac{1}{\sqrt{2}}(0,1,-i,0).
\end{aligned}
$$

The outgoing photon polarizations are

$$\epsilon_\gamma^{\mu *}(+1) = -\frac{1}{\sqrt{2}}(0, -\cos\theta, -i, -\sin\theta)$$

and $\epsilon_\gamma^{\mu *}(-1) = \frac{1}{\sqrt{2}}(0, -\cos\theta, i, -\sin\theta)$ whereas the nucleon spinors are

$$\bar{u}_N(\pm\tfrac{1}{2}) = \sqrt{E_N + M_N}(1, -\tfrac{\vec{\sigma}\cdot\vec{p_N}}{E_N+M_N})\chi_N^\dagger(\pm\tfrac{1}{2}),$$

where

$$\chi_N^\dagger(+\tfrac{1}{2}) = (\cos\tfrac{\theta}{2}, \sin\tfrac{\theta}{2})$$

and $\chi_N^\dagger(-\frac{1}{2}) = (-\sin\frac{\theta}{2}, \cos\frac{\theta}{2})$, where the $\pm$ refers to positive and negative helicities.

Rewriting the amplitude as

$$\mathcal{M}_{\Delta N\gamma} = \bar{u}_N\gamma_5(T_{1\Delta}\gamma.\epsilon_\gamma^* k^\mu + (-T_{1\Delta}(M_\Delta - M_N) + T_{2\Delta}M_\Delta k_0)\epsilon_\gamma^{*\mu})u_\mu, \qquad (84)$$

there are sixteen helicity amplitudes that we denote $\mathcal{M}_{\lambda_\Delta,\lambda_N,\lambda_\gamma}$ where λ_Δ, λ_N and λ_γ are respectively the helicity of the Δ, helicity of the nucleon and helicity of the γ. They are

$$\begin{aligned}
\mathcal{M}_{+\frac{3}{2},+\frac{1}{2},+1} &= \mathcal{M}_0(\frac{1}{2})\sqrt{3}\cos\frac{\theta}{2}\sin^2\frac{\theta}{2},\\
\mathcal{M}_{+\frac{3}{2},+\frac{1}{2},-1} &= \mathcal{M}_0(\frac{3}{2})\cos^3\frac{\theta}{2},\\
\mathcal{M}_{+\frac{3}{2},-\frac{1}{2},+1} &= -\mathcal{M}_0(\frac{3}{2})\sin^3\frac{\theta}{2},\\
\mathcal{M}_{+\frac{3}{2},-\frac{1}{2},-1} &= -\mathcal{M}_0(\frac{1}{2})\sqrt{3}\sin\frac{\theta}{2}\cos^2\frac{\theta}{2},\\
\mathcal{M}_{+\frac{1}{2},+\frac{1}{2},+1} &= \mathcal{M}_0(\frac{1}{2})\sin\frac{\theta}{2}(3\sin^2\frac{\theta}{2} - 2),\\
\mathcal{M}_{+\frac{1}{2},+\frac{1}{2},-1} &= \mathcal{M}_0(\frac{3}{2})\sqrt{3}\cos^2\frac{\theta}{2}\sin\frac{\theta}{2},\\
\mathcal{M}_{+\frac{1}{2},-\frac{1}{2},+1} &= \mathcal{M}_0(\frac{3}{2})\sqrt{3}\sin^2\frac{\theta}{2}\cos\frac{\theta}{2},\\
\mathcal{M}_{+\frac{1}{2},-\frac{1}{2},-1} &= \mathcal{M}_0(\frac{1}{2})\cos\frac{\theta}{2}(3\cos^2\frac{\theta}{2} - 2).
\end{aligned}$$

Note that the angular parts in these amplitudes are the Wigner d-functions $d^J_{M,M'}(\theta)$, where $M, M' = \frac{3}{2}, \frac{1}{2}, -\frac{1}{2}, -\frac{3}{2}$. The other eight helicity amplitudes are related to these first eight through

$$\mathcal{M}_{-\lambda_1,-\lambda_2,-\lambda_3} = (-1)^{\lambda_1+\lambda_2+\lambda_3}\mathcal{M}_{\lambda_1,\lambda_2,\lambda_3}.$$

$\mathcal{M}_0(\frac{3}{2})$ and $\mathcal{M}_0(\frac{1}{2})$ are

$$\begin{aligned}\mathcal{M}_0(\frac{3}{2}) &= -(M_\Delta^2 - M_N^2)(-2T_{1\Delta} + (M_N + M_\Delta)T_{2\Delta})/2, \\ \mathcal{M}_0(\frac{1}{2}) &= -(M_\Delta^2 - M_N^2)(-2M_N T_{1\Delta} + M_\Delta(M_\Delta + M_N)T_{2\Delta}) \\ &\quad /(2(3^{\frac{1}{2}}M_\Delta)).\end{aligned} \tag{85}$$

The decay width is

$$\Gamma(\lambda) = \int \frac{|\vec{p_N}|}{32\pi^2 M_\Delta^2}\frac{1}{(2J+1)}\sum_{MM'}|\mathcal{M}_0(\lambda)d^{\frac{3}{2}}_{M,M'}|^2 d\Omega, \tag{86}$$

where the term $\frac{\sum_{MM'}}{(2J+1)}$ corresponds to a sum over the 16 helicity states and average over the initial spin. Using the property of the $d^J_{M,M'}(\theta)$ function $\frac{1}{2J+1}\int \sum_{MM'}|d^J_{M,M'}|^2 d\Omega = 4\pi$, we obtain

$$\Gamma(\lambda) = \frac{|\vec{p_N}|}{8\pi M_\Delta^2}|\mathcal{M}_0(\lambda)|^2. \tag{87}$$

On the other hand, the helicity amplitudes given in P.D.G. are related to the partial width by

$$\Gamma(\lambda) = \frac{2|\vec{p_N}|^2 M_N}{\pi M_\Delta(2J+1)}|A(\lambda)|^2. \tag{88}$$

For the decay $\Delta \to N + \gamma$, the helicity amplitudes are $A(\frac{3}{2}) = -0.258 \pm 0.006$ and $A(\frac{1}{2}) = -0.140 \pm 0.005$. Solving for both equations (87) and (88), we extract the values

$$T_{1\Delta} = \quad 0.668 \pm 0.022,$$
$$T_{2\Delta} = \; - \; 0.305 \pm 0.047.$$

We note that values of these coupling constants can also be extracted directly from equation (87), by using the values of $\Gamma(\lambda)$ given in P.D.G. These values are $\Gamma(\frac{3}{2}) = (0.0044 \pm 0.0003)\Gamma$ and $\Gamma(\frac{1}{2}) = (0.0013 \pm 0.0001)\Gamma$, where $\Gamma = 0.120 \pm 0.005$ GeV is the full width of the Δ. Therefore, we obtain

$$T_{1\Delta} = \; \pm \; 0.668 \pm 0.084,$$
$$T_{2\Delta} = \; \mp \; 0.286 \pm 0.027,$$

and

$$T_{1\Delta} = \; \pm \; 20.553 \pm 0.423,$$
$$T_{2\Delta} = \; \mp \; 2.768 \pm 0.055.$$

In the calculation of the total and differential cross sections, the coupling constants extracted from the helicity amplitude data are used because they give the best fit.

As we have pointed out in chapter 3 that the second coupling term in the $\Delta\gamma N$-vertex could be absent, it is worth looking at the behavior of the helicity amplitudes if $T_{2\Delta} = 0$. In fact, with $T_{2\Delta} = 0$, the ratio between the two helicity amplitudes yields $\mathcal{M}_0(\frac{3}{2})/\mathcal{M}_0(\frac{1}{2}) = 3^{\frac{1}{2}} M_\Delta(M_\Delta - M)/M(3M_\Delta + M) \approx 0.14$. The avalaible data analysis gives $A(\frac{3}{2})/A(\frac{1}{2}) = -0.258/-0.140 = 1.79$ which is indeed inconsistent with $T_{2\Delta} = 0$. The point is that if the two helicity amplitudes are to be independent, the coupling $T_{2\Delta}$ must be kept arbitrary, and it has to be determined, along with the coupling $T_{1\Delta}$, by a fit to the helicity amplitude data. It is clear that with $T_{1\Delta} = 0.668$ and $T_{2\Delta} = -0.305$, the ratio $\mathcal{M}_0(\frac{3}{2})/\mathcal{M}_0(\frac{1}{2})$ gives a value around 2.19.

A similar calculation of coupling constants can be done for the $N^+(1520) \to \gamma + p$ and $N^0(1520) \to \gamma + n$ decays . The amplitude for $N^o\gamma N$ is

$$\mathcal{M}_{N^*\gamma N} = \bar{u}_N(T_{1N^o} g_{\mu\nu}\gamma_\lambda F^{*\lambda\nu} - T_{2N^o} g_{\mu\nu} p^\lambda_{N^o} F^{*\lambda\nu})u_\mu. \quad (89)$$

We recall that the parameters T_{1N^o} and T_{2N^o} contain the isoscalar and isovector terms and are written as $T_{1N^o} = k_s^{N^o(1)} + \tau_3 k_v^{N^o(1)}$ and $T_{2N^o} = k_s^{N^o(2)} + \tau_3 k_v^{N^o(2)}$, where $\tau_3 = \pm 1$ respectively for $N^+(1520)$ and $N^0(1520)$. The difference between the structures of $\mathcal{M}_{\Delta\gamma N}$ and $\mathcal{M}_{N^*\gamma N}$ is that $\mathcal{M}_{N^*\gamma N}$ does not have a γ_5 term in it. This is due to the fact that $N^*(1520)$, N and γ have natural parities.

The helicity amplitudes are respectively $A_p(\frac{3}{2}) = 0.166 \pm 0.005$, $A_p(\frac{1}{2}) = -0.024 \pm 0.009$, and $A_n(\frac{3}{2}) = -0.139 \pm 0.011$, $A_n(\frac{1}{2}) = -0.059 \pm 0.009$. Thus, we obtain

$$T_{1N^*} = \begin{cases} 0.620 \pm 0.062 & \text{for } \gamma N^{+*} p \\ -0.110 \pm 0.014 & \text{for } \gamma N^{0*} n \end{cases}$$

$$T_{2N^*} = \begin{cases} 0.350 \pm 0.045 & \text{for } \gamma N^{+*} p \\ 0.039 \pm 0.021 & \text{for } \gamma N^{0*} n. \end{cases}$$

By using the following values from P.D.G., namely $\Gamma(\frac{3}{2}) = (0.0049 \pm 0.0004)\Gamma$, $\Gamma(\frac{1}{2}) = (0.00020 \pm 0.00014)\Gamma$ for $N^+(1520) \to \gamma + p$, and $\Gamma(\frac{3}{2}) = (0.0035 \pm 0.0010)\Gamma$, $\Gamma(\frac{1}{2}) = (0.00070 \pm 0.0003)\Gamma$ for $N^0(1520) \to \gamma + n$, where $\Gamma = 0.120 \pm 0.010$ GeV is the full width of the $N(1520)$, the extracted coupling constants for the $\gamma N^+(1520)p$ vertex are

$$T_{1N^o} = \pm 0.663 \pm 0.072$$

$$T_{2N^o} = \pm 0.386 \pm 0.054$$

and

$$T_{1N^o} = \mp 0.319 \pm 0.025$$

$$T_{2N^o} = \pm 0.106 \pm 0.028.$$

For the $\gamma N^0(1520)n$ vertex, they are

$$T_{1N^o} = \pm 0.737 \pm 0.143$$

$$T_{2N^o} = \pm 0.471 \pm 0.094$$

and

$$T_{1N^o} = \mp 0.093 \pm 0.022$$

$$T_{2N^o} = \pm 0.053 \pm 0.032.$$

Again, the coupling constants extracted from the helicity amplitude data will be used in the calculation of the total and differential cross sections.

Appendix H

THE $N^o(1520, \frac{3}{2}^-) \rightarrow \Delta(\frac{3}{2}^+) + \pi(0^-)$ DECAY

The intrinsic spin of the final state is $S = \frac{3}{2}$. Thus, if $J = \frac{3}{2}$ and $S = \frac{3}{2}$, then $L = 0, 1, 2, 3$.

Using parity conservation, $P_{N^o} = P_\Delta P_\pi (-1)^L = (-1)^{L+1} = -1$, we derive that L must be an even number and that the possible values of J, S, L are respectively $\frac{3}{2}, \frac{3}{2}, 0$ or $\frac{3}{2}, \frac{3}{2}, 2$. This means that there are two independent partial-wave amplitudes that we denote ${}^4S_{\frac{3}{2}}$ and ${}^4D_{\frac{3}{2}}$ corresponding respectively to $L = 0$ and $L = 2$. In general, the parity eigenstate is

$$|J, M; \mu_1, \mu_2 > + \eta_1 \eta_2 (-1)^{J - s_1 - s_2} |J, M; -\mu_1, -\mu_2 >, \tag{90}$$

where J is the spin of the decaying particle. μ_1 and μ_2 are the helicities or spin components along the directions of motion of the daugther particles, s_1 and s_2 are their intrinsic spins, and η_1 and η_2 are their intrinsic parities. In the $N^o \rightarrow \Delta + \pi$, $\mu_2 = 0$ is the spin of the pion and we write equation (90) as

$$|J, M; \mu_1 > + \eta_1 \eta_2 (-1)^{J - s_1 - s_2} |J, M; -\mu_1 > . \tag{91}$$

Thus, The parity eigenstates for the decay are

$$\frac{1}{\sqrt{2}} \left(\left| \frac{3}{2}, M; \frac{3}{2} \right\rangle \; + \; \left| \frac{3}{2}, M; -\frac{3}{2} \right\rangle \right) ,$$

$$\frac{1}{\sqrt{2}}\left(\left|\frac{3}{2}, M; \frac{1}{2}\right\rangle + \left|\frac{3}{2}, M; -\frac{1}{2}\right\rangle\right) .$$

Recall that the $L - S$ coupling states are related to the helicity states by [74]

$$\begin{aligned} |J, M; \mu_1, \mu_2> &= \sum_{LS} \sqrt{\frac{2L+1}{2J+1}} < L, 0; S, \mu | J, \mu >< s_1, \mu_1; s_2, -\mu_2 | S, \mu > \\ &\quad \times |J, M; L, S > . \end{aligned}$$

Expanding each term in the previous helicity states, we obtain

$$\begin{aligned} \left|\frac{3}{2}, M; \frac{3}{2}\right\rangle &= \frac{1}{\sqrt{2}}\left|\frac{3}{2}, M; 0, \frac{1}{2}\right\rangle + \frac{1}{\sqrt{2}}\left|\frac{3}{2}, M; 2, \frac{3}{2}\right\rangle , \\ \left|\frac{3}{2}, M; -\frac{3}{2}\right\rangle &= \frac{1}{\sqrt{2}}\left|\frac{3}{2}, M; 0, \frac{1}{2}\right\rangle + \frac{1}{\sqrt{2}}\left|\frac{3}{2}, M; 2, \frac{3}{2}\right\rangle , \\ \left|\frac{3}{2}, M; \frac{1}{2}\right\rangle &= \frac{1}{\sqrt{2}}\left|\frac{3}{2}, M; 0, \frac{1}{2}\right\rangle - \frac{1}{\sqrt{2}}\left|\frac{3}{2}, M; 2, \frac{3}{2}\right\rangle , \\ \left|\frac{3}{2}, M; -\frac{1}{2}\right\rangle &= \frac{1}{\sqrt{2}}\left|\frac{3}{2}, M; 0, \frac{1}{2}\right\rangle - \frac{1}{\sqrt{2}}\left|\frac{3}{2}, M; 2, \frac{3}{2}\right\rangle . \end{aligned}$$

Hence, the parity eigenstates are

$$\begin{aligned} \frac{1}{\sqrt{2}}\left(\left|\frac{3}{2}, M; \frac{3}{2}\right\rangle + \left|\frac{3}{2}, M; -\frac{3}{2}\right\rangle\right) &= \frac{1}{\sqrt{2}}\left(\left|\frac{3}{2}, M; 0, \frac{3}{2}\right\rangle + \left|\frac{3}{2}, M; 2, \frac{3}{2}\right\rangle\right) , \\ \frac{1}{\sqrt{2}}\left(\left|\frac{3}{2}, M; \frac{1}{2}\right\rangle + \left|\frac{3}{2}, M; -\frac{1}{2}\right\rangle\right) &= \frac{1}{\sqrt{2}}\left(\left|\frac{3}{2}, M; 0, \frac{3}{2}\right\rangle - \left|\frac{3}{2}, M; 2, \frac{3}{2}\right\rangle\right) . \end{aligned}$$

The helicity amplitudes and partial-wave amplitude are related by the equations

$$\begin{aligned} \left\langle \frac{3}{2}, M|T|\frac{3}{2}, M; \frac{3}{2}\right\rangle &+ \left\langle \frac{3}{2}, M|T|\frac{3}{2}, M; -\frac{3}{2}\right\rangle = \\ \left\langle \frac{3}{2}, M|T|\frac{3}{2}, M; L=0, S=\frac{3}{2}\right\rangle &+ \left\langle \frac{3}{2}, M|T|\frac{3}{2}, M; L=2, S=\frac{3}{2}\right\rangle , \end{aligned} \quad (92)$$

and

$$\begin{aligned} \left\langle \frac{3}{2}, M|T|\frac{3}{2}, M; \frac{1}{2}\right\rangle &+ \left\langle \frac{3}{2}, M|T|\frac{3}{2}, M; -\frac{1}{2}\right\rangle = \\ \left\langle \frac{3}{2}, M|T|\frac{3}{2}, M; L=0, S=\frac{3}{2}\right\rangle &- \left\langle \frac{3}{2}, M|T|\frac{3}{2}, M; L=2, S=\frac{3}{2}\right\rangle , \end{aligned} \quad (93)$$

where 'T' is some transition operator.

The left-hand side terms of equations (92) and (93) are the angle independent parts of the helicity amplitudes that we denote $\mathcal{M}_{\mu_1}$, where $\mu_1 = \pm\frac{3}{2}, \pm\frac{1}{2}$.

Solving for the partial-wave amplitudes, we obtain

$$^4S_{\frac{3}{2}} =< \tfrac{3}{2}, M|T|\tfrac{3}{2}, M; L = 0, S = \tfrac{3}{2} >= \tfrac{1}{2}(\alpha_1 + \alpha_2)$$

and

$$^4D_{\frac{3}{2}} =< \tfrac{3}{2}, M|T|\tfrac{3}{2}, M; L = 2, S = \tfrac{3}{2} >= \tfrac{1}{2}(\alpha_1 - \alpha_2),$$

where α_1 and α_2 are respectively $\mathcal{M}_{\frac{3}{2}} + \mathcal{M}_{-\frac{3}{2}}$ and $\mathcal{M}_{\frac{1}{2}} + \mathcal{M}_{-\frac{1}{2}}$, and are expressed in terms of two coupling constants $T^1_{N^o\pi\Delta}$ and $T^2_{N^o\pi\Delta}$. They are

$$\begin{aligned}
\alpha_1 = & - 2M_{N^o}^{\frac{1}{2}}[((M_\Delta + M_{N^o})^2 - m_\pi^2)/M_{N^o}]^{\frac{1}{2}} T^2_{N^o\pi\Delta}, \\
\alpha_2 = & - [((M_\Delta + M_{N^o})^2 - m_\pi^2)/M_{N^o}]^{\frac{1}{2}}[(-(M_\Delta^2 - M_{N^o}^2)^2 + \\
& 2M_\Delta^2 m_\pi^2 + 2M_{N^o}^2 m_\pi^2 - m_\pi^4) T^1_{N^o\pi\Delta} + (2M_\Delta^2 + 2M_\Delta M_{N^o} + 2M_{N^o}^2 - \\
& 2m_\pi^2) T^2_{N^o\pi\Delta}]/(3M_\Delta M_{N^o}^{\frac{1}{2}}).
\end{aligned}$$

The decay width of $N^o(1520)$ into $\Delta\pi$ is calculated in a way that a subsequent decay of the unstable Δ into $N\pi$ is considered as seen in figure (48). Thus, the decay width of the process is

$$d\Gamma = \frac{1}{2M_{N^o}} \frac{\sum}{(2J_{N^o} + 1)} |\mathcal{M}|^2 d\Phi_3, \tag{94}$$

where the term $\frac{\sum}{(2J_{N^o}+1)}$ stands for an average over the spin of the $N^o(1520)$ and sum over the spins of the daughter particles, Δ and N. $\mathcal{M}$ is the amplitude of the full process $N^o \to \Delta\pi \to N\pi\pi$, and $d\Phi_3$ is the phase space written as

$$d\Phi_3 = (2\pi)^4 \int \frac{d^3p_1 d^3Q_1 d^3Q_2}{(2\pi)^9 (2E_1)(2w_1)(2w_2)} \delta^4(P - p_1 - Q_1 - Q_2), \tag{95}$$

where P, p_1, Q_1 and Q_2 are respectively the 4-momenta of the N^o, N, π_1 and π_2.

Using the amplitudes given in appendix C, $\mathcal{M}$ takes the form

$$\mathcal{M} = \bar{u}(p_1)\frac{f_{\pi\Delta N}}{m_\pi}\gamma_5 Q_1^\mu R_{\mu\nu}\gamma_5 T_2(T^1_{N^o\pi\Delta}Q_2^\nu Q_2^{\mu'} + T^2_{N^o\pi\Delta}g^{\nu\mu'})u_{\mu'}(P),$$

where $R_{\mu\nu}$, the propagator of the Δ, is given by

$$R_{\mu\nu} = \sum_{m_s=-\frac{3}{2}}^{m_s=\frac{3}{2}} \frac{\bar{u}_\mu(p_\Delta)u_\nu(p_\Delta)}{p_\Delta^2 - M_\Delta^2 + iM_\Delta\Gamma_\Delta}.$$

Squaring the amplitude, we find

$$|\mathcal{M}|^2 = \frac{\sum |\bar{u}(p_1)\frac{f_{\pi\Delta N}}{m_\pi}\gamma_5 Q_1^\mu u_\mu(p_\Delta)|^2 |\bar{u}_\nu(p_\Delta)\gamma_5 T_2(T^1_{N^o\pi\Delta}Q_2^\nu Q_2^{\mu'} + T^2_{N^o\pi\Delta}g^{\nu\mu'})u_{\mu'}(P)|^2}{|p_\Delta^2 - M_\Delta^2 + iM_\Delta\Gamma_\Delta|^2} \tag{96}$$

or

$$|\mathcal{M}|^2 = \sum \frac{|\mathcal{M}_1|^2|\mathcal{M}_2|^2}{|p_\Delta^2 - M_\Delta^2 + iM_\Delta\Gamma_\Delta|^2}, \tag{97}$$

where $\mathcal{M}_1$ and $\mathcal{M}_2$ are respectively the amplitudes of the processes $N^o \rightarrow \Delta\pi$ and $\Delta \rightarrow N\pi$, and Γ_Δ is the total width of the unstable Δ.

Now, going back to the decay width Γ and using the properties of the δ function given in equations (53) and (56), we can rewrite equation (94) as

$$\Gamma = \frac{1}{16(2\pi)^3 M_{N^o}^3} \int_{M_N+m_\pi}^{M_{N^o}-m_\pi} \frac{dm_\Delta}{m_\Delta |m_\Delta^2 - M_\Delta^2 + iM_\Delta\Gamma_\Delta|^2} \sum |\mathcal{M}_1|^2 \frac{\sum |\mathcal{M}_2|^2}{(2J_{N^o}+1)} \times \lambda^{\frac{1}{2}}(M_{N^o}^2, m_\Delta^2, m_\pi^2)\lambda^{\frac{1}{2}}(m_\Delta^2, M_N^2, m_\pi^2). \tag{98}$$

The expressions of the partial decay widths $\Gamma(^4S_{\frac{3}{2}})$ and $\Gamma(^4D_{\frac{3}{2}})$ are now obtained by replacing $\frac{\sum|\mathcal{M}_2|^2}{(2J_{N^o}+1)}$ respectively by $|^4S_{\frac{3}{2}}|^2$ and $|^4D_{\frac{3}{2}}|^2$. Experimental values of $\Gamma(^4S_{\frac{3}{2}})$ and $\Gamma(^4D_{\frac{3}{2}})$ are taken from PDG ($8\% \pm 3\%$ for the S-wave and $12\% \pm 2\%$ for the D-wave) and solving these equations, the coupling constants are derived.

We find

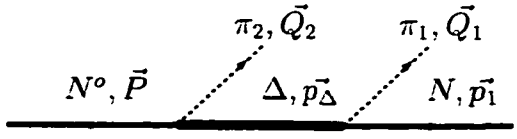

FIG. 48: The decay $N^o(1520) \to (N\pi)_\Delta \pi$.

$$T^1_{N^o\pi\Delta} = \pm 9.25 \pm 1.38$$

$$T^2_{N^o\pi\Delta} = \pm 0.33 \pm 0.05,$$

and

$$T^1_{N^o\pi\Delta} = \pm 10.79 \pm 1.74$$

$$T^2_{N^o\pi\Delta} = \pm 0.045 \pm 0.08.$$

In our calculation of differential and total cross section, we use

$$T^1_{N^o\pi\Delta} = -9.25 \pm 1.38$$

$$T^2_{N^o\pi\Delta} = -0.33 \pm 0.05$$

to obtain the best fit.

Bibliography

[1] P.D.B. Collins and A.D. Martin, Hadron Interactions (Adam Hilger LTD, Bristol, 1984).

[2] For a review, see: J. Hamber and G. parisi, Phys. Rev. **D27** (1983) 208 .

[3] *for a review, see*: L. J. Reinders, J. Rubinstein and S. Yazaki, Phys. Rep. **127** (1985) 1.

[4] *for a review, see*: F. Lenz, H. Griebhammer and D. Stoll, Lectures on QCD, (1997).

[5] *for a review, see*: J. Zeng, J. W. Van Orden and W. Roberts, CEBAF preprint CEBAF-TH-94-08; J. Zeng, PhD. Thesis, Old Dominion University, (1995); R. Koniuk and N. Isgur, Phys. Rev. **D21**, (1980) 1868.

[6] S. Capstick and N. Isgur, Phys. Rev. **D34**, (1986) 2809.

[7] J. W. Norbury, Can. J. Phys. **67**, (1989) 876.

[8] S. Fleck, B. Silvestre-Brac and J.-M. Richard, Phys. Rev. **D38**, (1991) 1659.

[9] D.B. Leinweber, R.M. Woloshyn and T. Draper, Phys. Rev. **D43**, (1988) 1519.

[10] S. Capstick and W. Roberts, Phys. Rev. **D47** (1993) 1994.

[11] R. Koniuk and N. Isgur, Phys. Rev. **D21** (1980) 1868.

[12] R. Koniuk and N. Isgur, Phys. Rev. **D44** (1980) 845.

[13] S. Frullani *et al.*, CEBAF proposal No. 91-011.

[14] G. S. Mutchler *et al.*, CEBAF proposal PR-89-024, G. S. Mutchler spokesperson.

[15] B. A. Mecking *et al.*, CEBAF proposal E-89-045, B. A. Mecking spokesperson.

[16] D. M. Manley and E. M. Saleski, Phys. Rev. **D45**, (1992) 4002.

[17] J. Beringer, πN Newsletter 7, (1992) 33.

[18] N. Grion *et al.*, Nucl. Phys. **A492**, (1989) 509.

[19] S. Capstick, Phys. Rev. **D46** (1992) 2864.

[20] S. Capstick and W. Roberts, Phys. Rev. **D49** (1994) 4570.

[21] Aachen-Berlin-Bonn-Hamburg-München collaboration, Phys. Rev. **175** (1968).

[22] G. Gialanella *et al.*, Nuovo Cimento **LXIII A** (1969) 892.

[23] F. Carbonara *et al.*, Nuovo Cimento **36A** (1976) 219.

[24] Cambridge Bubble Chamber Group, Phys. Rev. 155 (1967) 1477; Phys. Rev. **163** (1967) 1510.

[25] H. G. Hilpert *et al.*, Phys. Lett. **23** (1966) 707.

[26] A. Braghieri *et al.*, Phys. Lett. **B363** (1995) 46.

[27] H. Ströher, Private Communication.

[28] J. Napolitano *et al.*, CEBAF Proposal No. 93-033, J. Napolitano spokesperson.

[29] L. Lüke and P. Söding, Springer Tracts in Modern Physics **59** (1971) 39.

[30] E. Oset and J. A. Gomez-Tejedor, Nucl. Phys. **A571** (1994) 667.

[31] E. Oset and J. A. Gomez-Tejedor, Nucl. Phys. **A600** (1996) 413.

[32] R. M. Davidson, N. C. Mukhopadhyay, and R. S. Wittman, Phys. Rev. **43** (1991) 71.

[33] M. Vanderhaeghen *et al.*, Nucl. Phys. A **595** (1995) 219.

[34] Particle Data Group, R. M. Barnet *et al.*, Phys. Rev. **D54** (1996) 1.

[35] F. A. Berends, A. Donnachie, and D. L. Weaver, Nucl. Phys. **4**,103 (1967).

[36] G. F. Chew, M. L. Goldberger, F. E. Law and Y. Nambu, Phys. Rev. **106** (1957) 1345.

[37] R. L. Walker, Phys. Rev. **182**, 1729 (1969).

[38] D. H. Lyth, in Electromagnetic Interactions of Hadrons, edited by A. Donnachie and B. Shaw (Plenum, New York, 1978), p. 159.

[39] G. Goldstein *et al.*, Nucl. Phys. **B80** (1974) 164.

[40] M. G. Olsson and E. T. Osypowski, Nucl. Phys. **B87** (1975) 399; Phys. Rev. **D17** (1978) 174.

[41] S. Weinberg, Phys. Rev. **166** (1968) 1568.

[42] M. Vanderhaeghen *et al.*, Nucl. Phys. **A562** (1994) 521.

[43] S. Nozawa, B. Blankleider and T.-S.H. Lee, Nucl. Phys. **A513** (1990) 459.

[44] M. Gari and H. Hyuga, Nucl. Phys. **A264** (1976) 409.

[45] G. E. Brown and A. D. Jackson, The nucleon-nucleon interaction (North-Holland, Amsterdam, 1976).

[46] R. Machleidt, K. Holinde and C. Elster, Phys. Reports **149** (1987) 1.

[47] R. D. Peccei, Phys. Rev. **176** (1968) 1812; **181** (1969) 1902.

[48] L. M. Nath and B. K. Bhattacharyya, Z. Phys. **C5** (1980) 9.

[49] H. Haberzettl, Propagation of a massive spin-3/2 particle, nucl-th/9812043

[50] I. Blomqvist and J. M. Laget, Nucl. Phys. **A280** (1977) 405.

[51] R. M. Davidson *et al.*, Phys. Rev. **D43** (1991) 71.

[52] C. Carlson and N. C. Mukhopadhyay, Phys. Rev. Lett. **67**, (1991) 3745; Z. Li, V. Burkert, and Z. Li, Phys. Rev. **D46**, (1992) 70.

[53] C. Itzykson and J. Zuber, Quantum field theory, McGraw-Hill international book company, 1980.

[54] M. Benmerrouche, E. Tomusiak, Phys. Lett. **73**, (1994) 400.

[55] T. Oed, Rapport du stage de D.E.A., Institut des Sciences Nucléaires, Grenoble, France, 1996.

[56] J. D. Jackson, Rev. Mod. Phys. **37** (1965) 484.

[57] K. Gottfried and J. D. Jackson, Nuovo Cimento **34** (1964) 735.

[58] R. Miskimen *et al.*, Jefferson Laboratory Proposal 94-015.

[59] S. L. Adler, Phys. Rev. **177**, 2426 (1969); J. S. Bell and R. Jackiw, Nuovo Cimento **60A**, 47 (1969).

[60] J. S. Bell and R. Jackiw, Nuovo Cimento **60A**, 47 (1969).

[61] J. Wess and B. Zumino, Phys. Lett. **37B**, 95 (1971).

[62] E. Witten, Nucl. Phys. **B223**, 422 (1983).

[63] B. R. Holstein, Nucl. Phys. **A546**, 213 (1992).

[64] S. L. Adler, B. W. Lee, S. B. Treiman, and A. Zee, Phys. Rev. **D4**, 3497 (1971).

[65] M. Terent'ev, JETP Lett. **14**, 94 (1971).

[66] R. Aviv and A. Zee, Phys. Rev. **D5**, 2372 (1972).

[67] L.M. Nath, B. Etemadi, and J.D. Kimel, Phys. Rev. **D3**, (1971) 2153.

[68] P.A. Moldauer and K.M. Case, Phys. Rev. **102**, (1956) 279.

[69] C. Frondal, Suppl. Nuovo Cimento **9**, (1958) 416.

[70] W. Rarita and J. Schwinger, Phy. Rev. **60**, (1941) 61.

[71] A. Aurillia and H. Umezawa, Phys. Rev. **182**, (1969) 1682.

[72] K. Johnson and E.C.G. Sudarshan, Ann. Phys. (N.Y.) **13**, (1961) 126.

[73] M. Benmerrouche, R. M. Davidson, and N. C. Mukhopadhyay, Phys. Rev. **C39**, (1989) 2339.

[74] A. D. Martin and T. D. Spearman, Elementary Particle Theory, North Holland publishing company, Amsterdam (1970).

Vita

Andry M. Rakotovao
Department of physics
Old Dominion University
Norfolk, VA 23529

I was born in Antananarivo (Madagascar) in !967. In July 1994, I graduated from high school and in September 1995, after doing my national service, I entered the Chemistry and Physics department at the 'Ecole Normale Niveau 3' (EN3); University of Antananarivo. During my last academic year at the EN3, I was involved in a research project in the field of Statistical Physics. My main research of interest was the 'Percolation Theory'. In July 1990, I graduated from EN3 and received a diploma degree with honor. In 1992, I was enrolled in the Master's Degree program in Physics at Old Dominion University (ODU) and received my Master's Degree in August 1994. After that, I was admitted in the Ph.D program at ODU and since then, I have been working within the field of nuclear physics and studying the single and double pion photoproductions.

Typeset using LaTeX.